

ESD TDR 65-97
ESTI FILE COPY

ESD-TR-65-97

ESD RECORD COPY

RETURN TO
SCIENTIFIC & TECHNICAL INFORMATION DIVISION
(ESTI), BUILDING 1211

SR-98

ESTI PROCESSED

THE DESIGN OF RADAR SIGNALS DDC TAB PROJ OFFICER
 ACCESSION MASTER FILE

DATE _____

TECHNICAL REPORT NO. ESD-TR-65-97 ESTI CONTROL NR. **AL 46459**

CY NR 1 OF 1 CYS

JUNE 1965

E. N. Fowle

Prepared for

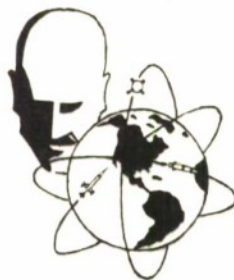
DIRECTORATE OF RADAR AND OPTICS

ELECTRONIC SYSTEMS DIVISION

AIR FORCE SYSTEMS COMMAND

UNITED STATES AIR FORCE

L. G. Hanscom Field, Bedford, Massachusetts



Project 750

Prepared by

THE MITRE CORPORATION

Bedford, Massachusetts

Contract AF 19(628)-2390

ESRRR

ADD611711

Copies available at Clearing House for Federal Scientific and Technical Information (formerly Office of Technical Services).

Qualified requesters may obtain copies from DDC. Orders will be expedited if placed through the librarian or other person designated to request documents from DDC.

When US Government drawings, specifications, or other data are used for any purpose other than a definitely related government procurement operation, the government thereby incurs no responsibility nor any obligation whatsoever; and the fact that the government may have formulated, furnished, or in any way supplied the said drawings, specifications, or other data is not to be regarded by implication or otherwise, as in any manner licensing the holder or any other person or corporation, or conveying any rights or permission to manufacture, use, or sell any patented invention that may in any way be related thereto.

Do not return this copy. Retain or destroy.

THE DESIGN OF RADAR SIGNALS

TECHNICAL REPORT NO. ESD-TR-65-97

JUNE 1965

E. N. Fowle

Prepared for

DIRECTORATE OF RADAR AND OPTICS

ELECTRONIC SYSTEMS DIVISION

AIR FORCE SYSTEMS COMMAND

UNITED STATES AIR FORCE

L. G. Hanscom Field, Bedford, Massachusetts



Project 750

Prepared by

THE MITRE CORPORATION

Bedford, Massachusetts

Contract AF 19(628)-2390

FOREWORD

The material on radar signal design in this report was presented by the author in lectures given during the two-week summer course on radar conducted at MIT in 1961. The lecture material was afterward expanded and prepared in written form for inclusion as Chapter 3 of a book entitled "Elements of High-Power Radar Design," edited by J. Freedman and L. Smullin of MIT. Now, in June 1965, it appears that plans for the book have been abandoned. Therefore, it seems desirable to make this material more generally available by issuing it as a technical report.

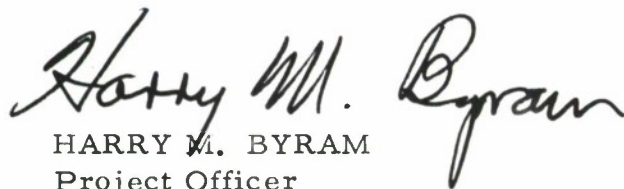
The ideas on signal design contained in this report have come from many sources, and these sources are acknowledged with care insofar as they are known to the author. The author is indebted to many of his colleagues; in particular, it is a pleasure to acknowledge many stimulating discussions with E. L. Key, R. Manasse, J. A. Sheehan, and R. D. Haggarty, of the MITRE Corporation, and with E. J. Kelly and R. C. Yost, of MIT Lincoln Laboratory.

ABSTRACT

This report discusses the design of radar signals. It is assumed that the radar receiver is matched to the signal so that the receiver output waveform, in the presence of signal Doppler frequency shift, is characterized by Woodward's two-dimensional signal correlation function. The signal correlation function is discussed, and certain of its properties are collected together. The problem of the detection of a target in the presence of many nearby targets is discussed, and an expression for the target capacity of a radar is developed in terms of the signal correlation function. There follows a discussion of the general problems of signal design for multiple target resolution and for detection of single targets in clutter. Signal waveforms are classified according to the type of modulation, and the design of waveforms of each type is considered in detail. The two-dimensional correlation function is given for each type of signal. Finally, the subject of techniques for generation and reception of signals is discussed.

REVIEW AND APPROVAL

Publication of this technical report does not constitute Air Force approval of the report's findings or conclusions. It is published only for the exchange and stimulation of ideas.



HARRY M. BYRAM
Project Officer
MITRE Project 750

CONTENTS

	<u>Page</u>
1.0 INTRODUCTION	1
2.0 THE SIGNAL CORRELATION FUNCTION AND THE PROBLEM OF RESOLUTION	3
2.1 Introduction	3
2.2 Some Properties of the Signal Correlation Function and Related Ambiguity Function	3
2.3 The Resolution of Two Nearby Targets	11
2.4 The Resolution of Multiple Targets	15
2.5 Signal Design for Multiple Target Resolution	19
2.6 Detection of a Target in Clutter	26
3.0 WAVEFORMS	29
3.1 Introduction	29
3.2 Amplitude-modulated Signals	34
3.3 Phase-modulated Signals	38
3.4 Uni-directional FM Signals	41
3.5 The Rectangular Linear FM Signal	47
3.6 A Rectangular Non-linear FM Signal	60
3.7 The Rectangular, Staircase FM Signal	65
3.8 Rectangular, Phase-reversal Signals	72
3.9 Amplitude- and Phase-modulated Signals	84
3.10 An Amplitude- and Phase-modulated Signal	88
3.11 Design of Phase-modulated Signals with Two-dimensional Correlation Functions of the Thumbtack Shape	96
3.12 Amplitude-modulated, Phase-reversal Signals with χ Functions of the Thumbtack Shape	109

CONTENTS (Cont'd.)

	<u>Page</u>
3.13 Amplitude-modulated, Phase-reversal Signals with Circularly Symmetric χ Functions	117
3.14 Pulse Burst Signals	121
3.15 Pulse Burst Signals with Non-uniform Repetition Intervals	130
3.16 Pulse Burst Signals with Jittered Carrier Frequency	134
4.0 TECHNIQUES	141
4.1 Introduction	141
4.2 General	142
4.3 Sideband Exchange	144
4.4 Lumped-constant Filters	147
4.5 Ultrasonic Delay Lines	165
4.6 Tapped Delay Lines	172
5.0 REFERENCES	179
6.0 BIBLIOGRAPHY	185

LIST OF ILLUSTRATIONS

<u>Figure No.</u>		<u>Page</u>
1	Sketch to illustrate the effect on probability of detection of an overlap of the two echoes and of signal-to-noise ratio.	14
2	Sketch of a pulse-train signal and its ambiguity function.	22
3	Sketch of the $ \chi $ function of a rectangular, constant-frequency signal.	36
4	Sketch of the $ \chi $ function of a constant-frequency signal with a Gaussian envelope.	38
5	Envelope of a signal with a Fourier transform that has a rectangular modulus and quadratic phase for (a) $TW = 10$, (b) $TW = 60$, and (c) $TW = 120$.	52
6	Block diagram of a linear FM pulse compression system.	53
7	Effect of Doppler frequency shift on linear FM pulse compression system.	55
8	$ \chi $ function of a signal with a rectangular envelope and linear frequency sweep.	57
9	Sketches to show (a) spectrum of receiver output before weighting, (b) receiver output waveform before weighting, (c) spectrum of receiver output waveform after weighting, (d) receiver output waveform after weighting.	59
10	The tangent FM signal.	63
11	Comparison of approximate and exact signal envelope and frequency sweep of non-linear FM signal.	64

LIST OF ILLUSTRATIONS (Cont'd.)

<u>Figure No.</u>		<u>Page</u>
12	The central region of the two-dimensional correlation function of the inverse-tangent signal with duration-bandwidth product of $50/\pi$.	66
13	Envelope and frequency vs. time of the staircase FM signal.	67
14	Block diagram of a filter whose impulse response is the staircase FM signal.	68
15	The staircase FM signal.	70
16	Sketch showing the frequency characteristics of the channels in Fig. 14.	71
17	A plus-minus code waveform.	74
18	Autocorrelation function of the 7th-order Barker code of Fig. 17.	75
19	The 13th-order Barker code waveform.	76
20	Block diagram of video filter used to generate and "match" 13-code waveform.	77
21	The two-dimensional correlation function of the 13-code signal.	79
22	Photograph of A-scope of a radar operating alternately with a simple pulse and with a 13-code signal of the same length.	80
23	Illustration of the method of suppression of the sidelobes of the 13-code autocorrelation function.	81

LIST OF ILLUSTRATIONS (Cont'd.)

<u>Figure No.</u>		<u>Page</u>
24	Block diagram of weighting network which controls amplitudes of the interior sidelobes of the 13-code autocorrelation function.	83
25	Photograph of a model of the $ \chi $ function of the linear FM Gaussian signal.	93
26	Observed linear FM Gaussian signal generated by applying a short pulse to a linear filter.	94
27	Output waveform of the filter matched to the linear FM Gaussian signal when the signal has zero Doppler shift.	94
28	Output waveform of the filter matched to the linear FM Gaussian signal when the signal has various Doppler shifts.	95
29	Solution of Eq. (152) for t_s , illustrated graphically (a) for $\tau > 0, \nu > 0$; (b) for $\tau < 0, \nu < 0$.	99
30	Solution of Eq. (152) for t_s , illustrated graphically (a) for $\tau < 0, \nu > 0$; (b) for $\tau > 0, \nu < 0$.	100
31	Solution of Eq. (152) for a symmetrical frequency sweep. (a) $\tau > 0, \nu > 0$; (b) $\nu > 0, \tau < 0$.	102
32	Envelope and frequency sweep of the vee-shaped linear FM signal.	104
33	$ \chi $ function of the vee-notch linear FM signal of Fig. 32.	105
34	Envelope and frequency sweep of a quadratic FM signal.	106

LIST OF ILLUSTRATIONS (Cont'd.)

<u>Figure No.</u>		<u>Page</u>
35	$ \chi $ function of the quadratic FM signal of Fig. 33.	107
36	The two-dimensional correlation function of the 13-code signal.	108
37	The ambiguity function of a 7-digit M-sequence.	115
38	$ \chi $ function of the truncated 7-digit M-sequence.	116
39	(a) Envelope of 10th order Hermite function signal for positive time (envelope is an even function about the origin); (b) a radial section of the envelope of the two-dimensional correlation function of the signal of part (a).	120
40	The radially symmetric two-dimensional correlation function associated with the 10th order Hermite function signal.	120
41	The time truncation of the periodic impulse train.	125
42	Central region of the χ function of the impulse train after truncation in time by the $(\sin \pi t/T)$ function.	125
43	Central region of the χ function of the periodic impulse train after truncation in time and frequency by $\sin y/y$ functions.	126
44	Sketch of the pulse-train signal after $\sin y/y$ time and frequency truncations.	126
45	Sketch of the central region of the χ function corresponding to rectangular time truncation and $\sin y/y$ spectrum truncation.	127

LIST OF ILLUSTRATIONS (Cont'd.)

<u>Figure No.</u>		<u>Page</u>
46	Sketch of the impulse-train signal after rectangular time truncation and $\sin y/y$ spectrum truncation.	128
47	(a) A simple pulse-burst signal; (b) the autocorrelation function of (a).	132
48	(a) A pulse-burst signal with non-uniform pulse spacing; (b) the autocorrelation function of (a).	132
49	Envelope of the two-dimensional correlation function for a non-uniformly spaced pulse train of N pulses.	133
50	Sketch of the χ function of a simple pulse-burst signal in a strip in the Doppler direction.	136
51	Sketch of the χ function of a pulse-burst signal whose frequency increases by f_s on successive pulses.	138
52	Sketch of a cross section in the τ direction of the χ function of Fig. 51.	138
53	Schematic to illustrate the process of sideband exchange.	146
54	Sketches illustrating the generation of a signal, its transmission and sideband exchange on reception.	148
55	A possible arrangement for realizing in the frequency domain a filter having an arbitrary frequency response.	150
56	Frequency response modulus (a) and group delay (b) of a linear phase, single-pole filter.	150
57	Pole-zero configuration which gives the frequency response of Fig. 56.	151

LIST OF ILLUSTRATIONS (Cont'd.)

<u>Figure No.</u>		<u>Page</u>
58	The frequency response modulus and group time delay of a bandpass filter.	152
59	Pole-zero configuration which gives the frequency response of Fig. 58.	153
60	Inverse-tangent group time delay characteristic.	154
61	The all-pass pole-zero arrangement whose delay approximates the inverse-tangent curve of Fig. 60.	154
62	The symmetrical constant-resistance lattice.	157
63	(a) The all-pass, constant-resistance lattice; (b) the constant-resistance network of (a) with equalized parasitic losses.	158
64	Pole-zero plot of (a) all-pass constant-resistance network of Fig. 63(a) and (b) loss-equalized, constant-resistance network of Fig. 63(b).	160
65	(a) and (b) Unbalanced bridged-tee equivalents of the constant-resistance lattice of Fig. 63(a); (c) and (d) Bridged-tee equivalents of lattice of Fig. 63(b).	161
66	Bridged-tee delay network of Fig. 65(c).	162
67	Alignment of bridged-tee network.	164
68	Bridged-tee networks in cascade.	166
69	Comparison of theoretical and experimental frequency dependence of delay for first longitudinal mode in a strip.	167

LIST OF ILLUSTRATIONS (Cont'd.)

<u>Figure No.</u>		<u>Page</u>
70	Photograph of one end of a strip ultrasonic delay line showing the piezo-electric transducer.	168
71	Insertion loss for a typical dispersive longitudinal strip delay line with a center frequency of about 2 megacycles and a mid band delay about one milli-second.	169
72	Photograph of a strip ultrasonic delay line.	171
73	Block diagram of a filter employing a tapped delay line.	173
74	Sketch to illustrate the method of generation of low-pass waveforms by use of tapped delay lines.	175
75	Sketch of the magnetostrictive acoustic wire delay line developed at Lincoln Laboratory.	177

1.0 INTRODUCTION

Central to the discussion of radar signal design is the signal correlation function and the related ambiguity function. It is recognized that the ambiguity function characterizes the degree to which a signal can be located in time and frequency. In Section 2.0 the subject of signal design is considered primarily from the standpoint of the signal correlation and ambiguity functions. First, we will collect some properties of the two functions. Then we will consider the problem of resolution and develop an expression for the target capacity of a radar in terms of the ambiguity function of the radar waveform and the target parameters. Three different idealized ambiguity function shapes — the ridge, the thumbtack, and the bed-of-spikes — are considered, and their utility and method of use in a multi-target environment is discussed.

In Section 3.0 signals are classified as to the type of modulation employed — amplitude modulation, phase or frequency modulation, and a combination of the two — and some aspects of the design of each type of signal are discussed. In every case some idea is given of the kinds of ambiguity function shapes that are possible with the various kinds of waveforms.

In Section 4.0 a number of the most important, well-developed techniques for the generation and reception of signals are considered, each in some detail.

Section 5.0 contains the list of references and, for convenience, a bibliography listing the referenced documents in alphabetical order.

2.0 THE SIGNAL CORRELATION FUNCTION AND THE PROBLEM OF RESOLUTION

2.1 Introduction

In this section we will tabulate some of the properties of the signal correlation function and the related ambiguity function and proceed then to discuss the problem of resolution in the context of the signal ambiguity function. Then we will develop an expression for the target capacity of a radar which depends upon, among other things, the ambiguity function of the radar signal. The specific dependence gives some insight as to how the signal ambiguity function ought to be shaped for various kinds of measurements and for various distributions of radar targets. Then the broad problem of signal design to achieve high target capacity is considered. The ideas developed for the problem of resolving multiple targets are then applied to the problem of detecting targets which are immersed in a clutter background.

2.2 Some Properties of the Signal Correlation Function and Related Ambiguity Function

The significance of the signal correlation function and the ambiguity function, and the manner in which these two functions enter the subject of detection theory has been discussed by Woodward^[1] and Siebert.^[2] A number of properties of the two functions have been collected by Siebert;^[3] since these are not too readily accessible in the literature, it seems worth while tabulating them here for easy reference.

Several notations are used in writing the signal correlation function. Woodward^[1] calls the signal correlation function $\chi(\tau, \nu)$, where*

*The Notation $\bar{u}(x)$ denotes the complex conjugate of $u(x)$.

$$\chi(\tau, \nu) = \int_{-\infty}^{\infty} u(t) \bar{u}(t + \tau) e^{-j2\pi \nu t} dt \quad , \quad (1)$$

while Siebert and others [4, 5] have used the symmetrical form, $\Theta(\tau, \omega)$, with

$$\Theta(\tau, \omega) = \int_{-\infty}^{\infty} u(t - \frac{\tau}{2}) \bar{u}(t + \frac{\tau}{2}) e^{-j\omega t} dt \quad . \quad (2)$$

In Eq. (1), ν is Doppler frequency in cycles per second; in Eq. (2), ω is Doppler frequency in radians per second. The relation between the two functions, χ and Θ , is simple. If we write $2\pi\nu = \omega$ and put $t = t' - \tau/2$ Eq. (1) becomes

$$\chi(\tau, \omega) = e^{j\frac{\omega\tau}{2}} \int_{-\infty}^{\infty} u(t - \frac{\tau}{2}) \bar{u}(t + \frac{\tau}{2}) e^{-j\omega t} dt \quad , \quad (3)$$

or

$$\chi(\tau, \omega) = e^{j\frac{\omega\tau}{2}} \Theta(\tau, \omega) \quad . \quad (4)$$

The functions χ and Θ thus are seen to differ only by a phase factor. Notice that

$$|\chi(\tau, \omega)| = |\Theta(\tau, \omega)| \quad .$$

The squared modulus of $\chi(\tau, \nu)$ or alternatively of $\Theta(\tau, \omega)$ is usually referred to as the ambiguity function, ψ . We have

$$\psi(\tau, \nu) = |\chi(\tau, \nu)|^2 \quad (5)$$

or

$$\psi(\tau, \omega) = |\Theta(\tau, \omega)|^2 \quad (6)$$

The χ notation of Woodward occurs naturally in analysis and is perhaps the most common in the literature, and for this reason the χ notation is used in this report. Because of its symmetry, however, manipulation of the Θ function yields neater results. Thus the properties of the signal correlation function are tabulated below in terms of the Θ function. The theorems on Θ functions are taken directly from Siebert^[1] with permission and with only minor changes. Proofs of the theorems are given only when the method of proof is not obvious.

We have the signal correlation function $\Theta(\tau, \omega)$, Eq. (2), repeated here as Eq. (7).

$$\Theta(\tau, \omega) = \int_{-\infty}^{\infty} u(t - \frac{\tau}{2}) \bar{u}(t + \frac{\tau}{2}) e^{-j\omega t} dt \quad (7)$$

Definitions

1. We assume that $u(t)$ is a reasonably well-behaved, complex-valued function of the real variable t . In particular, any integrals involving $u(t)$ are assumed to exist.

2. We define

$$\bar{U}(\omega) = \frac{1}{\sqrt{2\pi}} \int_{-\infty}^{\infty} u(t) e^{-j\omega t} dt \quad (8)$$

so that

$$u(t) = \frac{1}{\sqrt{2\pi}} \int_{-\infty}^{\infty} \bar{U}(\omega) e^{j\omega t} d\omega \quad (9)$$

3. We shall call a complex function $\Theta(\tau, \omega)$ of two real variables, τ and ω , a Θ function if and only if there exists a function $u(t)$ which is such that $\Theta(\tau, \omega)$ may be represented as in Eq. (7).

4. We shall call a real positive function $\psi(\tau, \omega)$ of two real variables, τ and ω , a ψ function if and only if there exists a function $u(t)$ which is such that

$$\psi(\tau, \omega) = |\Theta(\tau, \omega)|^2 = \left| \int_{-\infty}^{\infty} u(t - \frac{\tau}{2}) \bar{u}(t + \frac{\tau}{2}) e^{-j\omega t} dt \right|^2 \quad (10)$$

Theorems

1. $\Theta(\tau, \omega) = \bar{\Theta}(-\tau, -\omega)$.
2. If $\Theta(\tau, \omega)$ is a Θ function, it has the additional representations

$$\Theta(\tau, \omega) = \int_{-\infty}^{\infty} U(\mu - \frac{\omega}{2}) \bar{U}(\mu + \frac{\omega}{2}) e^{-j\mu\tau} d\mu \quad (11)$$

and

$$\Theta(\tau, \omega) = \frac{1}{\sqrt{2\pi}} \int_{-\infty}^{\infty} \int_{-\infty}^{\infty} u(\rho - \tau) U(\mu - \omega) e^{-j\mu\rho} e^{j\frac{\omega\tau}{2}} d\mu d\rho \quad (12)$$

3. If $\Theta(\tau, \omega)$ is a Θ function corresponding to $u(t)$, then $(1/\alpha)$ $\{\Theta[\alpha\tau, (\omega/\alpha)]\}$ is a Θ function corresponding to $u(\alpha t)$.

4. If $\Theta(\tau, \omega)$ is a Θ function corresponding to $u(t)$, then $\Theta(\tau, \omega + 2k\tau)$ is a Θ function corresponding to $\exp [jkt^2] u(t)$.

5. If $\Theta(\tau, \omega)$ is a Θ function corresponding to $U(\omega)$, then $\Theta(\tau + 2\alpha\omega, \omega)$ is a Θ function corresponding to $\exp [j\alpha\omega^2] U(\omega)$.

6. If $\Theta(\tau, \omega)$ is a Θ function corresponding to $u(t)$, then $\cos \varphi \Theta(\omega \sin \varphi + \tau \cos \varphi, \omega \cos \varphi - \tau \sin \varphi)$ is a Θ function corresponding to the time function

$$e^{-j\frac{t^2 \tan \varphi}{2}} \frac{1}{\sqrt{2\pi}} \int_{-\infty}^{\infty} \bar{U}(\omega) e^{-j\frac{\omega^2 \tan \varphi}{2}} e^{j\frac{\omega t}{\cos \varphi}} d\omega .$$

In other words, the property of being a Θ function is independent of a rotation in the coordinate axes.

7. If $\Theta(\tau, \omega)$ is a Θ function, then, along any straight line through the origin, $\{\Theta(\tau, \omega) / [\Theta(0, 0)]\}$ has the properties of a characteristic function; for example,

$$\int_{-\infty}^{\infty} \Theta(\tau \cos \varphi, -\tau \sin \varphi) e^{-j\omega\tau} d\tau \geq 0 \quad (13)$$

for all τ and ω .

8. A necessary and sufficient condition that $\Theta(\tau, \omega)$ be a Θ function is that

$$\frac{1}{2\pi} \int_{-\infty}^{\infty} \Theta(\tau, \omega - \mu) e^{j \frac{(\omega + \mu)\tau}{2}} d\tau \quad (14)$$

shall factor in the form $f(\mu) \bar{f}(\omega)$. If this condition is satisfied, then $U(\omega)$ can be identified with $f(\omega)$.

Proof:

Necessity follows directly upon substituting Eq. (11) into Eq. (14).

To prove sufficiency, assume that Eq. (14) factors and set $\mu = \varphi - (\rho/2)$ and $\omega = \varphi + (\rho/2)$. Then we have

$$\begin{aligned} \int_{-\infty}^{\infty} f(\varphi - \frac{\rho}{2}) \bar{f}(\varphi + \frac{\rho}{2}) e^{-j\varphi\xi} d\varphi &= \frac{1}{2\pi} \int_{-\infty}^{\infty} \left[\int_{-\infty}^{\infty} \Theta(\tau, \rho) e^{j\varphi\tau} d\tau \right] e^{-j\varphi\xi} d\varphi \\ &= \Theta(\xi, \rho) , \end{aligned}$$

which is valid if $f(\omega)$ is identified with $U(\omega)$.

9. An equivalent necessary and sufficient condition that $\Theta(\tau, \omega)$ be a Θ function is that

$$\frac{1}{2\pi} \int_{-\infty}^{\infty} \Theta(\tau - p, \omega) e^{j \frac{(\tau + p)\omega}{2}} d\omega \quad (15)$$

factor in the form

$$f(p) \bar{f}(\mu) .$$

If this condition is satisfied, then $u(t)$ may be identified with $f(t)$.

10. If $\Theta_1(\tau, \omega)$ and $\Theta_2(\tau, \omega)$ are both Θ functions and neither is identically zero, then $\Theta(\tau, \omega) = \Theta_1(\tau, \omega) + \Theta_2(\tau, \omega)$ is a Θ function if and only if $\Theta_1(\tau, \omega) = C\Theta_2(\tau, \omega)$, where C is a constant.

Proof:

The sufficiency of the condition is obvious. Necessity follows from Eq. (14) because we must have $U(\mu) \bar{U}(\omega) = U_1(\mu) \bar{U}_1(\omega) + U_2(\mu) \bar{U}_2(\omega)$ for all μ and ω . It is easily shown that this can be true only if $U_1(\mu)$ is proportional to $U_2(\mu)$; that is, if $\Theta_1(\tau, \omega)$ is proportional to $\Theta_2(\tau, \omega)$.

11. If $\Theta_1(\tau, \omega)$ and $\Theta_2(\tau, \omega)$ are both Θ functions, then both

$$\Theta'(\tau, \omega) = \int_{-\infty}^{\infty} \Theta_1(t, \omega) \Theta_2(\tau - t, \omega) dt \quad (16)$$

and

$$\Theta''(\tau, \omega) = \int_{-\infty}^{\infty} \Theta_1(\tau, \mu) \Theta_2(\tau, \omega - \mu) d\mu \quad (17)$$

are also Θ functions. In the case of Eq. (16)

$$U'(\omega) = U_1(\omega) U_2(\omega) \quad ,$$

and in the case of Eq. (17)

$$u''(t) = u_1(t) u_2(t) \quad .$$

Theorems 3, 4, 5 and 6 also apply, with obvious modifications, to ψ functions in place of Θ functions. In particular, the property of being a ψ function is independent of a rotation in axes. Other theorems are:

12. If $\psi(\tau, \omega)$ is a ψ function, then $\psi(\tau, \omega)$ is its own two-dimensional Fourier transform, i. e. ,

$$\frac{1}{2\pi} \int_{-\infty}^{\infty} \int_{-\infty}^{\infty} \psi(\tau, \omega) e^{-j\mu\tau} e^{j\omega p} d\tau d\omega = \psi(p, \mu) \cdot \quad (18)$$

13. If $\psi(\tau, \omega)$ is a ψ function, then

$$\frac{1}{2\pi} \int_{-\infty}^{\infty} \int_{-\infty}^{\infty} \psi(\tau, \omega) d\tau d\omega = \psi(0, 0) \geq \psi(\tau, \omega) \cdot \quad (19)$$

14. If $\psi(\tau, \omega)$ satisfies condition 12, and a fortiori, if $\psi(\tau, \omega)$ is a ψ function

$$\int_{-\infty}^{\infty} \int_{-\infty}^{\infty} \int_{-\infty}^{\infty} \int_{-\infty}^{\infty} \psi(\tau_2 - \tau_1, \omega_2 - \omega_1) g(\tau_1, \omega_1) \bar{g}(\tau_2, \omega_2) d\tau_1 d\tau_2 d\omega_1 d\omega_2 \geq 0 \quad (20)$$

for any function $g(\tau, \omega)$.

15. If $\psi_1(\tau, \omega)$ and $\psi_2(\tau, \omega)$ satisfy condition 12, and, a fortiori, if $\psi_1(\tau, \omega)$ or $\psi_2(\tau, \omega)$ are ψ functions, then

$$\psi(\tau, \omega) = \int_{-\infty}^{\infty} \psi_1(t, \omega) \psi_2(t - \tau, \omega) dt \quad (21)$$

also satisfies condition 12 but is not necessarily a ψ function.

Necessary and sufficient conditions for $\psi(\tau, \omega)$ to be a ψ function have not yet been discovered.

2.3 The Resolution of Two Nearby Targets

It frequently happens that radar targets are close enough together in range and radial velocity so that their echoes overlap. When the echoes overlap significantly, the detection and parameter estimation problems become considerably more complicated than is the case for isolated targets. The problem of determining whether there is one echo or more than one in an interval is called the resolution problem. In this section we will consider the problem of two nearby targets. In the next section the problem of many targets will be discussed.

Let us first consider the two-target problem in a qualitative way. Assume that we have a radar whose receiver is matched to a known signal, the echo from a stationary, point target. The input to the matched filter consists of noise and possible signals. At the filter output a threshold is set. When the filter output exceeds the threshold, we say a signal exists. The probability of noise alone exceeding the threshold is the so-called probability of false alarm. Let us assume that we are trying to decide whether there is a target at a range corresponding to t_0 . We ask: What is the effect on detection at t_0 of a possible second target at $t_0 + \tau$? We assume τ is small enough so that the matched filter response to a target at $t_0 + \tau$ would extend past the point t_0 . It is obvious that the possible second target has the effect of increasing the probability of false alarm, P_F , at the point of observation, t_0 . We can keep P_F constant by raising the threshold. Raising the threshold, however, reduces the probability of detection, P_D . Increasing the probability of the occurrence of the second target or reducing the separation, τ , would further reduce P_D , if P_F were held constant. So we see that

when the signal processing is predicated on isolated targets there is a loss in detection when the targets cease to be isolated.

One possible approach to the problem of resolving two nearby targets in noise is given by Helstrom. [6] Helstrom postulates that the range of both targets is exactly known and that the signal echo amplitudes are unknown. To resolve the signals, one constructs a separate filter to give a maximum-likelihood estimate of the amplitude of each signal. In the two-target case, two such filters are required. When taken at the proper time, the estimates of the amplitudes of the two signals are independent, and the estimates may be compared to a threshold. If the threshold is exceeded by the output of filter number one, for example, signal number one is said to be present, and so forth. The probabilities of false alarm and detection may be calculated for this process. If A^* is the estimate of actual amplitude A of one signal and if b is the threshold, we have for the probability of false alarm, P_F

$$P_F = P_r [|A^*| > b/A = 0] = 2 \operatorname{erfc} [b \sqrt{2(1 - \lambda^2)/N}] , \quad (22)$$

where

$$\operatorname{erfc} x = \frac{1}{\sqrt{2\pi}} \int_x^\infty e^{-t^2/2} dt .$$

N is the noise power per cycle and λ is a parameter which depends on the amount of overlap of the two signals, being zero for no overlap and one for complete overlap. As the amount of overlap increases, the parameter λ increases and the probability of false alarm increases.

The probability of detection of one signal is given by Helstrom

$$P_D = P_r [|A^*| > b/A \neq 0] = 1 - \operatorname{erfc} y_2 + \operatorname{erfc} y_1 , \quad (23)$$

where

$$y_1 = \sqrt{2(1 - \lambda^2)/N} (A + b)$$

and

$$y_2 = \sqrt{2(1 - \lambda^2)/N} (A - b)$$

We can hold the probability of false alarm constant by setting the threshold b in Eq. (22)

$$b = \frac{K_1}{\sqrt{2(1 - \lambda^2)/N}} , \quad (24)$$

where K_1 is a constant. With the above value of b the probability of detection becomes

$$P_D = 1 - \operatorname{erfc} y_2 + \operatorname{erfc} y_1 , \quad (25)$$

where

$$y_1 = \sqrt{\frac{2E}{N}} \sqrt{1 - \lambda^2} + K_1$$

and

$$y_2 = \sqrt{\frac{2E}{N}} \sqrt{1 - \lambda^2} - K_1 ,$$

where we have written $E = A^2$, the energy in the signal. The probability of detection is the shaded area in Fig. 1. As λ approaches 1, the unshaded region moves toward the origin, and its area increases, thus reducing the probability of detection. If the signal-to-noise ratio,

$$\frac{2E}{N} = \frac{K_2}{1 - \lambda^2}, \quad (26)$$

where K_2 is a constant, the probability of detection will be kept constant. The signal-to-noise ratio, then, must be increased as the overlap of the signals increases, to maintain a certain probability of detection when the probability of false alarm is held constant.

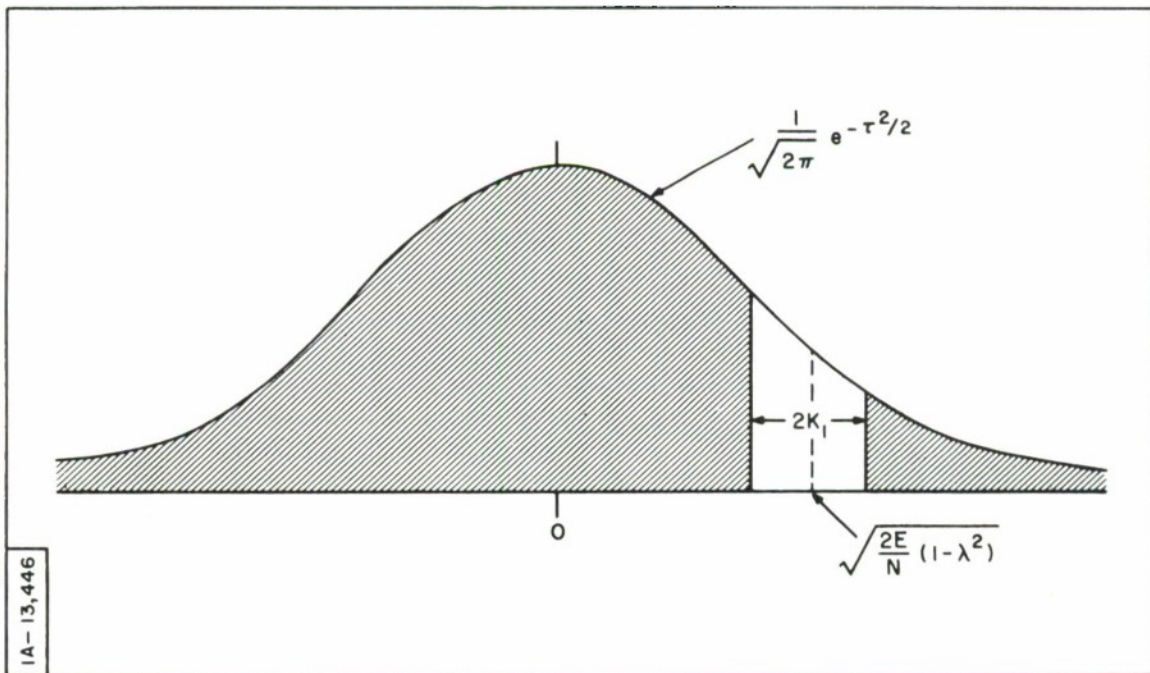


Fig. 1. Sketch to illustrate the effect on probability of detection of an overlap of the two echoes and of signal-to-noise ratio. Probability of detection is given by shaded area.

Thus we see that, even when elaborate signal processing methods are employed, a loss in detection occurs when two signals overlap. In the case considered, the range of both was assumed known exactly. As additional quantities are allowed to vary, for example, the range to the first target, the target separation, frequency shift, carrier phase and so forth, the processing required to make maximum-likelihood estimates of the unknowns becomes very complex. Detection is apparently impaired by each successive estimate of an unknown parameter made in the presence of noise.

The problem of the resolution of echoes from two nearby targets can be approached, alternatively, from the standpoint of signal design. To obtain the best probability of detection for a given probability of false alarm one should design the radar signal so that the responses from the expected targets do not overlap significantly. Not only does this approach give the best detection, but it results in the simplest signal processing as well.

2.4 The Resolution of Multiple Targets*

In the last section, the maximum-likelihood processing of the echoes from two targets was considered and expressions for probability of detection and false alarm were given. We saw that the probability of detection of either of the two targets decreased as the overlap of the echoes increased when the false alarm probability was held constant. Similar expressions could be developed for the three-target situation. It is clear that addition of a third target whose echo overlapped the first two echoes would have the effect of reducing further the probability of detection of any one target. As the number

* An excellent qualitative discussion of the multiple-target detection problem is given by Applebaum and Howells in Ref. 7.

of targets becomes large, it is clear that the probability of detection of any one target is going to be small if there is a significant amount of overlapping of the echoes. One should approach the multiple-target resolution problem, then, from the standpoint of signal design. The designer should find a signal which would optimize, as nearly as possible, the probability of detection of the individual targets. The ideal signal would be such that the echoes did not overlap at all. The optimum way (from the detection standpoint) to solve the multiple-target resolution problem is to avoid it, for when the signal is designed so that the echoes do not overlap, the multiple-target problem disappears. The signals are isolated and the receiver consists of an array of single target processors.

To design the signal so that the echoes do not overlap significantly, one must define some measure of total overlap of responses in a way which takes into account the number of targets, their cross sections, their probable distribution in time and Doppler frequency, and the detailed characteristics of the radar signal. Fowle, Kelly and Sheehan^[8] have defined as "interference" the mean energy from a complex of n objects with average cross section \bar{b} , distributed according to a probability density function $P(t, f)$. They get

$$E |c(\tau, \nu)|^2 = n\bar{b} \int_{-\infty}^{\infty} \int_{-\infty}^{\infty} \psi(\tau - t, \nu - f) P(t, f) dt df \quad (27)$$

where $\psi(\tau, \nu)$ is the single-target ambiguity function, Eq. (5), and the signal $u(t)$ is normalized to have unit energy so that $\psi(0, 0) = 1$ and $\int_{-\infty}^{\infty} \int_{-\infty}^{\infty} \psi(t, f) dt df = 1$. Here (τ, ν) is the point in the time-frequency plane at which the output of the single-target processor is observed. $E |e(\tau, \nu)|^2$ is a noisy background against which the detector must look for objects of interest.

If now at the point (τ, ν) we insert a target of energy b , we may form a signal-to-interference ratio, S/I ,

$$\frac{S}{I} = \frac{b}{n\bar{b} \int_{-\infty}^{\infty} \int_{-\infty}^{\infty} \psi(\tau - t, \nu - f) P(t, f) dt df}, \quad (28)$$

where $I = E |e(\tau, \nu)|^2$. Or, solving for n , and using the fact that $S = b$,

$$n = \frac{1}{(\bar{b}/I) \int_{-\infty}^{\infty} \int_{-\infty}^{\infty} \psi(\tau - t, \nu - f) P(t, f) dt df}. \quad (29)$$

We note that from Eq. (29) that \bar{b}/I need not be greater than unity.

An upper bound for n , N_{\max} , may be obtained as

$$N_{\max} = \frac{1}{(\bar{b}/I)_{\min} \int_{-\infty}^{\infty} \int_{-\infty}^{\infty} \psi(\tau - t, \nu - f) P(t, f) dt df}, \quad (30)$$

and this will be the maximum number of objects (in addition to the target of interest) which may be tolerated, subject to the constraints of a given $P(\tau, \nu)$, a given $\psi(\tau, \nu)$ and a given minimum (mean signal)-to-(mean interference) ratio.

If we write

$$\left(\frac{\bar{b}}{I}\right)_{\min} = \left(\frac{\bar{b}}{b_{\min}}\right) \left(\frac{S}{I}\right)_{\min}, \quad (31)$$

(since $S = b$), we see that the ratio $(\bar{b}/I)_{\min}$ may be partitioned into the product of an extremum of signal-to-interference ratio, and an extremum of dynamic range, either (but not both) of which is arbitrary.

A more careful treatment of this problem recognizes the fact that the integration in Eq. (27) through (30) should be extended only over that region of the t, f plane which is external to a small area which includes the point (τ, ν) , since echoes from objects very near (τ, ν) should properly be interpreted as targets of interest to the filter "tuned" to (τ, ν) . We should rewrite Eq. (30) for N_{\max} thus:

$$N_{\max} = \frac{1}{(\bar{b}/I)_{\min} \int \int_{R'} \psi(\tau - t, \nu - f) P(t, f) dt df}, \quad (32)$$

where R' is the τ, ν plane less an area centered at (τ, ν) .

It will frequently be true that the target distribution function, $P(t, f)$, will not be known. In that case, it is interesting to assume the objects uniformly distributed over a region in the t, f plane of area $T_T W_T$. Then, if we take

$$P(t, f) = \begin{cases} \frac{1}{T_T W_T}, & |t| < \frac{T_T}{2}, \quad |f| < \frac{W_T}{2}, \\ 0, & \text{otherwise,} \end{cases} \quad (33)$$

Eq. (32) becomes

$$N_{\max} = \frac{T_T W_T}{\left(\frac{\bar{b}}{b_{\min}}\right) \left(\frac{S}{I}\right)_{\min} \int \int_R \psi(\tau - t, \nu - f) dt df} \quad (34)$$

The integration in Eq. (34) is now over the region R , which is given by $|t| \leq T_T/2$ and $|f| \leq W_T/2$ with a small area excluded at $t = f = 0$.

Since n itself will usually be of a statistical nature, N_{\max} should be viewed as the average number of targets that the radar could separately detect (or resolve). That N_{\max} varies inversely with \bar{b}/b_{\min} , the dynamic range of range of target sizes, and $(S/I)_{\min}$, the minimum tolerable signal-to-interference ratio, appears quite plausible. The dependence of N_{\max} on $T_T W_T$ and on the double integral of $|\chi|^2$ is more interesting, however. We have the facts that the dimensionless quantity $T_T W_T$ is a measure of the intrinsic capacity of the target space. The target capacity of the radar can be increased over the intrinsic capacity by appropriate design of the radar signal.

2.5 Signal Design for Multiple Target Resolution

In the preceding section an expression for interference power was taken as a measure of the total overlap of the echoes from the multiple-target complex. From the expression for interference an expression was developed for N_{\max} , the average maximum number of targets that a radar can accommodate on an isolated target basis. In this section we investigate techniques of signal design which make it possible to reduce the interference (or to increase N_{\max}). The discussion will be cast in terms of several idealized signal ambiguity function shapes. The subject of the design of actual signals whose ambiguity functions approximate the ideal shapes will be reserved for Section 3.0.

We repeat the expression for interference $E |e(\tau, \nu)|^2$,

$$E |e(\tau, \nu)|^2 = \frac{\bar{n}\bar{b}}{T_T W_T} \int_R \int \psi(\tau - t, \nu - f) dt df \quad (35)$$

The integration in Eq. (35) is over the target space, which is assumed to have its center at the origin of the (τ, ν) plane. The interference will tend to be worst when the point of observation (τ, ν) is at the center of the target space, that is, at $\tau = \nu = 0$. Let us consider that case. Then we have

$$E |e(0, 0)|^2 = \frac{\bar{n}\bar{b}}{T_T W_T} \int_R \int \psi(t, f) dt df \quad ; \quad (36)$$

\bar{n} , \bar{b} and T_T in Eq. (36) are characteristics of the target complex and are beyond our control. The Doppler frequency spread of the target space, W_T , is proportional to carrier frequency; thus the interference may be reduced by increasing the carrier frequency. But generally the most promising way to reduce interference, and certainly the most interesting way, is to shape the ambiguity function, $\psi(\tau, \nu)$, in such a way as to reduce the value of the integral in Eq. (35).

We recall that $\psi(0, 0) = 1$ and that

$$\int_{-\infty}^{\infty} \int_{-\infty}^{\infty} \psi(t, f) dt df = 1 \quad , \quad (37)$$

because of the normalization of the signal, $u(t)$. While the total volume under $\psi(t, f)$ is thus constrained, the value of the integral $\int \int_R \psi(t, f) dt df$ may be reduced by shaping $\psi(t, f)$ to cause some of the volume under ψ to lie outside the target space, that is, outside the region R . *

Accuracy requirements in the measurement of range and radial velocity will determine the shape of the ambiguity function near its peak. For example, if accurate estimates are required of both range and radial velocity, the central response of the ambiguity function must have the shape of a narrow spike. In addition, if the interference is to be low, the spike should be surrounded by a clear space, that is, a region where ψ is zero or very small. A signal consisting of a train of equally spaced pulses has an ambiguity function of the correct general shape. The pulse train signal and its ambiguity function are sketched in Fig. 2. The ambiguity function is identically zero except in strips oriented in the Doppler direction. The spacing of the strips is, of course, the spacing between pulses, Δ , and the strips have a width of 2δ where δ is the pulse length. In the strips where ψ has value, the volume is primarily concentrated at points spaced at intervals of $1/\Delta$ in Doppler frequency. As shown in Fig. 2, the central peak has significant value over a region, the area of which is approximately equal to $\delta/m\Delta$, where $m\Delta$ is the total time duration of the train of pulses. Notice that the central response is surrounded by an approximately clear space of dimensions Δ in range by $1/\Delta$ in Doppler.

We should use the pulse train signal in the multiple-target problem by scaling the radar parameters to cause echoes from objects in the target

* A very good general discussion of signals and the shapes of their χ functions is given by Siebert in Ref. 9.

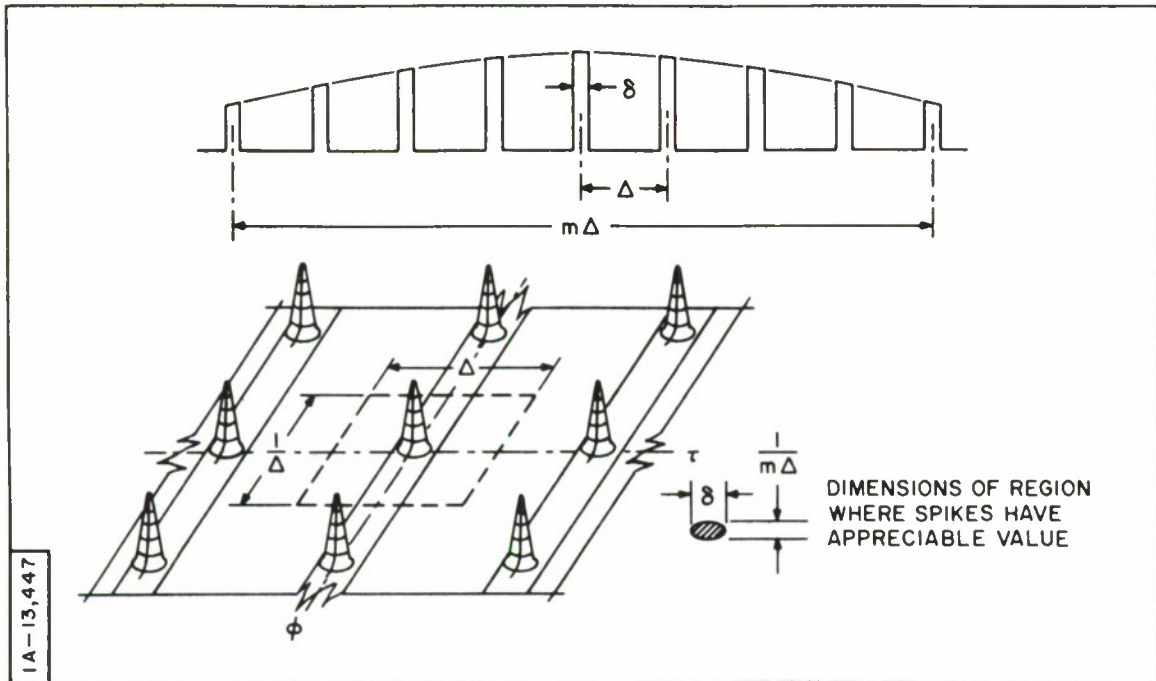


Fig. 2. Sketch of a pulse-train signal and its ambiguity function.

space to fall within the clear space surrounding the central response in Fig. 2. To scale the radar parameters properly, we would set Δ , the interval between pulses in the train, equal to T_T , the time extent of echoes from the multiple targets. Next we select the carrier frequency, f_o , to spread the objects in Doppler frequency sufficiently to fill the dimension $1/\Delta$ in Fig. 2. To do this we would set

$$W_T = \frac{2V_R}{C} f_o \leq \frac{1}{\Delta} \quad , \quad (38)$$

where V_R is the total spread of the multiple-target complex in radial velocity, and C the velocity of light. This would yield for the carrier frequency f_o

$$f_o \leq \frac{C}{2V_R \Delta} \quad (39)$$

The required range and radial-velocity accuracies can be achieved by making δ sufficiently small and $m\Delta$ sufficiently large. The region R in Eq. (36) by the above discussion consists of the space Δ by $1/\Delta$ about the origin in Fig. 2. We can estimate the volume under ψ in R . The volume under the central response is roughly

$$\begin{aligned} \text{volume} &= \text{height at origin} \times \text{area of base} \\ &\cong 1 \times \frac{\delta}{m\Delta} \\ &= \frac{1}{\text{signal time-bandwidth product}} \quad , \end{aligned} \quad (40)$$

and the volume under ψ in R will be of the same order of magnitude. Then the interference is approximately

$$E|e(0, 0)|^2 \cong \frac{\bar{n}b}{(T_T W_T)(T_S W_S)} \quad , \quad (41)$$

where $T_S W_S$ is the signal time-bandwidth product. The interference is thus reduced by a factor $1/T_S W_S$, which can be of the order of 10^{-4} or 10^{-5} when the signal is a properly designed pulse train.

If the requirements of the radar system do not include estimation of both range and Doppler frequency simultaneously, other signal designs may be employed to reduce the volume under ψ inside the target space. For example,

if it is sufficient to detect the targets and measure their range only, then one may choose a signal whose ambiguity function has the shape of a thin ridge oriented in the Doppler direction. The volume under ψ in R may be reduced, by making the ridge extend in Doppler far beyond W_T , the Doppler extent of the target complex. A signal whose ambiguity function has the general shape of a thin ridge oriented in the Doppler direction is the short, constant-frequency pulse. A pulse of length δ has an ambiguity function having a width in the range direction of about δ and an extent in the Doppler direction of about $1/\delta$. The pulse length δ would be chosen so that the ridges corresponding to the objects in the multiple-target complex would not overlap significantly.

If the simple pulse signal is made to have a large duration, the signal ambiguity function assumes the shape of a thin ridge oriented in the range direction. If the duration, δ , is made much greater than T_T , the extent of target echoes in time, the volume under ψ in R , and hence the interference, is reduced. Targets may then be separated by their differences in radial velocity. This is the CW radar case.

Another type of signal which may be useful in multiple-target situations is the large time-bandwidth product, frequency-modulated signal whose frequency variation is uni-directional with time. Such signals tend to have ambiguity functions of the shape of a thin ridge, except in this case the ridge is at an angle to both the time and frequency axes. An example of this type of signal is the so-called "tangent FM" signal described by Key, Fowle, and Haggarty.^[10] Another such FM signal is the familiar linear FM or "chirp" signal described by Cook,^[11] Klauder et al.,^[12] Fowle et al.,^[13] Jacobus,^[14] and others.

In the discussion up to this point we have explicitly assumed that the dense target complex was bounded in time and Doppler frequency. When the target complex extends so far in time and Doppler that it is not practical to

design the signal to cause any of the volume under ψ to lie outside the target space, we have

$$\int_R \int \psi(t, f) dt df \cong (\text{signal energy})^2 = 1 \quad , \quad (42)$$

and N_{\max} becomes

$$N_{\max} \cong \frac{T_T W_T}{\left(\frac{\bar{b}}{b_{\min}}\right) \left(\frac{S}{I}\right)_{\min}} \quad (43)$$

Now it is meaningful to speak of target capacity in terms of a density or target capacity per unit area in range-radial velocity space. To do this we may write for T_T

$$T_T = \frac{R_T}{C} \quad ,$$

and for W_T

$$W_T = \frac{2V}{C} f_o \quad ,$$

where R_T is twice the extent of the target complex in range, V the spread in radial velocity, f_o the radar carrier frequency, and C the velocity of propagation. Then we have N_{\max} per unit area in the range-radial velocity plane given by

$$\frac{N_{\max}}{R_T V} = \frac{2}{C^2} \frac{f_o}{(\bar{b}/b_{\min}) (S/I)_{\min}} \quad (44)$$

The target capacity per unit area may only be increased by increasing the carrier frequency when the target complex is of large extent in range and radial velocity, as shown by Eq. (44).

2.6 Detection of a Target in Clutter*

In the situation that exists when an isolated target is imbedded in clutter at $\tau = \nu = 0$, it is meaningful to speak of the signal-to-interference ratio, S/I

$$\frac{S}{I} = \frac{b}{n\bar{b} \int_{-\infty}^{\infty} \int \psi(t, f) P(t, f) dt df} \quad (45)$$

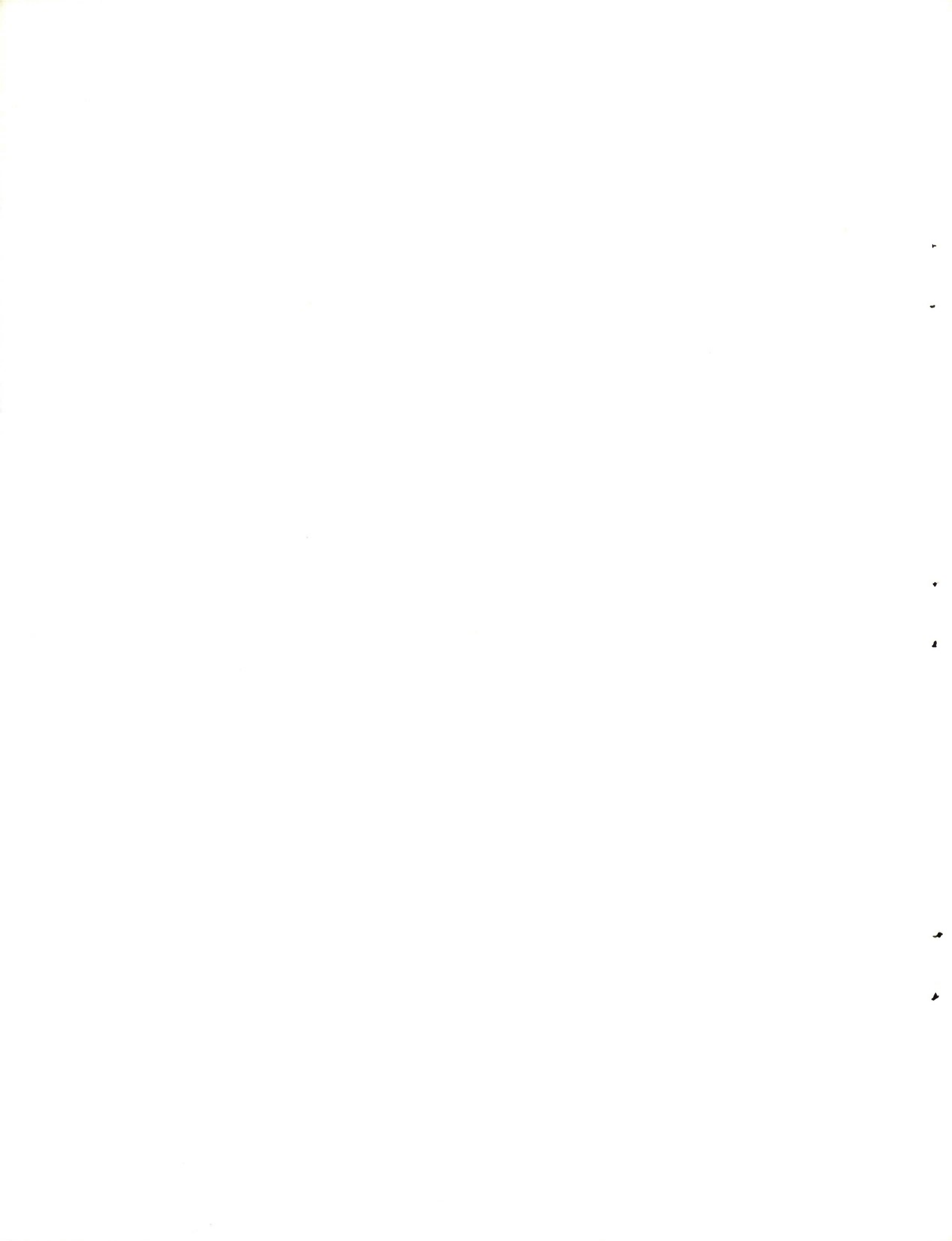
where n is very large and \bar{b} very small so that the product $(n\bar{b})$ is finite.

If the clutter is assumed to be uniformly distributed over time T_c and Doppler frequency shift W_c , the expression for the signal-to-interference ratio becomes

$$\frac{S}{I} = \frac{T_c W_c}{(\sigma/b) \int_R \int \psi(t, f) dt df} \quad (46)$$

* This section follows Fowle, Kelly, and Sheehan, Ref. 8. For a treatment of the problem of the detection of a target in clutter distributed in range only, see Manasse, Ref. 15.

where we have written $\sigma = n\bar{b}$ to signify an "average clutter cross section." The region R now includes the entire clutter space. Quite obviously, all the commentary about the problems of detection in the multiple-target situation apply to the case of a target in clutter. In addition, it is possible that the clutter cross section, σ , may be reduced by appropriate choice of carrier frequency. As previously mentioned, once the interference is lowered to a point where targets of suitably small cross section can be detected, there is little motivation for going farther and exploring the structure of the clutter, even if that could be done. When the clutter is of very great extent in time and Doppler, as in the unbounded multiple-target situation, the only method available for reduction of interference is that of increasing the radar carrier frequency.



3.0 WAVEFORMS

3.1 Introduction

As a preliminary to a discussion of the design of radar waveforms, it is most appropriate to assert that no one waveform is ideal in all operating situations. A particular waveform can be very useful in one situation and less than optimum in another. Hence, in the design of a versatile radar it is conceivable that provision should be made for the transmission, at the option of the operator, of any one of several waveforms.

For example, the radar operator might want to perform with a long-range, high-power radar a sequence of operations somewhat like the following:

- (1) Search a given region of space for targets with potentially large velocity toward or away from the radar; upon detection of an echo, measure coarse range and velocity.
- (2) Following reception of an echo, determine whether the target is single or multiple.
- (3) Measure with increased accuracy the range and radial velocity of the object (or objects).
- (4) Distinguish between genuine signal echoes and bogus echoes.

In the search mode, because of the possible large velocities and correspondingly large Doppler frequency shifts, it is necessary to provide in the radar receiver a bank of matched filters spaced uniformly in frequency over the anticipated Doppler band. Many filters may be necessary in some cases. In the search mode the only important parameter of the signal is the energy it contains (all signals of equal energy received in matched filters give the same probability of detection of isolated targets). The radar operator,

looking for possible distant targets, would thus begrudge a waveform design which made his transmission inefficient. Also, the waveform should be simple. Simple signals generally have simple matched filters, and simple matched filters are desirable when a large number of them must be built, paid for, and maintained. For the search mode a signal consisting of a rectangular burst of constant frequency sinusoid might serve well. With the flat-topped signal the transmitter can be operated in the saturated mode at maximum efficiency.

When an echo is received, the coarse range and radial velocity of the object are measured. To determine whether there is one object or several nearby objects the operator might switch to a different signal — one of large bandwidth with an autocorrelation function having a very narrow central peak and very low sidelobes. In general, echoes somewhat more widely separated in time than the duration of the central part of the autocorrelation function may be resolved, and the lower the sidelobes, the greater the permissible ratio of the cross sections of the resolvable nearby objects. Signal-to-noise ratio is always important, but to answer the question of whether there is one or many objects, ultra-low sidelobes are important, too, and one might use a less efficient signal than that employed in Operation 1 to get the low sidelobes. For example, one might use an amplitude- and phase-modulated signal, say, a linear FM signal with a Gaussian envelope or a simple amplitude-modulated, pulse-burst signal. The former would provide high resolution in range and the latter high resolution in both range and Doppler.

To perform Operation 3, that is, to measure with greater accuracy the range and radial velocity of an object, the operator might transmit a very complicated signal having an ambiguity function of the thumb-tack shape. Such a signal, as we shall see, might have a symmetrical (about the center of the pulse) frequency sweep and more or less constant envelope. The matched filter

for such a signal can be very complex to design, build, and align and, hence, very costly. One would not want to make a filter bank consisting of many such filters. However, one might make, say, three such filters tuned to different frequencies so that their responses overlapped at the minus 1- or minus 2-db points. One could steer the bank of three filters to the approximate frequency of the echo (measured in Operation 1) and refine the measurement of frequency (and hence of radial velocity) by interpolating between the filter outputs and at the same time, refine the measurement of range made in Operation 1.

Finally, the operator, by hypothesis, has the problem of distinguishing between genuine and bogus echoes. There are a number of things the operator could do. For example, he could detect certain kinds of bogus echoes by transmitting several highly structured signals in succession and observing the output of the respective matched filters. If the output waveform did not have the shape of the signal autocorrelation function in each case, the operator should suspect that the echoes were not genuine.

It should be clear, of course, that there are other equally valid signals and procedures for solving the operating problems postulated in the example. The reader can invent his own. The above discussion serves to illustrate, however, the point made earlier that no one signal solves all radar operating problems in an optimum way and that it is not unreasonable in the design of a radar to provide several signals to serve various purposes. In fact, this is frequently done.

In the preceding section we classified signal correlation function (and the related ambiguity function) shapes and gave a discussion which indicated something of the utility of the various shapes in regard to the accuracy of target parameter estimation and to the resolution of multiple targets. It would be pleasant if there were a method of synthesizing a signal to have a

specified two-dimensional correlation function. Sussman [5] and others [16] have studied the general problem of signal correlation function synthesis but have not produced useful general methods. In the last analysis the signal designer must choose a signal, calculate its two-dimensional correlation function, and continue the process until he finds a satisfactory signal whose χ function is also satisfactory for his purpose. In this process he may, of course, be guided by experience.

In this section we will classify signals by type of modulation, that is, whether amplitude modulation, phase modulation, or a combination of the two. We will try to see what kinds of χ -function shapes are possible with the various kinds of modulation in the signal and, where possible, see how to control the χ -function shape, at least over a limited region. For purposes of convenience we will distinguish between "compact" signals (energy concentrated into one time interval) and "distributed" signals. An example of the former is a single rectangular pulse; an example of the latter is a burst of pulses spaced at intervals in time. Compact signals are treated in the first 12 sub-sections, and distributed signals are treated in the 3 sub-sections which follow.

In the discussion which follows we will assume that the signal $s(t)$ is

$$s(t) = u_e(t) \cos [2\pi f_o t + \varphi(t)] , \quad (47)$$

where $u_e(t)$ is called the envelope and $\varphi(t)$ is called the phase modulation. We will assume that narrow band conditions apply and represent $s(t)$ as the real part of $s_c(t)$ where

$$\begin{aligned} s(t) &= R_e \left\{ s_c(t) \right\} \\ &= R_e \left\{ u_e(t) \exp j\varphi(t) \exp j2\pi f_o t \right\} . \end{aligned} \quad (48)$$

We let

$$u(t) = u_e(t) \exp j\varphi(t) \quad . \quad (49)$$

The function $u(t)$ is usually referred to as the complex modulation of the signal. Notice that $u(t)$ completely defines the signal except for the carrier frequency which is, at this point, of no particular concern. For simplicity, then, we shall refer to $u(t)$ as the signal in the material which follows, unless otherwise noted. The Fourier transform of $u(t)$ will be $U(f)$ where

$$U(f) = U_m(f) \exp j\theta(f) \quad . \quad (50)$$

The two-dimensional signal correlation function $\chi(\tau, \nu)$ has the two representations, one in terms of $u(t)$ and the other in terms of $U(f)$ thus:

$$\chi(\tau, \nu) = \int_{-\infty}^{\infty} u(t) \bar{u}(t + \tau) \exp(-j2\pi \nu t) dt \quad (51)$$

$$= \int_{-\infty}^{\infty} \bar{U}(f) U(f + \nu) \exp(-j2\pi f \tau) df \quad . \quad (52)$$

The complex conjugate of $u(t)$ is denoted by $\bar{u}(t)$. Notice that along the τ axis

$$\chi(\tau, 0) = \int_{-\infty}^{\infty} u(t) \bar{u}(t + \tau) dt \quad (53)$$

$$= \int_{-\infty}^{\infty} U_m^2(f) \exp(-j2\pi f \tau) df \quad . \quad (54)$$

The first Eq., (53), shows $\chi(\tau, 0)$ to be the complex signal autocorrelation function, and the second line, Eq. (54), shows $\chi(\tau, 0)$ to be the Fourier transform of the square of the modulus of the signal spectrum. From the latter relation we may deduce that the effective duration of $\chi(\tau, 0)$ is inversely proportional to the bandwidth of the signal. Along the ν axis

$$\chi(0, \nu) = \int_{-\infty}^{\infty} \bar{U}(f) U(f + \nu) df \quad (55)$$

$$= \int_{-\infty}^{\infty} u_e^2(t) \exp(-j2\pi\nu t) dt \quad (56)$$

$\chi(0, \nu)$ is given by the complex autocorrelation of the signal spectrum and, alternatively, by the Fourier transform of the square of the signal envelope, $u_e(t)$. The extent of $\chi(0, \nu)$ is thus inversely proportional to the duration of the signal. It should be noted, however, that the function $\chi(\tau, \nu)$ is not in general determined in the τ, ν plane by its behavior on the τ and ν axes.

3.2 Amplitude-modulated Signals

When the signal is merely amplitude modulated, $u(t) = u_e(t)$, and $\varphi(t) = 0$. $U(f)$ is then determined solely by the envelope, $u_e(t)$. We have for $\chi(\tau, \nu)$

$$\chi(\tau, \nu) = \int_{-\infty}^{\infty} u_e(t) u_e(t + \tau) \exp(-j2\pi\nu t) dt \quad (57)$$

To show how the ambiguity function shape is related to the envelope shape, let us calculate the ambiguity function for two amplitude-modulated signals. First let us consider a signal with a rectangular envelope. We take

$$u_e(t) = \begin{cases} 1, & 0 \leq t \leq T \\ 0, & \text{otherwise} \end{cases}, \quad (58)$$

We substitute Eq. (58) into Eq. (57) and integrate to obtain for $\chi(\tau, \nu)$

$$\chi(\tau, \nu) = \begin{cases} \exp [j\pi\nu(\tau - T)] (T - \tau) \frac{\sin \pi\nu(\tau - T)}{\pi\nu(\tau - T)}, & 0 \leq \tau \leq T \\ \exp [j\pi\nu(\tau + T)] (T + \tau) \frac{\sin \pi\nu(\tau + T)}{\pi\nu(\tau + T)}, & -T \leq \tau \leq 0 \\ 0, & \text{otherwise} \end{cases}, \quad (59)$$

Along the ν axis (that is, $\nu = 0$) we have

$$\chi(\tau, 0) = \begin{cases} T - \tau, & 0 \leq \tau \leq T \\ T + \tau, & -T \leq \tau \leq 0 \\ 0, & \text{otherwise} \end{cases}, \quad (60)$$

and along the τ axis we have

$$\chi(0, \nu) = \exp(-j\pi\nu T) T \frac{\sin \pi\nu T}{\pi\nu T}. \quad (61)$$

The function $|\chi(\tau, \nu)|$ is sketched in Fig. 3. The section of $|\chi|$ along the τ axis is triangular in shape with an extent of $2T$; this section is the auto-correlation function of the envelope $u_e(t)$. In the ν direction the section of $|\chi|$ is the Fourier transform of $u_e^2(t)$. The extent of $|\chi|$ in the τ direction is effectively, T , the reciprocal of the bandwidth of the signal. The extent of $|\chi|$ in the ν direction is effectively the reciprocal of the signal duration.

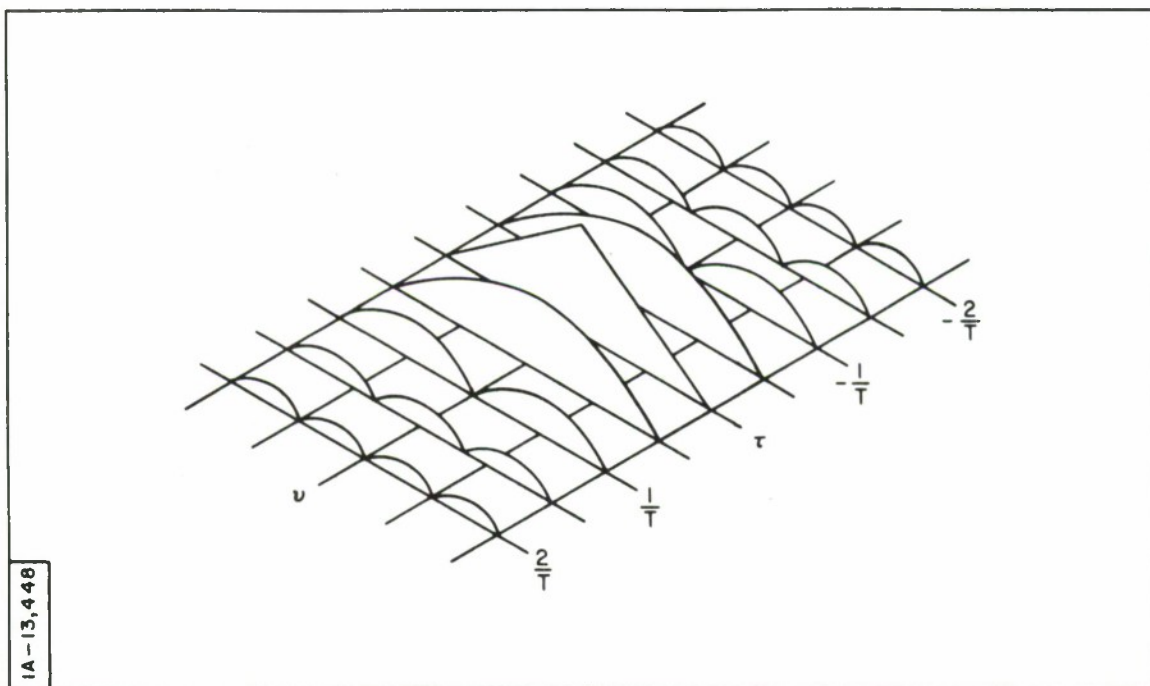


Fig. 3. Sketch of the $|\chi|$ function of a rectangular, constant-frequency signal. Profiles are shown vs. time at intervals of $1/2T$ in Doppler where T is the signal duration. (Taken from Applebaum and Howells, Ref. 7, with permission.)

Next, as a second example, let us consider a signal with a Gaussian envelope. We take

$$u_e(t) = \exp(-t^2) \quad (62)$$

The signal correlation function becomes

$$\chi(\tau, \nu) = \int_{-\infty}^{\infty} \exp(-t^2) \exp-(t + \tau)^2 \exp(-j2\pi \nu t) dt \quad (63)$$

We complete the square in the exponent in Eq. (63) and use the relation

$$\int_{-\infty}^{\infty} \exp\left(-\frac{y^2}{2\sigma^2}\right) dy = \sqrt{2\pi} \sigma \quad (64)$$

to obtain for $\chi(\tau, \nu)$

$$\chi(\tau, \nu) = \sqrt{\frac{\pi}{2}} \exp(j\pi\nu\tau) \exp\left[-\left(\frac{\tau^2}{2} + \frac{\pi^2\nu^2}{2}\right)\right]. \quad (65)$$

Notice that in Eq. (65) sections of $|\chi|$ taken in the τ direction are all Gaussian of constant width between e^{-1} points. The effect of a Doppler shift is to reduce the amplitude of the peak. The signal correlation function of the Gaussian signal is sketched in Fig. 4.

The two examples above serve to illustrate somewhat the extent to which the signal correlation function may be shaped by shaping only the signal envelope, $u_e(t)$. In both of these cases $|\chi|$ has appreciable value over approximately the interval $1/W$ (where W is the bandwidth of the signal) in the τ direction and $1/T$ in the ν direction. In both cases TW is approximately equal to one. The volume under $|\chi|$ is thus largely contained in a unit area centered about the origin of the τ, ν plane, and $|\chi|$ has approximately unit height in this region. The width of $|\chi|$ in the τ direction can be decreased by increasing W (that is, by decreasing T) and target range may thus be measured more accurately in presence of noise. However, decreasing T has the effect of increasing the extent of $|\chi|$ in the ν direction and reducing our ability to measure frequency shift. In the following sections we will show that a combination of amplitude and phase modulation will permit the time-bandwidth

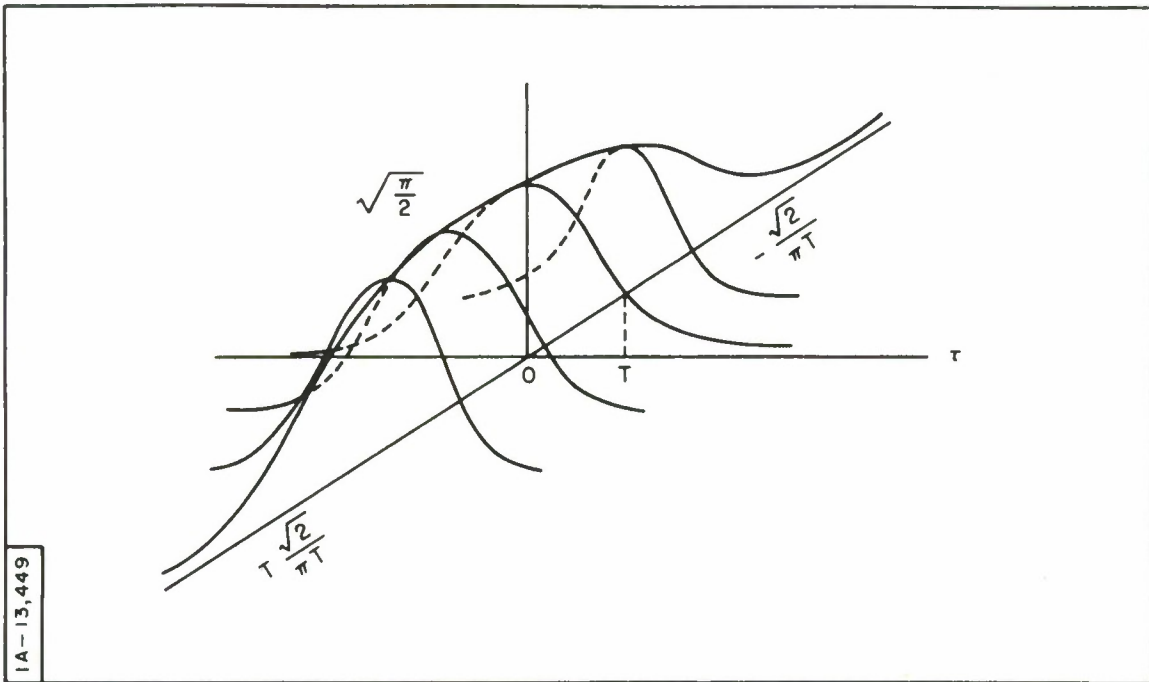


Fig. 4. Sketch of the $|\chi|$ function of a constant-frequency signal with a Gaussian envelope.

product to be much greater than one, and that with a large time-bandwidth product a great deal more control over the shape of $|\chi(\tau, \nu)|$ is possible.

3.3 Phase-modulated Signals

We will say a signal is phase modulated when its structure and that of $\chi(\tau, \nu)$ is largely determined by the phase modulation and is relatively independent of the amplitude modulation. We have seen that the extent of χ on the τ axis is reciprocally related to the signal bandwidth and that the extent on the ν axis depends on the reciprocal of the signal duration. Simple amplitude-modulated signals have time-bandwidth products of approximately one. By phase

modulation we can make the bandwidth much greater than the reciprocal of the duration, and hence, it is possible by phase modulation to make χ narrowly confined in both the τ and ν directions, subject, of course, to the volume constraint on $|\chi|^2$. However, we will see that phase modulation achieved by sweeping the frequency in one direction does not necessarily narrowly confine the peak of χ in the τ, ν plane. To confine χ to an area of $1/W$ by $1/T$ in the τ, ν plane it is necessary that the frequency sweep be symmetrical, that is, down and up or vice versa. But confining χ in the τ and ν directions is not always necessary or desirable. We will see that by sweeping the frequency in one direction we can control the shape of χ in a narrow strip about the τ axis. We will develop a procedure for designing signals to do this and give some examples. Then we will extend our results to see what can be said about phase-modulated signals whose χ -functions are narrowly confined in both the τ and ν directions. We will also consider phase modulation achieved by making step changes in the phase of the signals, and see what kinds of χ functions are associated with this kind of signal.

If the range of expected Doppler frequency shifts is small and if measurement of Doppler frequency is not desired, then a suitable shape for $|\chi(\tau, \nu)|$ would be a narrow ridge perpendicular or nearly perpendicular to the time axis. The ridge should be sharp enough to permit a sufficiently accurate determination of range to be made in the presence of noise, and it should fall away quickly enough in range to make the interference due to echoes from nearby objects small. With $\nu = 0$, the signal correlation function becomes $\chi(\tau, 0)$ which is, of course, the signal autocorrelation function, and the problem of shaping $|\chi(\tau, \nu)|$ in a narrow strip about the τ axis becomes that of designing the signal to have a desirable autocorrelation function.

If the only problem were that of designing a signal whose autocorrelation function were short, the solution would be easy: a simple signal of short duration. But in general the easy solution is not acceptable because the returning signal echo is detected in noise on the basis of the energy it contains, and energy in the echo is proportional to energy in the transmitted signal. To get high energy in a short signal requires high voltages in the transmitter, leading eventually to arcing, etc; frequently it is not possible to get sufficient energy in a short signal, and recourse must be had to long signals whose autocorrelation functions are narrow. The problem of designing a relatively long, rectangular, phase-modulated signal to have an autocorrelation function of short duration and specified shape has been treated, by Key, Fowle, and Haggarty [10] and, independently, by Watters. [17] The solution for the phase modulation when the signal envelope is constrained and of arbitrary shape (that is, non-rectangular) and duration has been given by Fowle. [18] We will first treat the general rectangular signal case and then consider examples to illustrate the design procedures. Then we will discuss an approximation to a smooth frequency sweep: a rectangular signal whose frequency changes by discrete steps at intervals during the signal duration. Next we will discuss rectangular signals with phase modulation obtained by making step changes in the phase at intervals during the signal's duration. Following that, we will return to smooth frequency sweeps and consider the general problem of designing a signal of arbitrary envelope shape to have a specified autocorrelation function, and, finally, we will give an example of an amplitude- and phase-modulated signal.

3.4 Uni-directional FM Signals*

Here our purpose is to consider how to design a signal of rectangular envelope and given duration so that the $|\chi|$ function of the signal will have a specified shape along the τ axis. By controlling the shape of the $|\chi|$ function along the τ axis we will, in fact, shape the $|\chi|$ function in a strip on either side of the τ axis. Such a signal will be useful when the range of expected Doppler shifts is less than the width of the strip. We have for $\chi(\tau, 0)$

$$\chi(\tau, 0) = \int_{-\infty}^{\infty} |U(f)|^2 \exp(-j2\pi f\tau) df \quad (66)$$

Specification of $\chi(\tau, 0)$ determines $U_m(f)$, the modulus of the signal spectrum, thus:

$$U_m(f) = \left[\int_{-\infty}^{\infty} \chi(\tau, 0) \exp(j2\pi f\tau) d\tau \right]^{1/2} \quad (67)$$

At this point we have specified the modulus of the signal (i. e. , that it be rectangular) and the modulus of the Fourier transform of the signal, $U_m(f)$. The question is, what phase functions must be associated with these moduli to make a Fourier pair? We must find an expression for $\Theta(f)$, for example, to make

*Early work in FM signal design is described in the patents of Sproule and Hughes in England, [19] Dicke [20] and Darlington [21] in the U. S. , and Cauer in Germany. [22] The material in this section is based upon Key et al. [10] Watters, [17] and Fowle. [18]

$$\left| \int_{-\infty}^{\infty} U_m(f) \exp j\Theta(f) \exp (j2\pi ft) df \right| = |u(t)|, \quad (68)$$

where $|u(t)| = \text{constant}$ during the signal duration. Eq. (68) is an integral equation of an unusual kind; it is not clear how the solution for $\Theta(f)$ should proceed. The problem is further complicated by the fact that an exact solution for $\Theta(f)$ does not, in general, exist, because the moduli of a Fourier pair may not be arbitrarily specified. Worse still, a concise set of necessary and sufficient conditions on two functions to be the moduli of a Fourier pair does not exist. How then are we to proceed to solve the problem we have formulated?

Fortunately there is a way. An approximate expression for $\Theta(f)$ in terms of the specified moduli may be gotten from Eq. (68) by the method of stationary phase. As we will see, the approximate expression for $\Theta(f)$ together with the initially specified $U_m(f)$ will satisfy Eq. (68) with good accuracy under certain circumstances even for modest signal time-bandwidth products.

To begin the approximate solution for $\Theta(f)$, we write for $u(t)$

$$u(t) = \int_{-\infty}^{\infty} U_m(f) \exp j\Theta(f) \exp (j2\pi ft) df \quad (69)$$

According to the principle of stationary phase,* the integral of an oscillatory function, such as Eq. (68) above, has little value except in the vicinity of points where the phase is "stationary" or where the derivative of the phase is zero. The phase in Eq. (68) is $\beta(f)$ where $\beta(f) = 2\pi ft + \Theta(f)$, and the derivative, $\beta'(f)$, is

* For a discussion of the method of stationary phase, see Sneddon, Ref. 23.

$$\beta'(f) = 2\pi t + \Theta'(f) \quad (70)$$

where the prime denotes differentiation with respect to f . The phase is stationary at the point $f = \lambda$, which makes $\beta'(f) = 0$. Then we have

$$\Theta'(\lambda) = -2\pi t \quad (71)$$

In the stationary phase method, $\beta(f)$ is expanded in a Taylor's series about the stationary point, λ , and terms of higher degree than second are dropped. The resulting equation can be integrated to give the following approximate expression for $u(t)$:

$$u(t) \cong \sqrt{2\pi} \frac{U_m(\lambda)}{\sqrt{|\Theta''(\lambda)|}} \exp j [2\pi\lambda t + \Theta(\lambda) \pm \pi/4] \quad (72)$$

where the $+$ sign is taken in the exponent for $\Theta''(\lambda) > 0$ and $-$ for $\Theta''(\lambda) < 0$. Equation (72) above assumes that only one stationary point exists at time t , and this is adequate for our purpose. We note that $u_e(t)$ and $\phi(t)$ are given approximately by

$$u_e(t) \cong \sqrt{2\pi} \frac{U_m(\lambda)}{\sqrt{|\Theta''(\lambda)|}} \quad (73)$$

and

$$\phi(t) \cong 2\pi\lambda t + \Theta(\lambda) \pm \pi/4 \quad (74)$$

The trouble with the solutions for $u_e(t)$ and $\phi(t)$ above is that they are functions of the variable λ , and λ is, as yet, an unknown function of t , given in Eq. (71). In the special case which is of interest here, $u_e(t)$ is required to be constant. With $u_e(t)$ constant, Eq. (73) becomes

$$\Theta''(\lambda) = k U_m^2(\lambda) \quad , \quad (75)$$

and the phase, $\Theta(f)$, is given by two integrations of Eq. (75) with $\lambda = f$. We get

$$\Theta(f) = k \int_{-\infty}^f \int_{-\infty}^x U_m^2(y) dy dx \quad . \quad (76)$$

By definition, the group time delay $T(f) = -\Theta'(f)/2\pi$; we differentiate Eq. (76) to obtain for $T(f)$

$$T(f) = k_1 \int_{-\infty}^f U_m^2(x) dx \quad , \quad (77)$$

where k_1 is a constant.

Up to this point, we have obtained the following result: If we associate with an arbitrary spectral modulus a group delay proportional to the integral of the square of the modulus, we then have the Fourier transform of a function that has an approximately constant envelope. In other words, we have the result that

$$\int_{-\infty}^{\infty} U_m(f) \exp \left[jk \int_{-\infty}^f \int_{-\infty}^x U_m^2(y) dy dx \right] \exp (j2\pi f t) df \quad (78)$$

$$\cong \begin{cases} A \exp j\varphi(t), & \text{for } t \text{ such that a} \\ & \text{stationary point exists,} \\ 0, & \text{elsewhere,} \end{cases}$$

where A is a constant. We have the final question to answer: What is the phase modulation, $\varphi(t)$? To get an approximate expression for $\varphi(t)$, we differentiate Eq. (74) with respect to t . We get

$$\varphi'(t) \cong 2\pi\lambda + \left[2\pi t + \frac{d\Theta(\lambda)}{d\lambda} \right] \frac{d\lambda}{dt} \quad (79)$$

The term in brackets in Eq. (79) is zero by Eq. (71). Then we have

$$\varphi'(t) \cong 2\pi\lambda \quad (80)$$

If we define the instantaneous frequency $f(t) = \varphi'(t)/2\pi$, Eq. (80) becomes

$$f(t) \cong \lambda \quad (81)$$

The instantaneous frequency at time t is thus given approximately by λ , the frequency which makes the integrand in Eq. (69) stationary. Another relation between λ and t can be gotten from Eq. (71). We have

$$t = - \frac{\Theta'(\lambda)}{2\pi} . \quad (82)$$

But $-\Theta'(\lambda)/2\pi$ is, according to the discussion above, the group time delay, $T(\lambda)$, and Eq. (82) becomes

$$t = T(\lambda) . \quad (83)$$

If we use Eq. (83) in Eq. (81), we get

$$f [T(\lambda)] \cong \lambda , \quad (84)$$

which shows that instantaneous frequency and group time delay are approximately inverse functions. That is, we have

$$T(\lambda) = f^{-1}(\lambda) , \quad (85a)$$

and, in addition

$$f(t) = T^{-1}(t) . \quad (85b)$$

Using Eq. (85b) we can write for $\varphi'(t)$

$$\varphi'(t) = 2\pi T^{-1}(t) . \quad (86)$$

We integrate Eq. (86) to get for $\varphi(t)$

$$\varphi(t) = 2\pi \int_{-\infty}^t T^{-1}(x) dx . \quad (87)$$

$\varphi(t)$ in Eq. (87) is given by the integral of the inverse of the group delay, $T(f)$, which depends only on the spectral modulus $U_m(f)$ and upon the fact that the envelope $U_e(t)$ is required to be constant.

Let us now summarize the procedure that we have given for the design of unidirectional FM signals. The problem is to design a constant amplitude signal to have a specified duration and an autocorrelation function of specified shape and duration. Specification of the autocorrelation function determines the modulus of the signal spectrum. We then associate with the modulus of the signal spectrum a group time delay characteristic proportional to the integral of the squared spectral modulus to obtain the approximate transform of a constant amplitude signal. Because $U_m^2(f)$ is non-negative, the group delay, Eq. (77) will either monotonically increase or decrease with frequency, depending on the sign of k_1 . Since the instantaneous frequency and group time delay are approximately inverse by Eq. (85), the instantaneous frequency will be a monotonic function of time. A little thought will show that if the group delay increases with increasing frequency, the instantaneous frequency will increase with time and vice versa. In the two sections which follow we will consider signal design examples that will illustrate the ideas we have developed in this section.

3.5 The Rectangular Linear FM Signal

We will consider the linear FM signal for two reasons. First, it illustrates in the simplest way the FM signal design ideas we have developed and second, the linear FM signal is a widely used and useful radar signal. To put the linear FM ideas in terms which fit our development, let us suppose that we want a rectangular signal whose χ function along the τ axis has the following form,

$$\chi(\tau, 0) = \frac{1}{T_1} \frac{\sin \pi t/T_1}{\pi t/T_1} \quad (88)$$

The effective duration of the signal autocorrelation function above is T_1 . We set $T_1 = 1/W$. The Fourier transform of $\chi(\tau, 0)$ is $U_m^2(f)$. We perform the transformation and obtain for $U_m^2(f)$

$$U_m^2(f) = \begin{cases} 1, & -\frac{W}{2} < f < \frac{W}{2} \\ 0, & \text{otherwise} \end{cases} \quad (89)$$

The modulus of the signal spectrum, $U_m(f)$, is

$$U_m(f) = \begin{cases} 1, & -\frac{W}{2} < f < \frac{W}{2} \\ 0, & \text{otherwise} \end{cases} \quad (90)$$

We find the group delay $T(f)$ required, with $U_m(f)$ [Eq. (90)], to make the Fourier transform of a rectangular signal by means of Eq. (77). We have two choices, one corresponding to a frequency sweep whose frequency increases with time, the second to a frequency which decreases with time. To find the former, we set

$$\begin{aligned} T(f) &= K \int_{-W/2}^f df \\ &= K(f + \frac{W}{2}) \quad , \quad -\frac{W}{2} < f < \frac{W}{2} \end{aligned} \quad (91)$$

We find K by requiring that the signal have duration T_2 where $T_2 \gg T_1$. The signal duration is given approximately by the range of delay through which $T(f)$ varies. Hence we set

$$T\left(\frac{W}{2}\right) = T_2 \quad , \quad (92)$$

and find that

$$K = \frac{T_2}{W} \quad . \quad (93)$$

Hence

$$T(f) = \begin{cases} \frac{T_2}{W} \left(f + \frac{W}{2} \right) , & -\frac{W}{2} < f < \frac{W}{2} \\ 0 , & \text{otherwise} \end{cases} \quad . \quad (94)$$

We can find the instantaneous frequency vs. time by use of Eq. (83) which says

$$t = T(\lambda) \quad , \quad (95)$$

where λ , by Eq. (81), is the instantaneous frequency. We set

$$t = \frac{T_2}{W} \left(\lambda + \frac{W}{2} \right) \quad (96)$$

and solve for λ . We find that

$$\lambda = \begin{cases} W \left(\frac{t}{T_2} - \frac{1}{2} \right) , & 0 < t < T_2 \\ 0 , & \text{otherwise} \end{cases} \quad . \quad (97)$$

It is apparent in Eq. (97) that the instantaneous frequency increases with time from $-W/2$ to $+W/2$.

In order to find the second solution for $T(f)$ we re-write Eq. (77), changing the limits of integration thus,

$$T(f) = K \int_f^{W/2} df \quad , \quad (98)$$

and require that $T(-W/2) = T_2$. We obtain for $T(f)$

$$T(f) = \begin{cases} \frac{T_2}{W} \left(\frac{W}{2} - f \right) \quad , & -\frac{W}{2} < f < \frac{W}{2} \\ 0 \quad , & \text{otherwise} \end{cases} \quad (99)$$

We find the frequency vs. time, λ , corresponding to $T(f)$ in Eq. (99), to be

$$\lambda = \begin{cases} W \left(\frac{1}{2} - \frac{t}{T_2} \right) \quad , & 0 < t < T_2 \\ 0 \quad , & \text{otherwise} \end{cases} \quad (100)$$

which shows that the frequency decreases with time from $+W/2$ to $-W/2$.

It is well to note here that we have been trying to design a band-limited signal to be time limited as well. Paley and Wiener show that it is impossible for a function to be both time limited and band limited.* As the

* See Theorem 10 of Paley and Wiener, Ref. 24.

time-bandwidth product of the signal increases, however, the above restriction appears to lose force, and a better and better approximation to a time-limited signal is possible. Klauder et al.^[12] calculate the envelope of a signal whose spectrum has a rectangular modulus and linear group delay. Their results are given in Fig. 5 for several TW products. For $TW \cong 10$, the envelope is not very rectangular. For $TW \cong 60$ the approximation is better; finally for $TW \cong 120$, the approximation is fairly good. As the TW product increases, the envelope will become more and more nearly rectangular although, of course, never exactly rectangular. For modest TW products it can be shown that the frequency vs. time is quite linear except near the ends of the pulse, and that the fraction of the pulse over which the frequency is approximately linear increases as the TW product increases.

The linear FM signal can be generated in a number of ways. The most common way is to apply an impulse (i. e. , a short pulse) to a composite filter with a frequency response that has an approximately rectangular modulus and a group delay that is linear with frequency. The signal can also be generated by sweeping an oscillator in frequency at a uniform rate and holding the amplitude constant. In the latter case it is the spectrum that has the ripple and is only approximately rectangular. We will say more about the techniques that are available to generate and receive signals in Section 4. 0.

In Fig. 6 we show schematically a radar which employs a matched filter receiver. The transmitter is represented as an equivalent linear filter whose impulse response is the linear FM signal. The system operates in the following way. The impulse response of the transmitter bandpass filter in Fig. 6 is a $\sin \pi Wt/\pi Wt$ waveform of duration $T_1 = 1/W$. The $\sin \pi Wt/\pi Wt$ pulse is dispersed in the all-pass filter in a manner which, according to the previous discussion, gives a waveform of nearly constant amplitude with

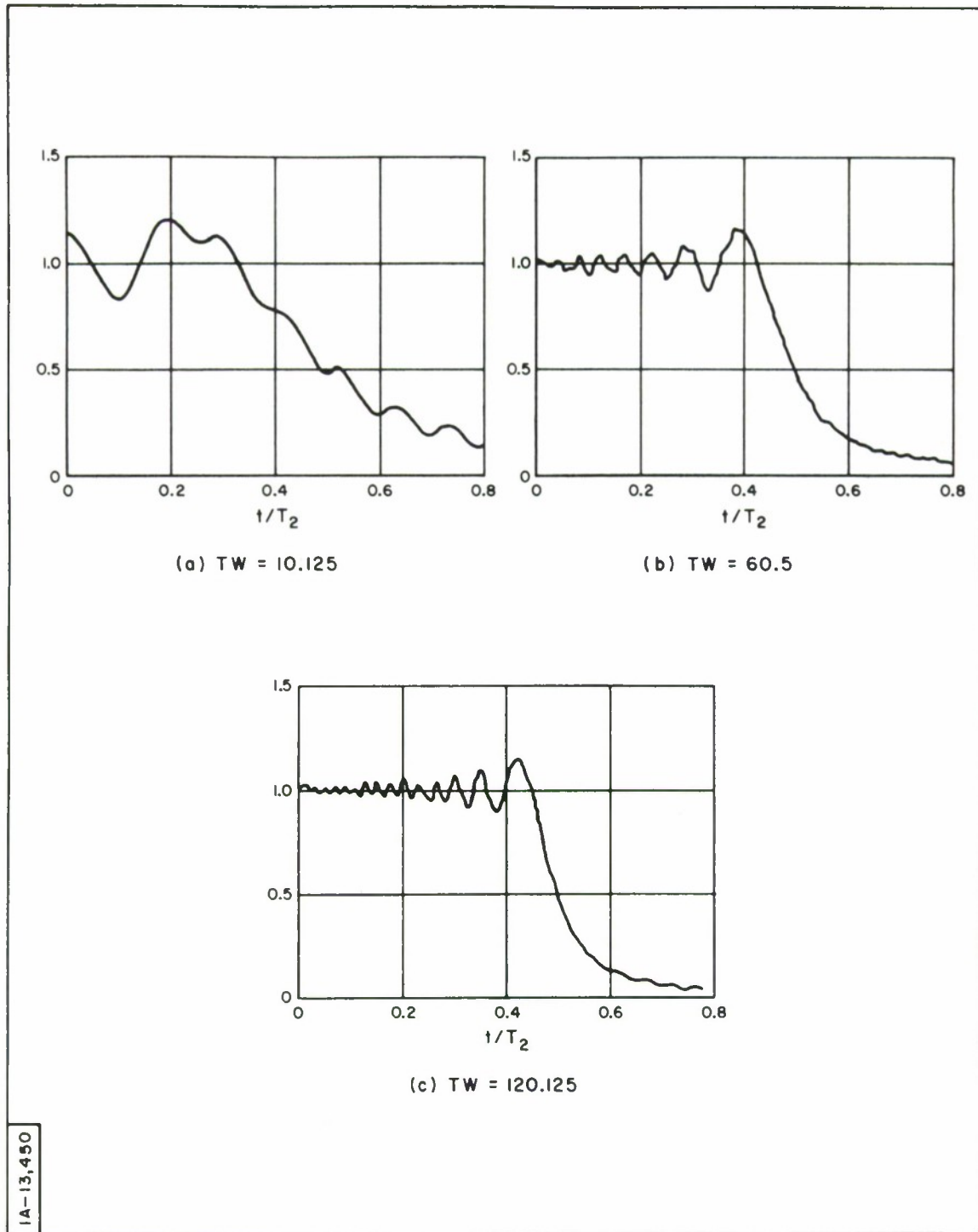


Fig. 5 Envelope of a signal with a Fourier transform that has a rectangular modulus and quadratic phase for (a) $TW = 10$, (b) $TW = 60$, and (c) $TW = 120$. (Taken from Klauder et al, Ref. 12, with permission.)

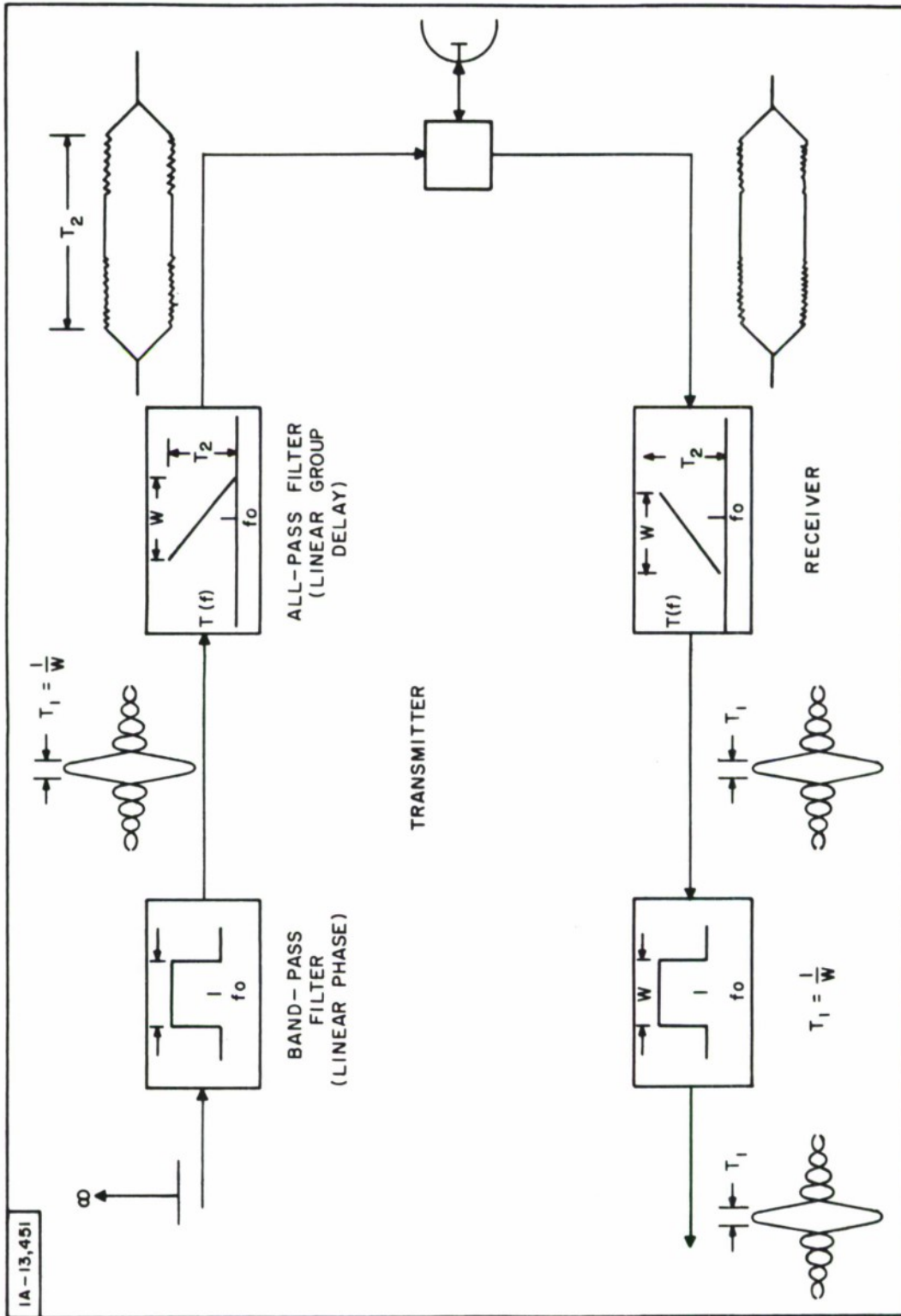


Fig. 6 Block diagram of a linear FM pulse compression system.

duration T_2 . The ratio of the duration of the waveforms is $T_2/T_1 = TW$, the time-bandwidth product. The dispersed waveform, which we call the signal, is transmitted. A replica of the signal, attenuated and delayed, is presented to the receiver. The receiver, in this case a matched filter, is shown as an equivalent linear filter whose impulse response is the signal inverted in time. The dispersed signal echo is compressed in the receiver all-pass filter, the output waveform of which is again $\sin \pi Wt/\pi Wt$. The signal then passes, in this case without change in shape, through the bandpass filter to the receiver output terminal.

When the echo returns with a Doppler frequency shift (due to reflection from an object moving radially with respect to the radar), we have the situation in the receiver illustrated in Fig. 7. In Fig. 7(a) the receiver frequency response is shown centered at f_0 . The signal spectrum is shown shifted up in frequency from f_0 by f_d , the Doppler shift. The moduli of the frequency functions of the signal and the receiver multiply and the group delay characteristics add, to give the modulus and group delay, respectively, of the receiver output waveform [Fig. 7(b)]. The effect of the Doppler shift is two-fold. First, the bandwidth of the output waveform is reduced and its duration correspondingly increased, and second, the signal appears at the output terminals advanced in time by ΔT which is proportional to f_d . When the Doppler shift is negative, the signal is delayed in time by ΔT . As the output waveform broadens because of Doppler shift in the signal, the resolving power of the radar (the ability to make echoes from nearby objects distinct or non-overlapping) decreases. The time shift which results from the Doppler shift causes an error to be made in the estimate of the range to the target. But, regardless of Doppler shift, the group delay of the waveform at the receiver output is constant (non-dispersive) and the output waveform thus is free of phase modulation.

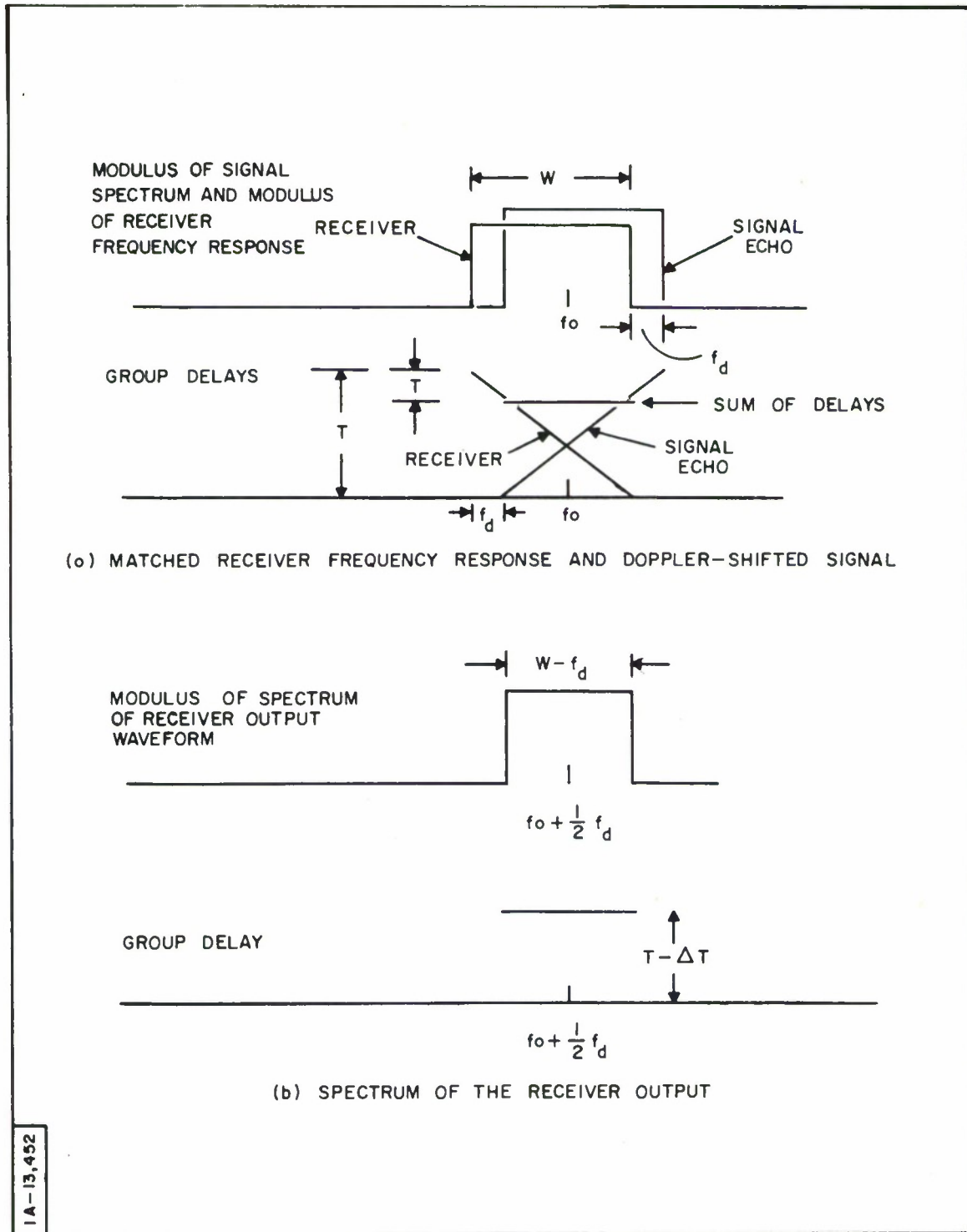


Fig. 7 Effect of Doppler frequency shift on linear FM pulse compression system.

Fig. 8 shows a model of the two-dimensional correlation function, $|\chi(\tau, \nu)|$, corresponding to a signal of rectangular envelope and exactly linear instantaneous frequency. The TW product of the signal is 10. The profiles in Fig. 8 are taken vs. time at intervals in Doppler equal to one-tenth of the signal bandwidth. The profile with the tallest peak is the envelope of the signal autocorrelation function; the peak occurs at the origin of the τ, ν plane. The most significant feature of the function is the ridge which runs at an angle to the time and Doppler axes. Elsewhere in the plane the function is low.

We might consider how the linear FM signal could be used. The duration of the signal we will assume will be determined by the energy requirements for detection and the available transmitter peak power. The bandwidth of the signal should be large enough to give the desired resolution in range. The duration of the signal at the receiver output in Fig. 6 is approximately T_1 , and $T_1 = 1/W$, where W is the bandwidth. To resolve echoes which are separated by an interval in time equal to T_1 , a bandwidth of at least W is required. It is possible, depending on the parameters of the radar, that the error in the estimate of range caused by Doppler shifts is negligible. For example, the error in the estimate of time of arrival, ΔT , of a Doppler shifted signal can be shown to be

$$\Delta T = f_d \frac{T}{W} , \quad (101)$$

where f_d is the Doppler shift, T the signal duration and W the signal bandwidth. The Doppler shift $f_d = 2v_R f_o/c$ where v_R is the radial velocity of the target, f_o the radar operating frequency, and C the speed of light. If the radar transmitting at 400 Mcps a 100 μ sec signal of 1 Mc bandwidth looks at an airplane traveling at 600 miles/hr toward the radar, the resulting error

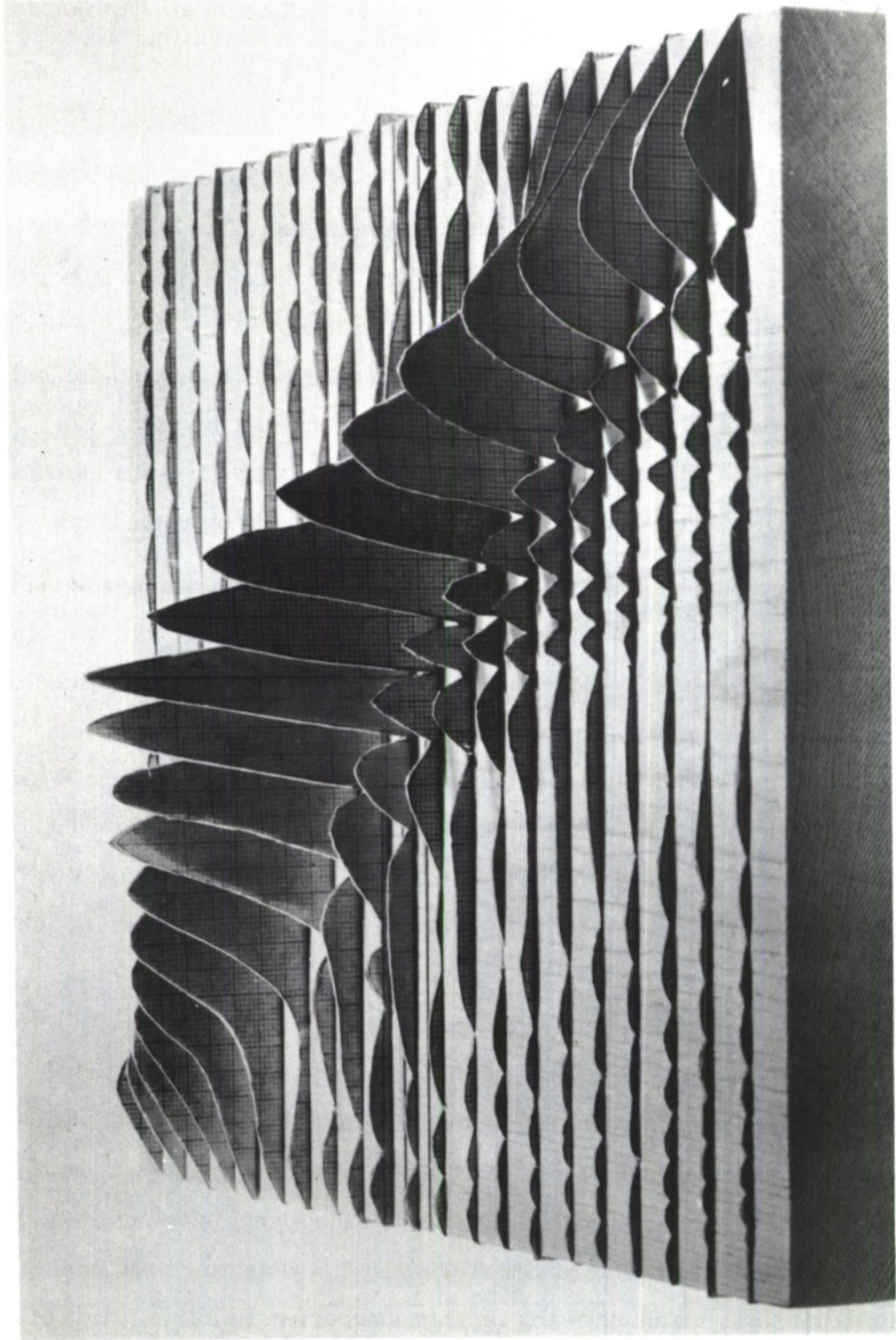


Fig. 8 $|x|$ function of a signal with a rectangular envelope and linear frequency sweep. $TW = 10$. Profiles are vs. time at intervals in Doppler of one-tenth of the signal bandwidth. (Photo courtesy of C.E. Cook, Sperry-Rand Corporation.)

in the estimate of range will be of the order of 40 feet, in all likelihood a negligible error.

However, the same radar measuring the range to a satellite traveling toward it at 4 miles/sec would be in error by about 970 feet, and 970 feet might not be negligible. What can be done to eliminate the error? One thing that could be done would be to measure the range to the target on a number of successive pulses, and from the measured values of range compute the range rate or velocity of the target. With range rate known, one could compute the Doppler shift and correct the measured values of range by use of Eq. (101). In addition, one could reduce the range error caused by Doppler shift to a negligible value by making the signal bandwidth W sufficiently large.

One disadvantage of the linear FM signal is the shape of the autocorrelation function of the signal. When it is desired to resolve two echoes close together in time, it is desirable to use a signal that has an autocorrelation function that falls off rapidly and smoothly from its peak. In this way the receiver response due to one signal may fall to a low value before the response to a nearby echo occurs, and the resolving power of the radar is enhanced. The autocorrelation function of the linear FM signal falls off as $1/t$ (which is not very fast) and it is oscillatory, which is to say that it has sidelobes. In most applications it is desirable to suppress the sidelobes, while at the same time preserving the rectangular signal shape and its approximately linear frequency sweep. The sidelobes of the autocorrelation function arise, of course, because of the rectangular shape of the signal spectrum. The usual method of suppressing the sidelobes is to weight or taper the frequency characteristic of the receiver, leaving the shape of the signal spectrum, and hence the signal envelope, rectangular. The spectrum weighting problem here is exactly the same mathematically as that of tapering the illumination of an

antenna to reduce sidelobes, a problem treated by Taylor^[25] and others.

Figure 9 shows: (a) the unweighted spectrum of the receiver output and (b) the associated $\sin \pi Wt/\pi Wt$ time function, and (c) the general shape of the spectrum after weighting and (d) the associated time function. Notice that the effect of tapering is to broaden the output waveform, usually by a factor of about two. The weighted receiver is, of course, no longer a matched filter to the signal, and a loss in the detection capability of the system results. This loss is usually about 1 to 1-1/2 db, and in many cases is not serious. The reader is referred to the paper by Klauder et al^[12] for a thorough discussion of the details of the problem of suppressing the sidelobes of the autocorrelation function of the rectangular linear FM signal.

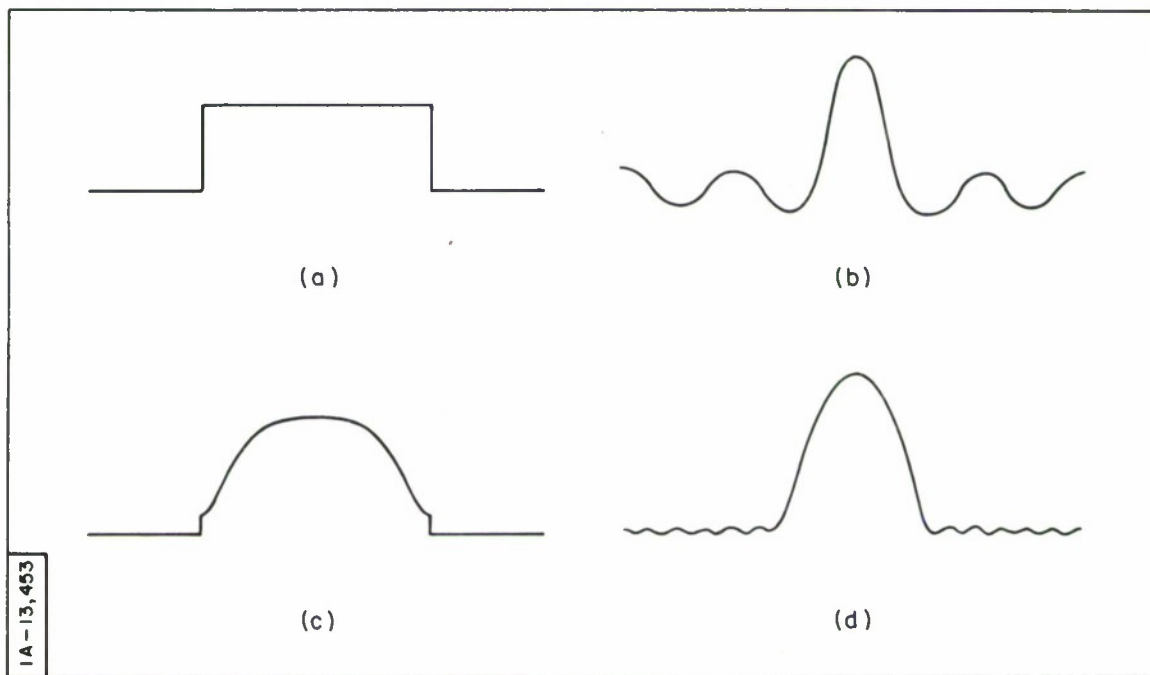


Fig. 9 Sketches to show (a) spectrum of receiver output before weighting, (b) receiver output waveform before weighting, (c) spectrum of receiver output waveform after weighting, (d) receiver output waveform after weighting.

3.6 A Rectangular Non-linear FM Signal*

Earlier in this section we gave a method for the design of rectangular, phase-modulated signals of large time-bandwidth product to have a specified autocorrelation function. In the preceding section we applied these ideas to design a rectangular signal of large TW product whose autocorrelation function was of the form $\sin \pi W\tau / \pi W\tau$. In most applications it is desirable to have a signal whose autocorrelation function has sidelobes of low rms value (so that the sidelobes of echoes from many nearby targets will not build up and obscure echoes from objects of small cross section) and whose peak sidelobes are low (to avoid ambiguities; i. e., is it a sidelobe or a second nearby target?). The objectionable sidelobes of the linear FM autocorrelation function are usually suppressed by mismatching the receiver at some loss in detection.

As a second example of the procedure, let us design a signal to have an exponential autocorrelation function. The exponential shape falls off smoothly (i. e., does not oscillate and cause ambiguities) and with adequate bandwidth can be made to fall off rapidly. With such a signal the receiver can be an ideal matched filter, because no mismatching, with the attendant losses in detection, is necessary. For the envelope of the autocorrelation function we take

$$\chi(\tau, 0) = \exp \left\{ -2\pi W |\tau| \right\} \quad . \quad (102)$$

The duration of $\chi(\tau, 0)$ between e^{-1} points is $T_1 = 1/\pi W$. We take the Fourier transform of $\chi(\tau, 0)$ above to get $U_m^2(f)$, the square of the signal spectrum. We obtain

* The example in this section is taken from Key et al., Ref. 10.

$$U_m^2(f) = \frac{1}{\pi W} \frac{1}{1 + \left(\frac{f}{W}\right)^2} \quad (103)$$

To be the Fourier transform of a rectangular signal, the modulus $U_m(f)$ must be associated with a group delay characteristic proportional to the integral of $U_m^2(f)$ as shown by Eq. (77). As in the previous example, there are two possibilities: one corresponds to a signal whose frequency increases with time, the other corresponds to a signal whose frequency decreases with time. To obtain the group delay corresponding to the former signal we write

$$T(f) = k \int_{-\infty}^f U_m^2(f) df \quad , \quad (104)$$

which yields, using Eq. (103),

$$T(f) = \frac{k}{\pi} \left[\frac{\pi}{2} + \tan^{-1} \frac{f}{W} \right] \quad (105)$$

We find k by setting $T(\infty) = T$, the desired pulse length, and obtain $k = T$. The frequency vs. time, λ , is obtained from Eq. (105) by use of Eq. (95), here repeated as Eq. (106):

$$t = T(\lambda) \quad (106)$$

We obtain for λ

$$\lambda = W \tan \frac{\pi}{T} \left(t - \frac{T}{2} \right) \quad (107)$$

The signal autocorrelation function, its spectrum and group delay, envelope, and frequency vs. time are all illustrated in Fig. 10. The amplitude of the envelope is found by use of Parseval's law, which requires that

$$\int_{-\infty}^{\infty} U_m^2(f) df = \int_{-\infty}^{\infty} u_e^2(t) dt \quad (108)$$

We obtain

$$u_e(t) = \begin{cases} \frac{1}{\sqrt{T}} & , \quad 0 < t < T \\ 0 & , \quad \text{otherwise} \end{cases} \quad (109)$$

We should emphasize, of course, that the procedure we have followed is approximate. For a suitably large time-bandwidth product (here the time-bandwidth product may be taken, again, as TW) the Fourier transform of the spectral modulus, the square root of Eq. (103) together with the group delay, Eq. (105), should have a rectangular envelope and the instantaneous frequency given by Eq. (107). Key et al. [10] have by numerical integration determined the Fourier transform of the modulus and group delay cited above. Their results are shown in Fig. 11. For $TW = 5/\pi$ in Fig. 11 (a), the envelope is within about ± 4 percent of being constant. For $TW = 50/\pi$ [Fig. 11 (b)], the envelope is constant to within the limits of accuracy of the numerical calculation (about 0.25 %). In this example, where the signal spectrum is a smooth, continuous function, the method of signal design we have outlined yields good results for TW products of the order of 10.

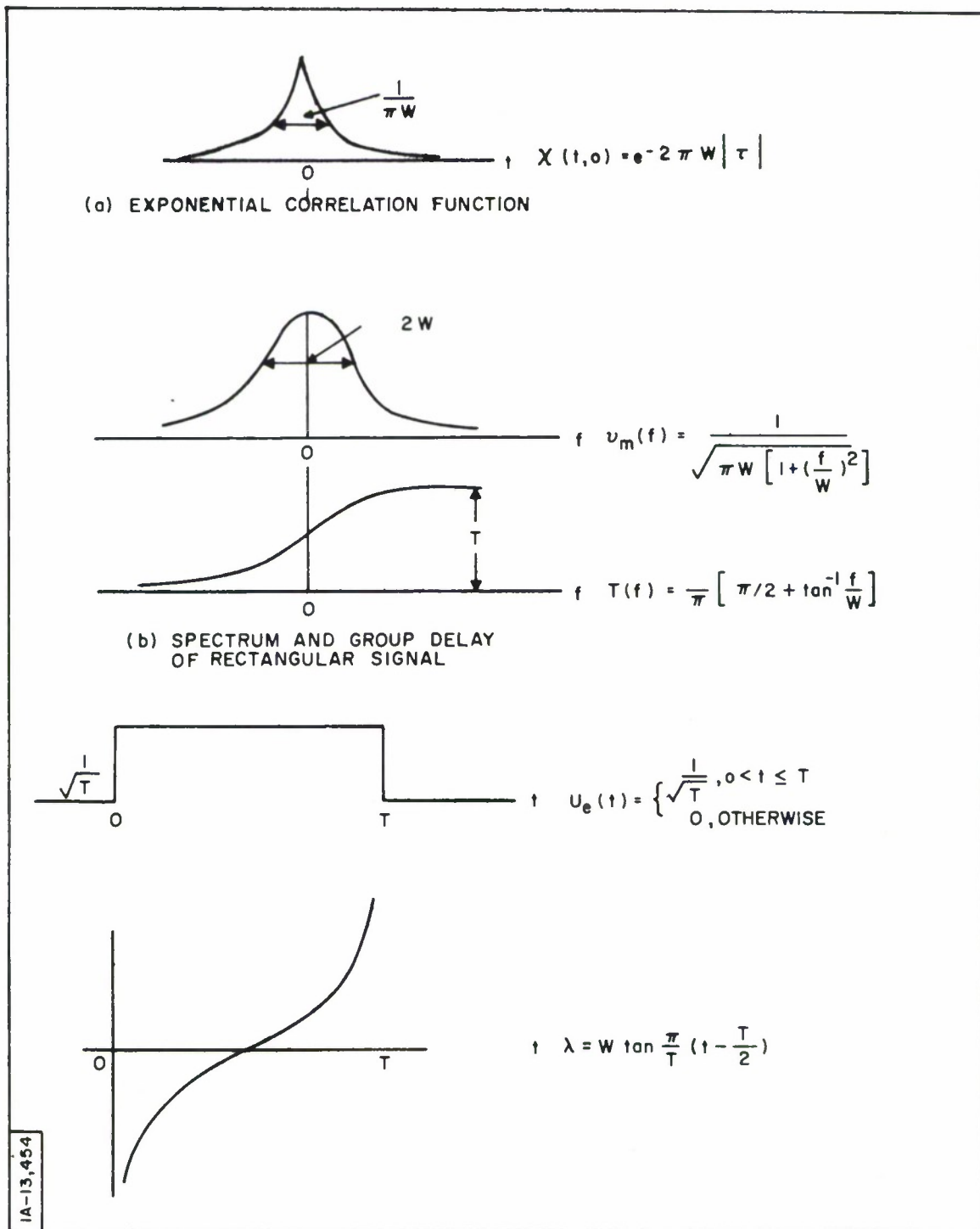


Fig. 10 The tangent FM signal.

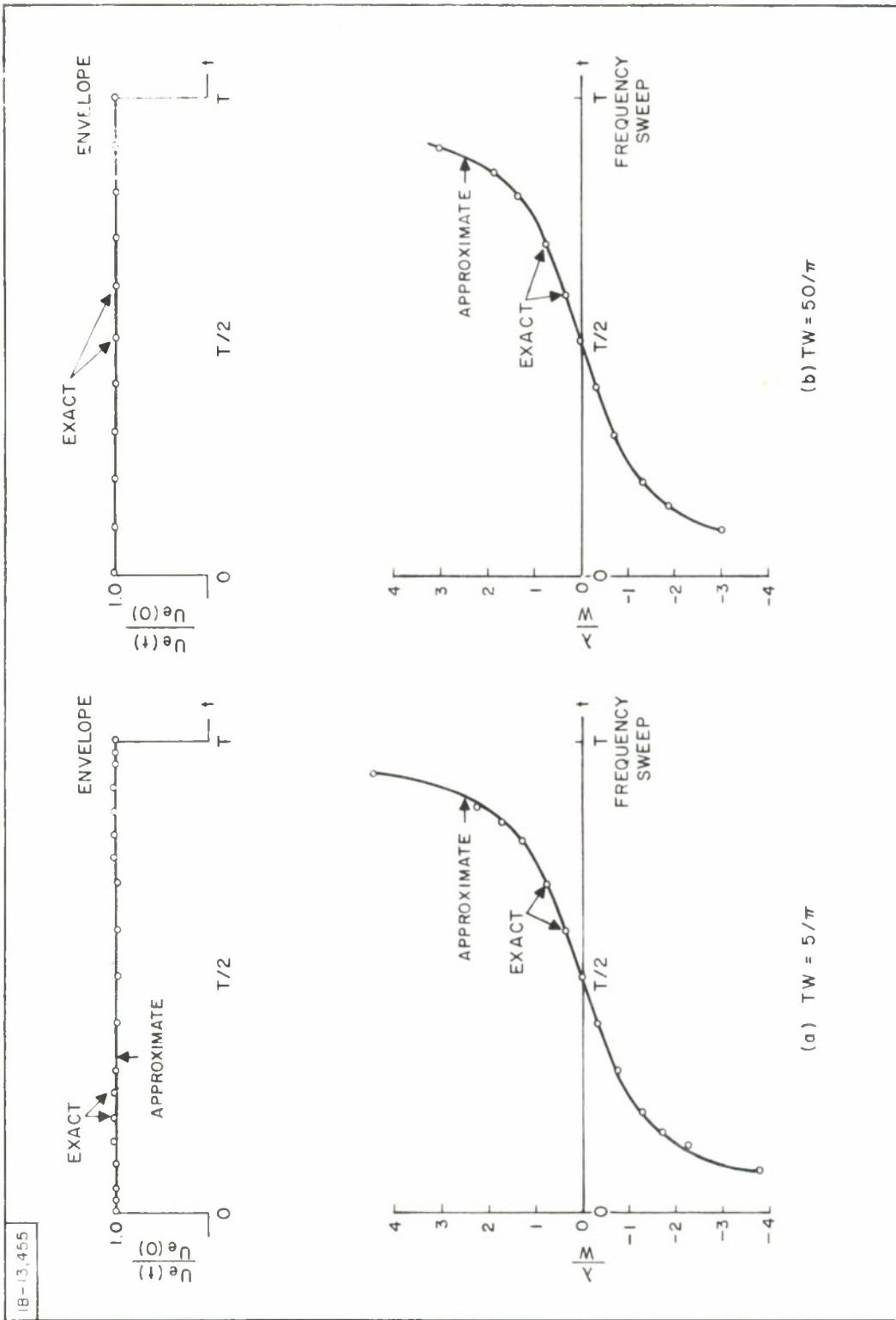


Fig. 11 Comparison of approximate and exact signal envelope and frequency sweep of non-linear FM signal for (a) $TW = 5/\pi$, and (b) $TW = 50/\pi$.

As in the case of the linear FM signal considered previously, the signal can be generated in a linear fashion by applying an impulse to a linear filter or by sweeping properly the frequency of an oscillator.

In this example the signal and receiver have non-linear group delay characteristics. The non-linear group delay permits the signal spectrum and hence the autocorrelation function to be of controlled shape while the signal has rectangular shape for efficient transmission. The receiver is exactly matched to the signal, and the maximum detection capability is obtained. The group delay characteristic of the receiver output is constant only for zero Doppler shift; when the signal is Doppler shifted, the delay of the receiver output becomes dispersive and hence, in general, the peak of the receiver output will fall off more rapidly with Doppler shift than it does with the linear FM signal.

The modulus of the two-dimensional signal correlation function of the tangent FM signal is shown in Fig. 12. Notice that $|\chi(\tau, \nu)|$ is sharply peaked at the origin. With the sharp peak, there is some possibility of locating the signal in time and Doppler frequency and hence, of measuring both parameters with a single pulse. (This was not possible with the linear FM signal.) We will later get some insight into the problem of designing frequency-modulated signals to have sharply peaked two-dimensional correlation functions; we will see then that non-linear frequency sweeps (or non-linear group delay characteristics) are required.

3.7 The Rectangular, Staircase FM Signal

A smooth frequency sweep can be approximated crudely by a frequency pattern which changes in steps at intervals in time. Such signals are useful in many applications and will be discussed briefly here.

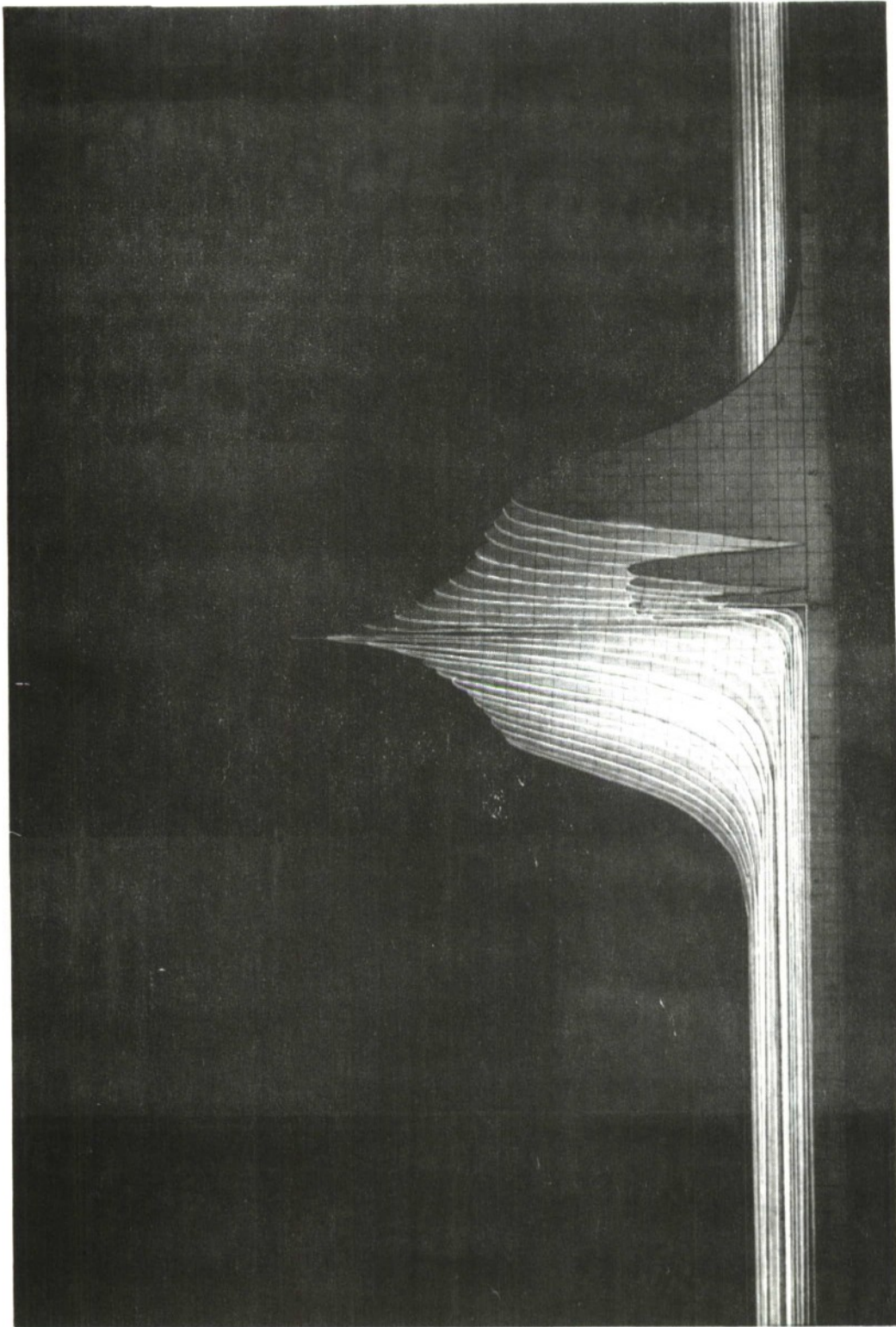


Fig. 12 The central region of the two-dimensional correlation function of the inverse-tangent signal with duration-bandwidth product of $50/\pi$. The signal is 100 time units long. The region shown extends about 20 time units on either side of the origin. Profiles are taken vs. time at intervals in Doppler equal to $1/4T$, where T is the signal duration.

Let us suppose that we have a rectangular signal whose frequency changes by equal steps at equal intervals of time, as shown in Fig. 13. The signal is a stepwise approximation to a linear FM signal. The signal duration is nT , and the bandwidth with the frequency step $W = 1/T$ is approximately nW , making the duration-bandwidth product n^2TW .

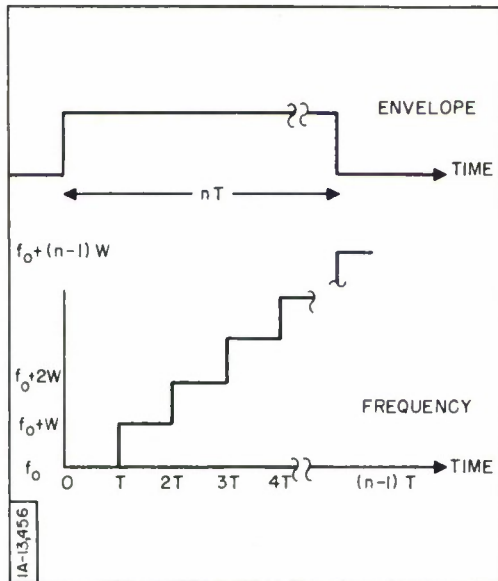


Fig. 13 Envelope and frequency vs. time of the staircase FM signal.

Consider the block diagram of a filter shown in Fig. 14 whose impulse response is the staircase FM signal. The impulse is applied to a bank of $\sin f/f$ filters arranged in parallel. Each filter has an impulse response which is a rectangular pulse of constant frequency and duration T , and the filter responses are spaced at intervals of W in frequency. The response of the k th filter is delayed by kT and all pulses are added to form a long-duration signal of constant amplitude.

The matched filter for the signal is required to have an impulse response which is a replica of the signal inverted in time. The matched filter for the staircase FM signal is simply the filter of Fig. 14 with delay lines rearranged so that the longest delay, nT , appears on the first line, next to longest on the second and so on, with zero delay on the bottom line. When

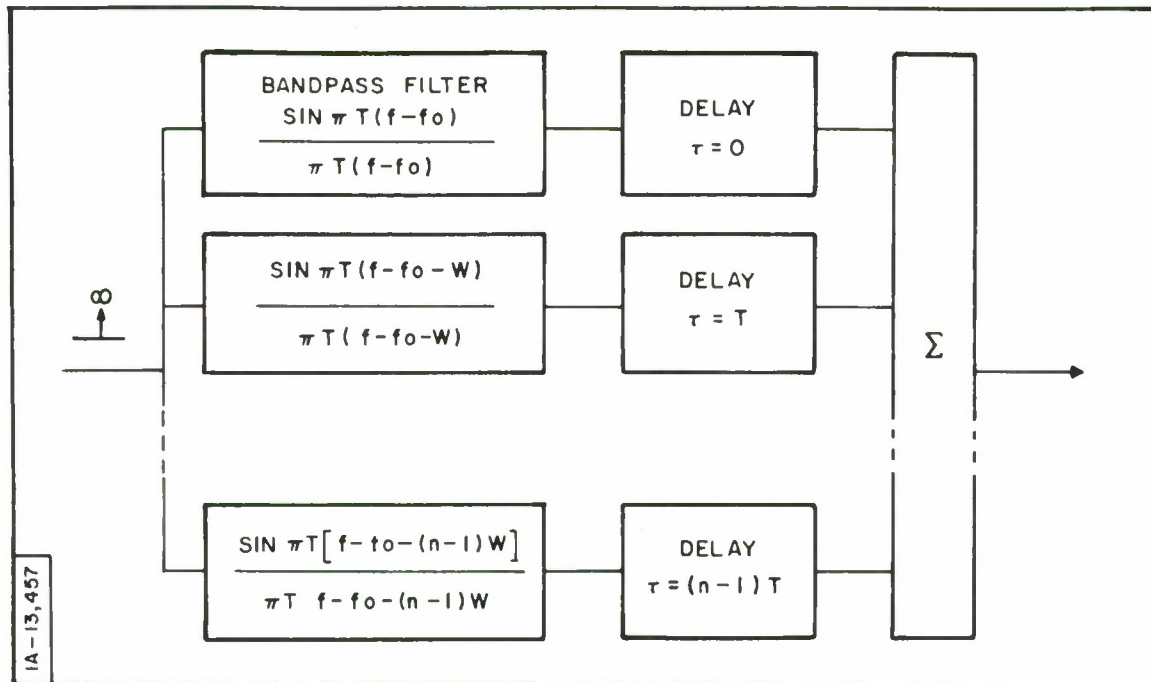


Fig. 14 Block diagram of a filter whose impulse response is the staircase FM signal.

the signal is inserted into the matched filter, after an interval $t = nT$ all of the pulses appear simultaneously at the output and add together. During this interval, $nT < t \leq (n+1)T$, the matched filter output $e(t)$ may be written as

$$e(t) = \sum_{k=0}^{n-1} a(t) \cos 2\pi (f_0 + kW) t \quad (110)$$

$$= \text{Re} \left\{ \sum_{k=0}^{n-1} a(t) \exp j2\pi (f_0 + kW) t \right\}, \quad (111)$$

where

$$a(t) = \begin{cases} T - |t| & , \quad -T \leq t \leq T \\ 0 & , \quad \text{otherwise} \end{cases} \quad (112)$$

is the autocorrelation function of the envelope of the short pulse of duration T . Equation (111) is a simple geometric progression and may be summed to obtain for $e(t)$

$$e(t) = a(t) \cos 2\pi t \left[f_o + \frac{n-1}{2} W \right] \frac{\sin \pi n W t}{\sin \pi W t} \quad (113)$$

Notice that the waveform $e(t)$ has a carrier frequency of $[f_o + (n-1) W/2]$, the mean frequency of the signal. The waveform without the carrier is sketched in Fig. 15. The duration of the signal at the 3-dB points is approximately $1/nW$. The compression ratio, C , is the ratio of the signal duration to the duration of the receiver output. We have

$$C = \frac{nT}{1/nW} = n^2 TW \quad (114)$$

The interesting thing is the fact that the compression ratio goes as n^2 , where n is the number of sub-pulses.

It should be noted that the receiver output waveform exists in time for an interval about equal to twice the duration of the signal, that is, $(2n-1)T$. Physically, the extended duration of the receiver output is due to cross-channel leakage. The bandpass filters in Fig. 14 overlap in frequency as shown in

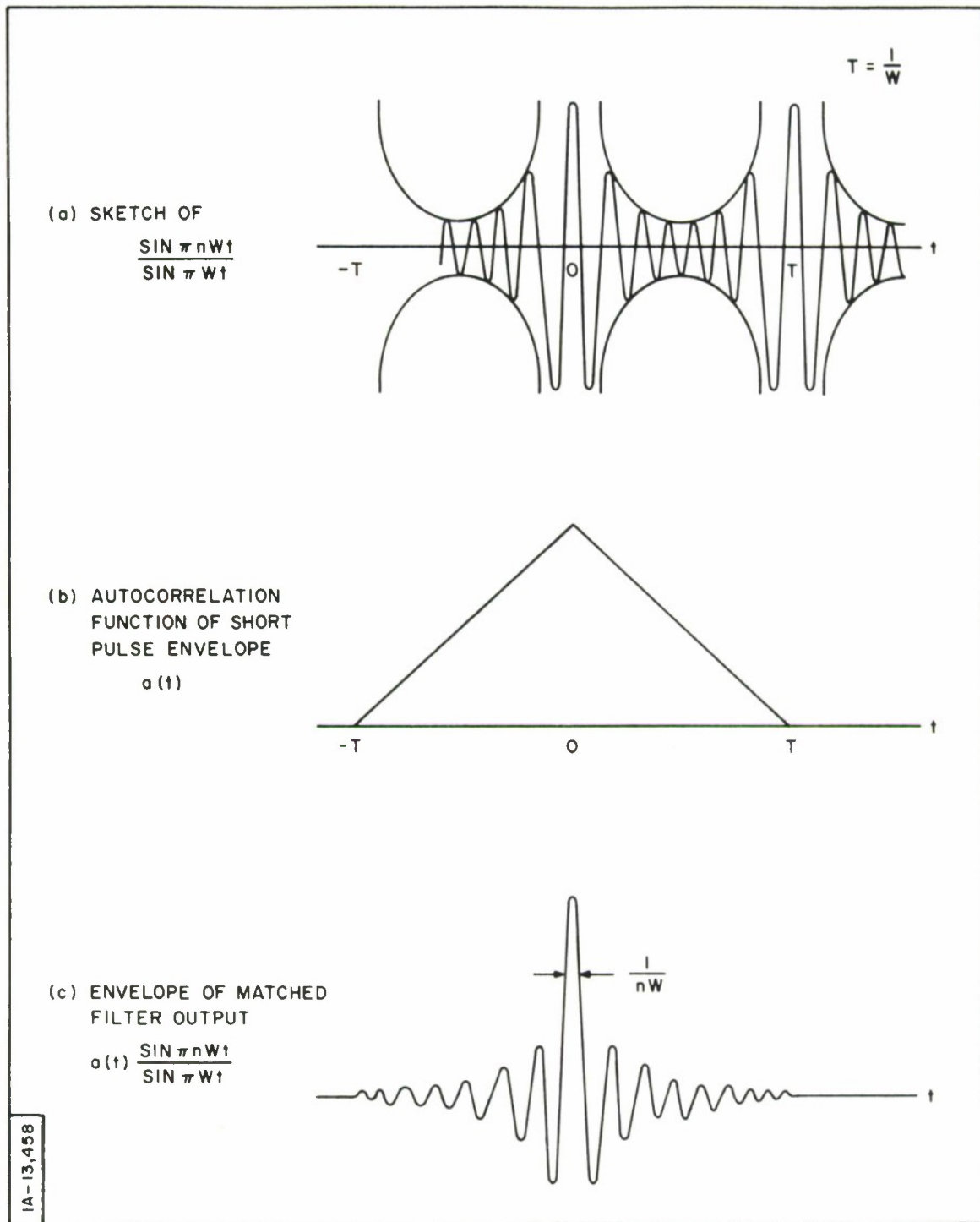


Fig. 15 The staircase FM signal.

Fig. 16, and, hence, respond somewhat to sub-pulses centered in the passband of other channels. When a signal leaks through a wrong channel, it appears at the output at a time different from that at which the peak occurs. The leakage is distributed over an interval of about nT on either side of the peak.

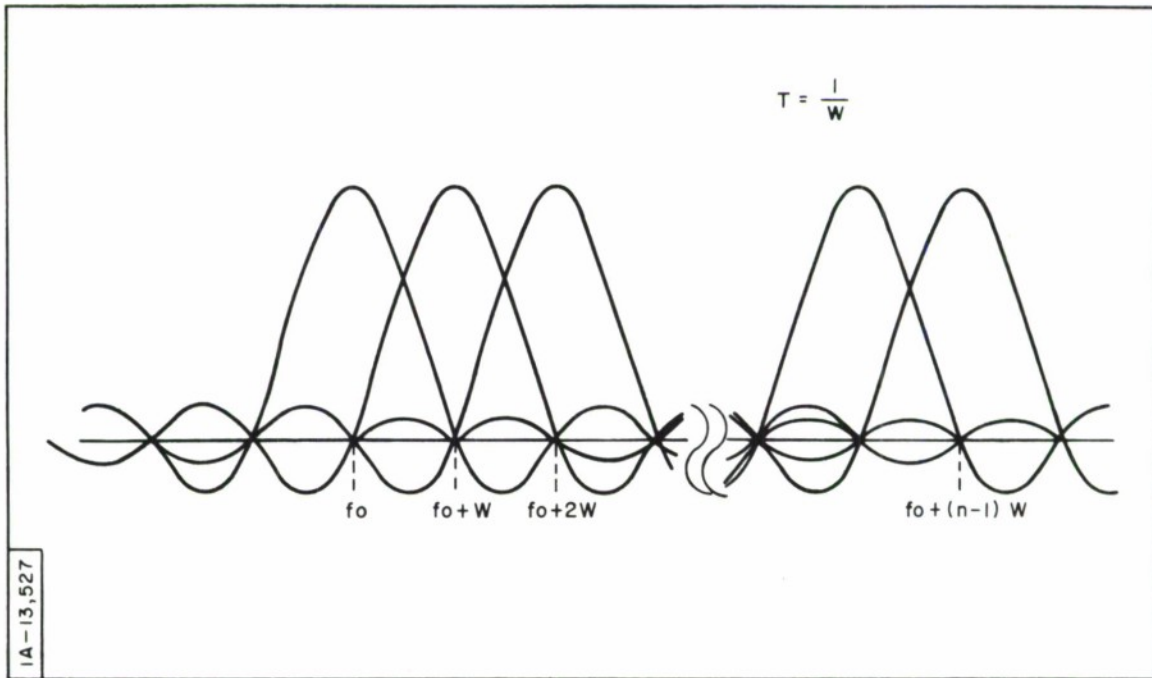


Fig. 16 Sketch showing the frequency characteristics of the channels in Fig. 14.

Analytically, the leakage may be viewed as the sidelobes of the signal autocorrelation function. The sidelobes are difficult to calculate, and usually the calculation is not made. The sidelobes may be suppressed by weighting in a way similar to that done for the linear FM signal. In the case of the staircase FM signal, however, one may insert a complex weighting function in each channel and adjust each channel separately in turn to suppress the sidelobes. Signal-to-sidelobe ratios of 30 db or better may be achieved in this way.

The staircase FM signal is useful over a range of Doppler frequencies which is less than the reciprocal of the signal duration, nT . Over a wide Doppler range, the two-dimensional signal correlation function generally resembles that of the linear FM signal, being a ridge at an angle to both the time and Doppler axes.

The individual channels of the filter shown in Fig. 14 have only bandwidth W . From many components, each of narrow bandwidth, a wide-band system can be fashioned in this way. This is frequently an advantage in practice.

3.8 Rectangular, Phase-reversal Signals

In previous sections we have considered various methods for increasing the bandwidth of a signal of given duration. We have discussed some methods of modulating the phase and/or frequency of the signal to do this. These methods so far have yielded signals whose two-dimensional correlation functions have a useful shape only in a relatively narrow region on either side of the τ axis. In this section we will consider another kind of phase-modulated signal, which is useful, again, over a narrow Doppler region.

The bandwidth of a constant frequency pulse can be increased by making step changes in the phase at intervals during the pulse. One could make the phase steps any amount, but in the most commonly used phase-step signals the step is π radians. A signal of duration Δ is divided into n parts and the phase of each part (taken with respect to a phase reference) is set at either zero or π .

The autocorrelation function of the phase reversal signal may be shown to have an envelope which is the autocorrelation function of the plus-minus code waveform. We take the signal, $s(t)$, to be

$$s(t) = a(t) \cos[2\pi f_o t + \varphi_k(t)] \quad , \quad (115)$$

where $\varphi_k(t)$ is the phase code; the corresponding complex form, $s_c(t)$, in the narrow band case is

$$s_c(t) = a(t) \exp j\varphi_k(t) \exp(j2\pi f_o t) \quad . \quad (116)$$

We see in Eq. (116) that the complex modulation, $u(t)$, is

$$u(t) = a(t) \exp j\varphi_k(t) \quad . \quad (117)$$

Since $\varphi_k(t)$ is either zero or π , $\exp j\varphi_k(t)$ is either (+1) or (-1); and with $a(t)$ given by

$$a(t) = \begin{cases} 1 & , \quad 0 < t < \Delta \\ 0 & , \quad \text{otherwise} \end{cases} \quad , \quad (118)$$

$u(t)$ is purely real, that is, either plus one or minus one. A possible $u(t)$ for a phase-coded signal is shown in Fig. 17. The autocorrelation function of $s(t)$, $A(\tau)$, is given by the real part of the complex autocorrelation of $s_c(t)$. That is,

$$\begin{aligned} A(\tau) &= \text{Re} \left\{ \int_{-\infty}^{\infty} s_c(t) \bar{s}_c(t + \tau) dt \right\} \\ &= \text{Re} \left\{ e^{-j2\pi f_o \tau} \int_{-\infty}^{\infty} u(t) \bar{u}(t + \tau) dt \right\} \quad . \end{aligned} \quad (119)$$

Since $u(t)$ is real,

$$A(\tau) = \cos 2\pi f_0 \tau \int_{-\infty}^{\infty} u(t) u(t + \tau) dt \quad (120)$$

The envelope of $A(\tau)$ is thus seen to be the autocorrelation function of $u(t)$.

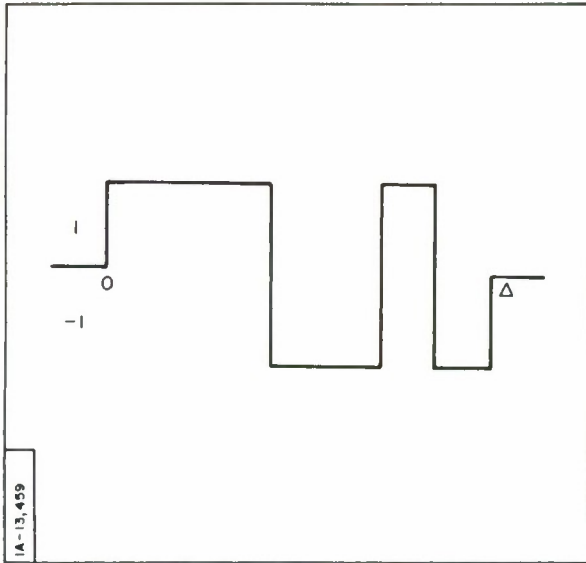


Fig. 17 A plus-minus code waveform.

The sequence of phases in $u(t)$ may be chosen randomly or according to a code. If the sequence is chosen at random, it is likely that the autocorrelation function of the signal will have rather large sidelobes. To control the sidelobes the sequence will be chosen according to a carefully selected binary code.

Plus-minus or binary codes having satisfactory (in some sense) autocorrelation functions have been investigated by Zierler, [26] Lerner, [27] Elspas, [28] Barker, [29] and many others. Three-phase codes have been investigated by DeLong. [30] We will not here attempt to discuss codes in general but rather refer the reader to the literature. Instead, we will illustrate our remarks about phase-reversal codes in general by using for an example a particular class of codes called "Barker codes" or "optimum words."

An n^{th} order Barker code is a sequence of plus ones and minus ones of length n which has the property that its autocorrelation function has a peak value of n and has uniformly spaced sidelobes, all of unit height. The plus-minus code shown previously in Fig. 17 is actually a 7th order Barker code; its autocorrelation function is shown in Fig. 18. Table 1 lists all of the known Barker codes. The highest code of odd-order has been shown to be 13, and it has been shown that higher order codes, should they exist, must have orders which are even and perfect squares. So far none of the latter have been found.

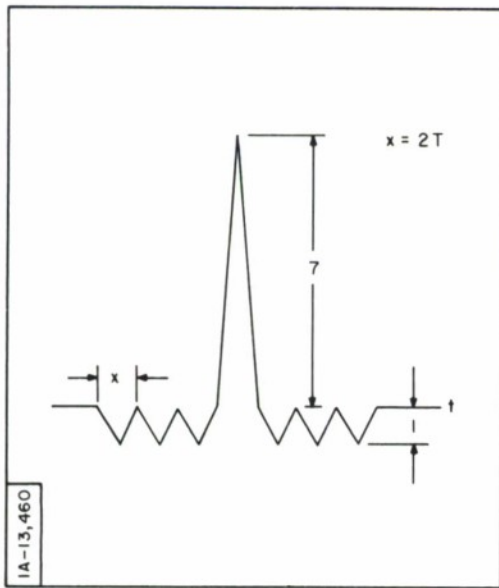


Fig. 18 Autocorrelation function of the 7th order Barker code of Fig.17.

Table 1

Barker Codes

Order	Code
3	++-
4	++-+
5	+++--
7	+++---+
11	+++----++-
13	++++---++-+-

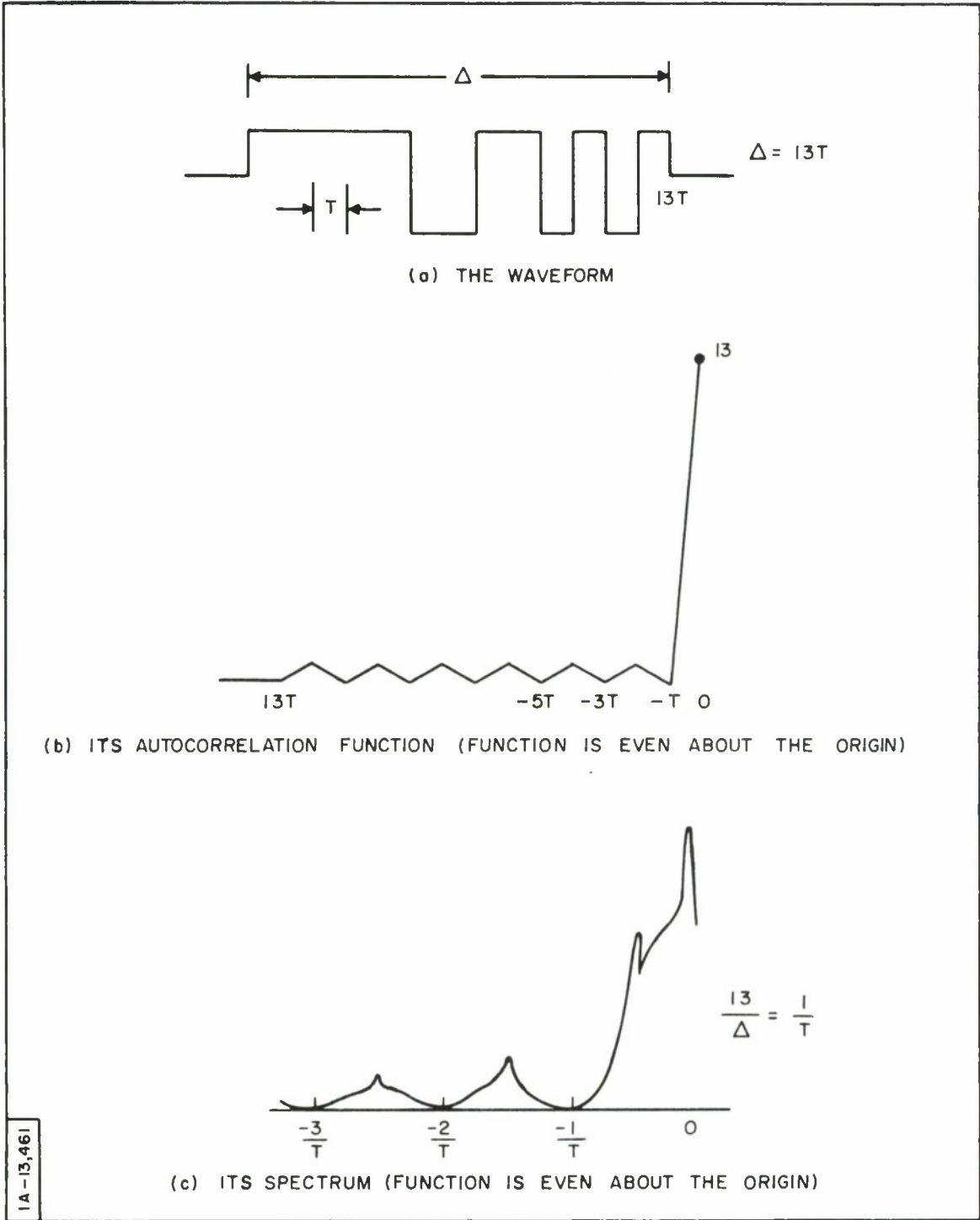


Fig. 19 The 13th order Barker code waveform.

The highest order Barker code, of length 13, has been used as a phase-reversal code in a radar signal. The 13-code waveform, its auto-correlation functions, and its spectrum are shown in Fig. 19. The spectrum has the bandwidth associated with a simple pulse of duration $\Delta/13$. The time bandwidth product, TW , is then

$$TW = \Delta \times \frac{13}{\Delta} = 13 \quad (121)$$

The block diagram of a tapped delay line filter that may be used to generate the 13-code signal is shown in Fig. 20. Discussion of the design, however, will be reserved for Section 4.0, where tapped delay line techniques are considered.

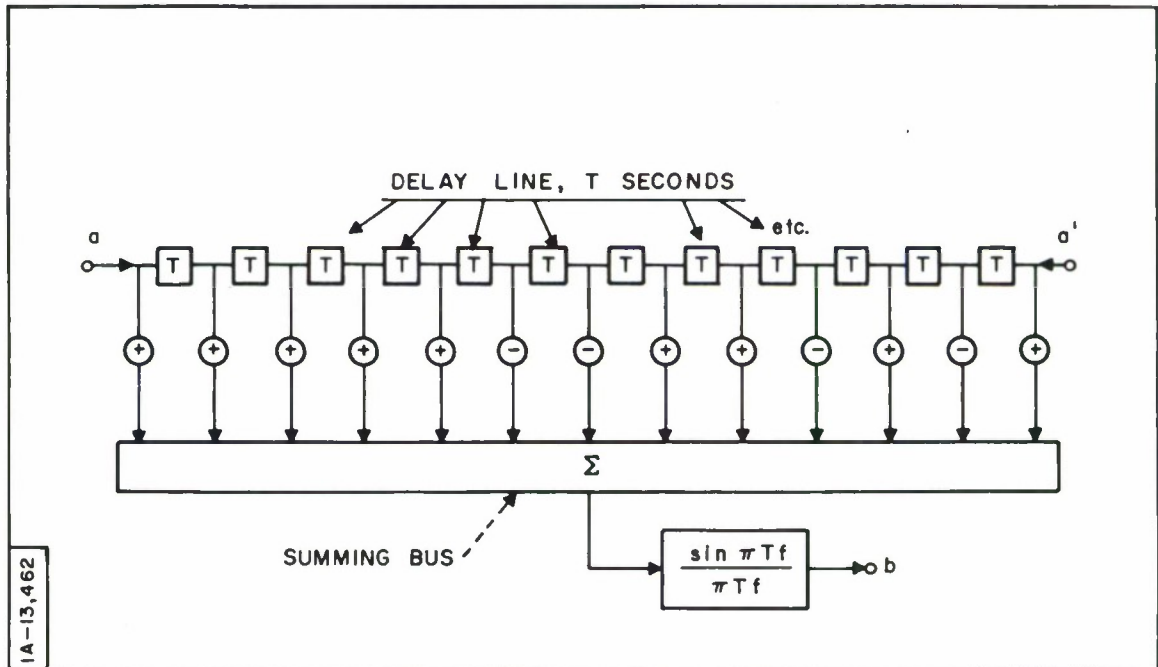


Fig. 20 Block diagram of video filter used to generate and "match" 13-code waveform.

A model of the modulus of the two-dimensional signal correlation function of the 13-code signal is shown in Fig. 21. The profiles are taken in the time direction at intervals of $1/4\Delta$ in Doppler frequency. For clarity, only one-half of the time-Doppler plane is shown. The zero-Doppler profile, the 13-code autocorrelation function, is the first profile. For a Doppler shift of $1/4\Delta$ (the second profile), the sidelobe levels are fairly constant although the height of the peak does decrease somewhat. However, for Doppler shifts $\nu > 1/4\Delta$, the surface is terrible. Hence, the earlier remarks on the utility of the signal in a narrow Doppler strip.

Figure 22 shows a photograph of the receiver output waveforms of a radar operating alternately with a simple uncoded signal (top) and a 13-code signal of the same duration (bottom). In the top trace one can see a ground clutter return on the left, followed by a return from a single moving target, and finally a return from several nearby moving targets. But how many? In the bottom trace the radar views the same targets as in the top trace. Notice on the left that the rms value of the clutter return is much decreased and that the position of the isolated target can be much more accurately fixed in time, and finally, that there were three targets in the overlapping returns of the top trace. In the bottom trace the echoes stand out clearly without overlapping.

But notice also that the sidelobes of the autocorrelation function are visible in the lower trace and are bothersome. The question always arises: Is it a sidelobe or a nearby small target?

The sidelobes may be suppressed in this case by a simple method given by Key, Fowle, and Haggarty. [31] The sidelobe suppression method makes use of the fact that the central part of the autocorrelation function and the sidelobes are all triangles. Because of this geometric similarity, it is possible to suppress the sidelobes by adding to the signal autocorrelation

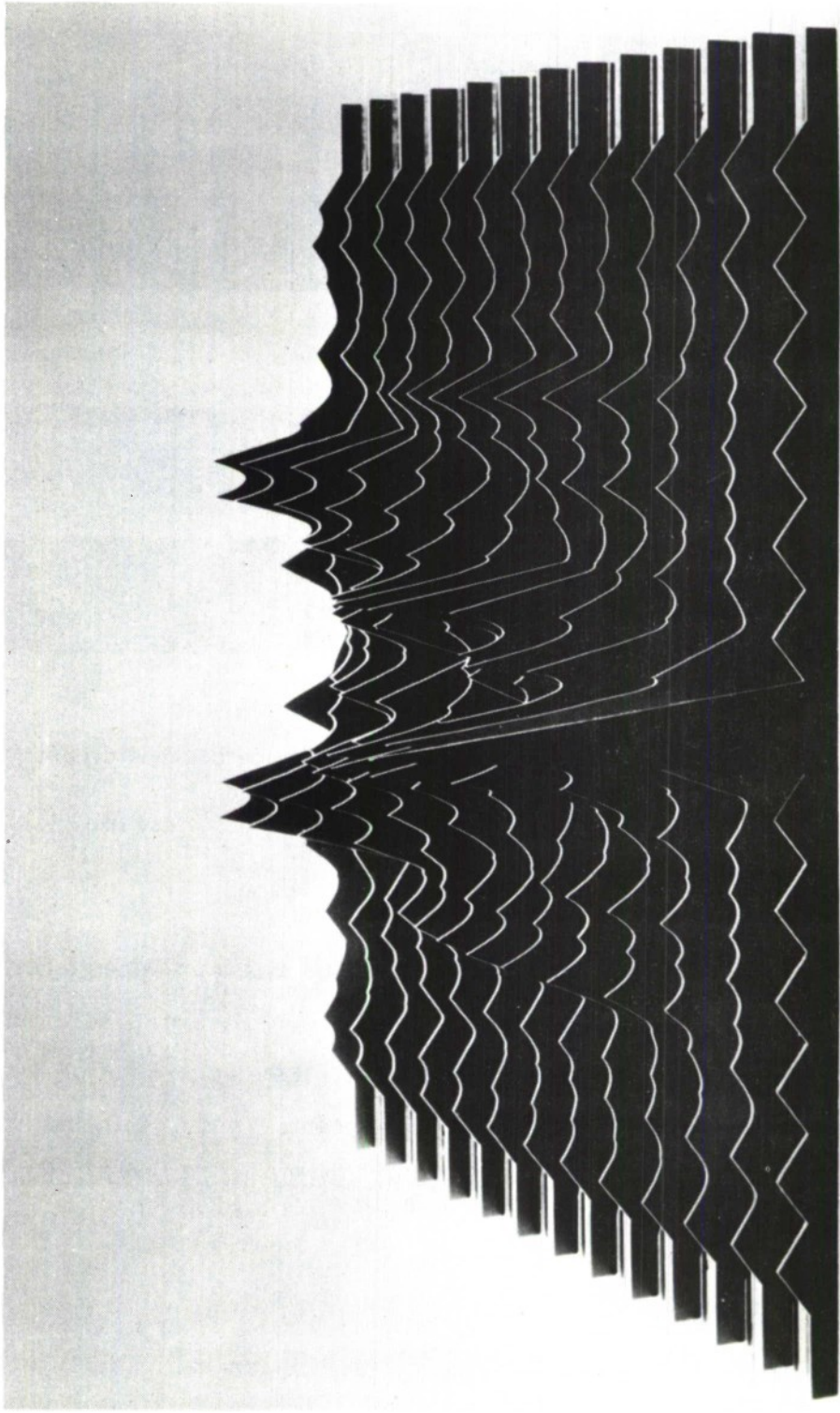


Fig. 21 The two-dimensional correlation function of the 13-code signal. Profiles are taken vs. time at intervals of $1/4 \Delta$ in Doppler, where Δ is the 13-code signal duration. (Taken from Key et al., Ref. 31, with permission.)

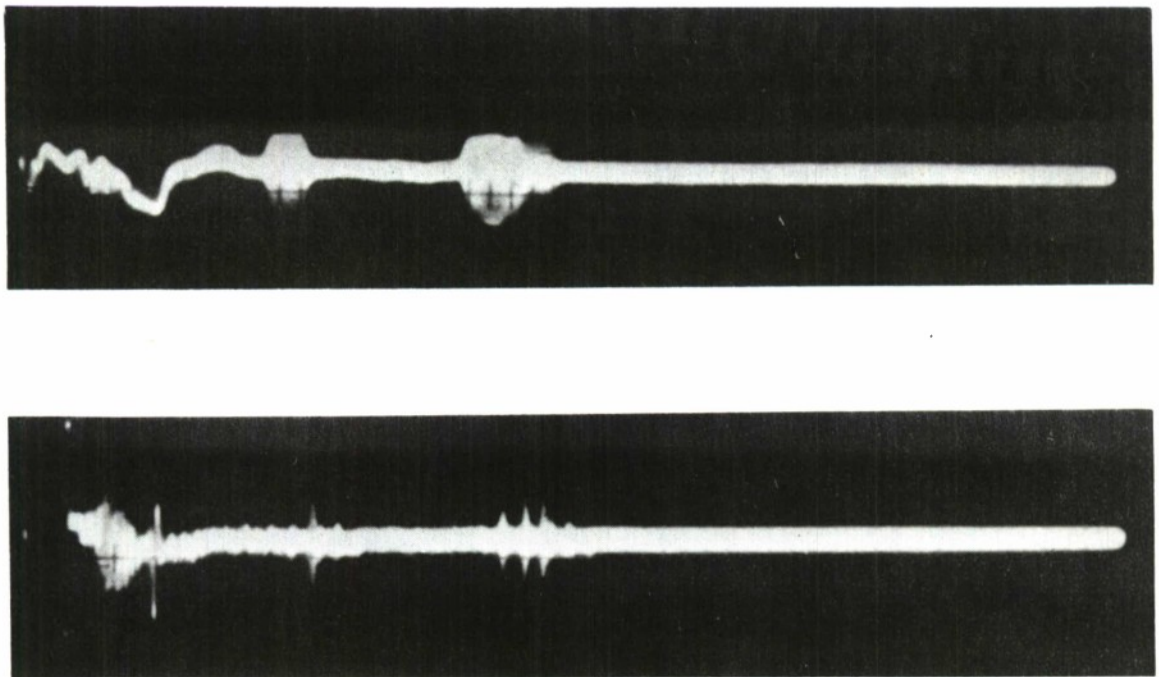


Fig. 22 Photograph of A-scope of a radar operating alternately with a simple pulse and with a 13-code signal of the same length. Top: simple pulse operation. Bottom: 13-code signal operation. (Courtesy of G.B. Tiffany, of The MITRE Corporation.)

function properly scaled replicas of the autocorrelation functions which are relatively advanced and delayed in time.* Figure 23 illustrates this process. Here a weighted and shifted replica of the autocorrelation function is shown for each of the 12 sidelobes and for the central peak. Weights are found for each so that they add up to produce $g(t)$ shown at the bottom of Fig. 23. We have for $g(t)$

*The method of Key et al. [31] is very general and may be applied to shape waveforms at bandpass as well as at video.

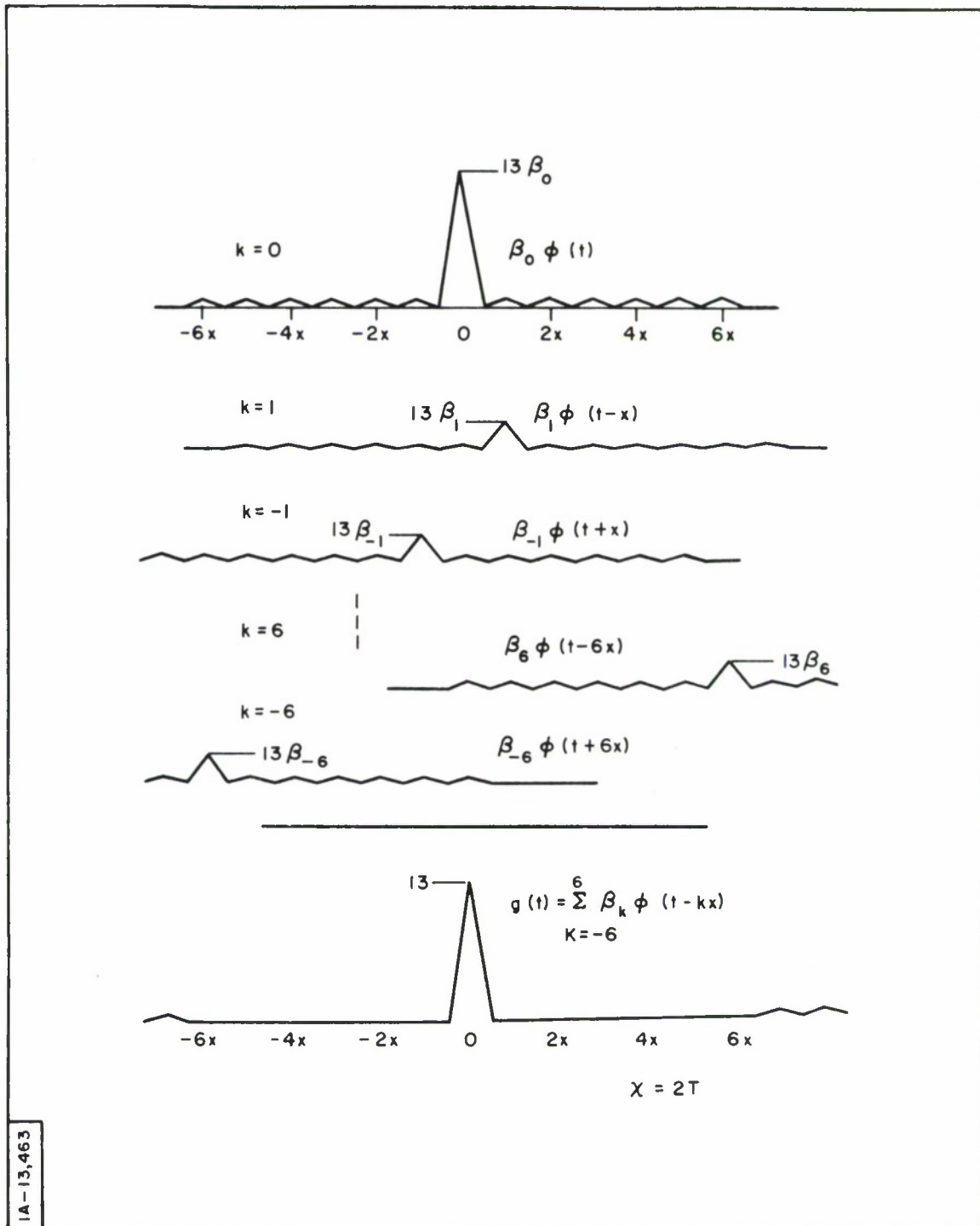


Fig. 23 Illustration of the method of suppression of the sidelobes of the 13-code autocorrelation function.

$$g(t) = \sum_{k=-6}^6 \beta_k \varphi(t - kx) \quad , \quad (122)$$

where $\varphi(t)$ is the 13-code autocorrelation function. We let t assume the values $-6x, -5x, \dots, 0, +x \dots +6x$ in succession. For each value of t we specify the value we want $g(t)$ to have and set it equal to the sum on the right. In this way a set of 13 equations is generated whose solution yields the values of the weighting coefficients, β_k . If the weighted waveform is made symmetrical, $\beta_{-k} = \beta_k$ and the number of equations reduces to 7. In Fig. 23, $g(t)$ has been made zero where the original sidelobes were. New sidelobes farther out in t are created, of course, and these may be suppressed in the same way, if desired. Table 2 gives the weighting coefficients which reduce the 6 sidelobes on either side of the central peak to zero, and Fig. 24 shows the block diagram of the sidelobe suppression network.

Table 2
Weighting Coefficients for the Suppression of
Sidelobes of 13-Code Autocorrelation Function

$\beta_0 = 1.047722182$	$\beta_4 = -0.0542686157$
$\beta_1 = -0.0407328662$	$\beta_5 = -0.0580662589$
$\beta_2 = -0.0455717223$	$\beta_6 = -0.0614606642$
$\beta_3 = -0.0500941064$	

When the original sidelobes are suppressed to zero, the ratio of the amplitude of the peak to the maximum sidelobe is increased to 42 (32.4 db) from the initial value of 13 (22.3 db). The loss in detection due to mismatching the receiver to suppress the sidelobes in this way is of the order of 0.25 db.

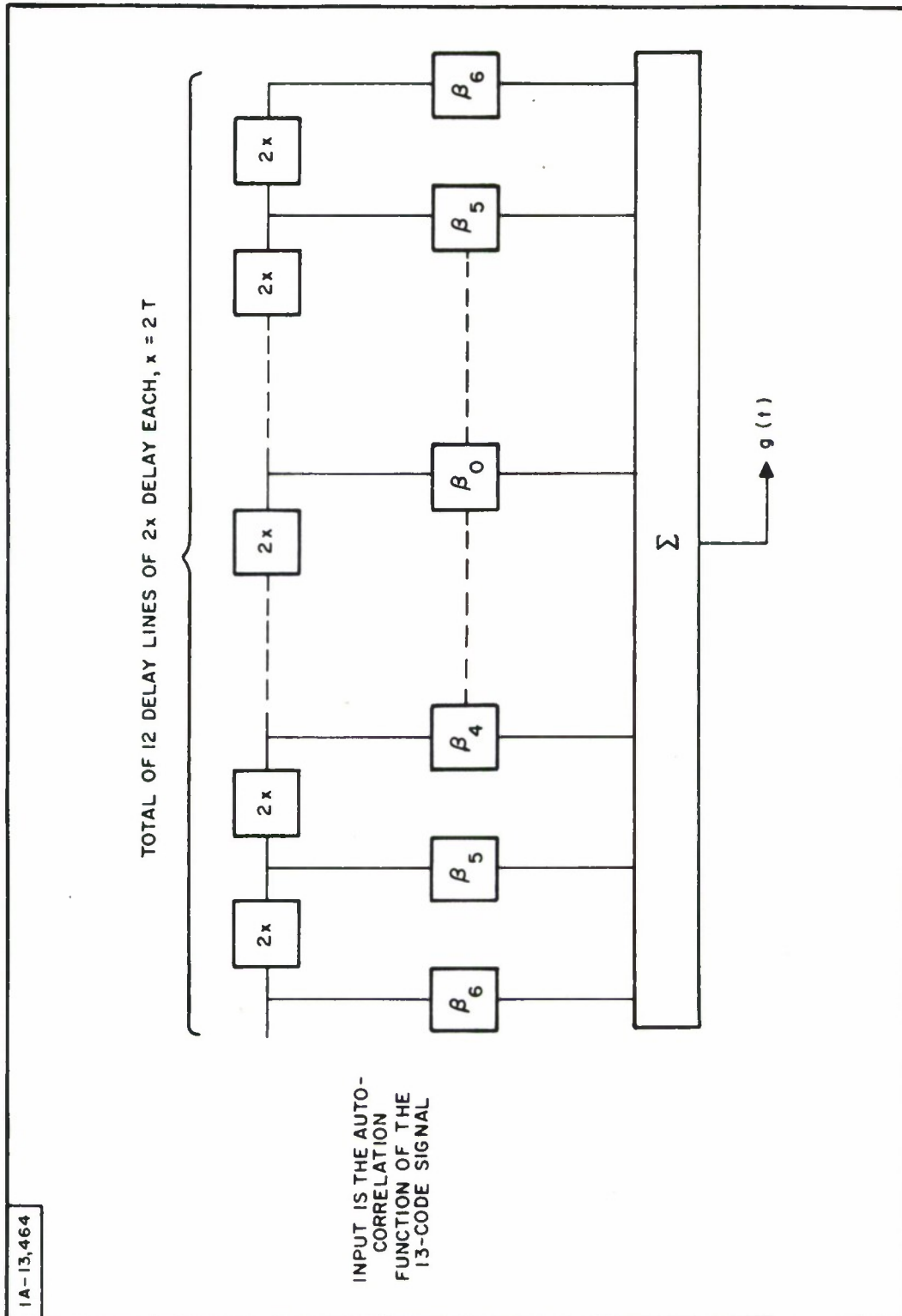


Fig. 24 Block diagram of weighing network which controls amplitudes of the interior sidelobes of the 13-code autocorrelation function.

3.9 Amplitude- and Phase-modulated Signals *

Earlier in Section 3.0 we derived a method of designing a rectangular signal of large TW product to have a specified autocorrelation function. By controlling the autocorrelation function, one in fact shapes the two-dimensional signal correlation function in a narrow strip on either side of the τ axis. The χ function associated with a rectangular signal, however, is not a smooth function over a very large time-Doppler region. For example, the χ function associated with the rectangular, tangent FM signal, shown in Fig. 12, begins to have an oscillatory character for $\nu > 1/T$ where T is the signal duration. In many cases some improvement in the shape of a χ function might be obtained if the requirement were relaxed that the signal have a rectangular envelope.

In this section we will extend the method of designing FM signals to cover signals of arbitrary envelope shape. To put it another way, we will give a method for determining the phase characteristics necessary to the construction of a Fourier pair when, initially, the signal envelope and the modulus of the signal spectrum are specified.

We may begin with the statement that $u(t) = u_e(t) e^{j\varphi(t)}$ is, by definition, the inverse Fourier transform of $U(f) = U_m(f) e^{j\Theta(f)}$ thus,

$$u_e(t) \exp j\varphi(t) = \int_{-\infty}^{\infty} U_m(f) \exp j\Theta(f) \exp j2\pi f t \, df \quad . \quad (123)$$

We can control the signal shape by specifying $u_e(t)$, and the autocorrelation function by specifying $U_m(f)$. When $u_e(t)$ and $U_m(f)$ are independently

* This section follows Fowle in Ref. 32.

specified, we need a method of finding $\varphi(t)$ and $\Theta(f)$ to make $u(t)$ and $U(f)$ a Fourier pair.

We should point out that it is not possible in general to specify independently the modulus of a function and the modulus of its Fourier transform. The two moduli must satisfy certain constraints, the full details of which Fourier theory does not make clear. However, as the time-bandwidth product of the signal increases, these constraints seem to lose force, and independently specified moduli may be realized in a Fourier pair in some cases with very good accuracy.

The derivation of expressions for $\varphi(t)$ and $\Theta(f)$ begins with the approximate relations, Eq. (72), calculated from Eq. (69) by the method of stationary phase. We have Eq. (73), which relates the two moduli with the second derivative of one of the phase functions,

$$u_e(t) \cong \sqrt{2\pi} \frac{U_m(\lambda)}{\sqrt{|\Theta''(\lambda)|}} \quad . \quad (124)$$

The relation between λ and t , Eq. (71), is given by one of the unknown functions thus,

$$2\pi t = -\Theta'(\lambda) \quad . \quad (125)$$

We must first find a relation between λ and t in terms of the known functions, the moduli $u_e(t)$ and $U_m(f)$. To do this we square Eq. (124), and substitute in it the expression for $\Theta''(\lambda)$ obtained by differentiating Eq. (125) with respect to λ . We obtain

$$u_e^2(t) dt = U_m^2(\lambda) d\lambda \quad , \quad (126)$$

which upon integration yields

$$P(t) = Q(\lambda) + C \quad , \quad (127)$$

where P and Q are the indefinite integrals of $u_e^2(t)$ and $U_m^2(f)$, respectively, and C is a constant of integration. Equation (127) may be solved for either t or λ . We may solve for t and substitute for t in Eq. (125) to obtain for $\Theta'(\lambda)$

$$\Theta'(\lambda) = -2\pi P^{-1} [Q(\lambda) + C] \quad . \quad (128)$$

We integrate Eq. (128) and substitute $f = \lambda$ to obtain for $\Theta(f)$

$$\Theta(f) = -2\pi \int P^{-1} [Q(f) + C] df \quad . \quad (129)$$

We may find an expression for $\varphi'(t)$ by solving Eq. (127) for λ and substituting into Eq. (80). We obtain for $\varphi'(t)$,

$$\varphi'(t) = 2\pi Q^{-1} [P(t) - C] \quad , \quad (130)$$

from which we get $\varphi(t)$ by integration,

$$\varphi(t) = 2\pi \int Q^{-1} [P(t) - C] dt \quad . \quad (131)$$

Equations (129) and (131) give $\varphi(t)$ and $\Theta(f)$ entirely in terms of the specified functions $u_e(t)$ and $U_m(f)$ and are, therefore, the results we sought. We have derived the following approximate Fourier pair

$$u_e(t) \exp j2\pi \int Q^{-1}[P(t) - C] dt \cong \mathcal{F}^{-1} \left\{ U_m(f) \exp -j2\pi \int P^{-1}[Q(f) + C] df \right\} . \quad (132)$$

We may obtain another corresponding pair of relations for $\varphi(t)$ and $\Theta(f)$ by conjugating Eq. (132). Conjugation of Eq. (132) has the effect of changing the direction of the frequency sweep, so that of the two expressions for $\varphi(t)$, one corresponds to an upward frequency sweep and the other to a downward sweep.

There are several comments that are appropriate at this point. First, as shown earlier, the group delay characteristic, $-\Theta'(f)/2\pi$, and the instantaneous frequency, $\varphi'(t)/2\pi$, are approximately inverse functions. The frequency sweep (and hence the group time delay) is ordinarily a non-linear function. The exception, of course, occurs when the signal envelope and spectral modulus are required to have the same functional form; then, frequency vs. time and group delay vs. frequency are linear, as the reader may demonstrate. The argument given above is predicated on the assumption that the signal time-bandwidth product is large. Just how large quite obviously depends on the shape of the signal envelope and spectral modulus and upon the accuracy desired. If both envelope and spectrum are smooth, continuous functions, the method described can give excellent results for TW products as small as 3 or 4. If one modulus is smooth and continuous and the other rectangular, TW products of the order of 10 give very good results, as we saw in the example of the rectangular, tangent FM signal of Key et al. [31] discussed earlier.

Finally, if both moduli are required to be rectangular, as in the linear FM example considered earlier, (a requirement which, by the way, expressly violates Paley-Wiener Theorem 10), TW products of the order of 100 or more are required to get good results.

3.10 An Amplitude- and Phase-modulated Signal

To illustrate the method described in the preceding section let us assume that we want a signal whose autocorrelation function has a Gaussian shape and whose envelope also has a Gaussian shape. Let us take for the desired autocorrelation function

$$\chi(\tau, 0) = \sqrt{\frac{\pi}{2}} \exp - \frac{\pi^2 T^2 W^2}{2} \left(\frac{\tau}{T}\right)^2 \quad (133)$$

The squared spectrum $U_m^2(f)$ is given by the Fourier transform of $\chi(\tau, 0)$ thus,

$$\begin{aligned} U_m^2(f) &= \mathcal{F} \{ \chi(\tau, 0) \} \\ &= \frac{1}{W} \exp - 2 \left(\frac{f}{W}\right)^2, \end{aligned} \quad (134)$$

which gives

$$U_m(f) = \frac{1}{\sqrt{W}} \exp - \left(\frac{f}{W}\right)^2 \quad (135)$$

In addition, we require that the envelope $u_e(t)$ be Gaussian thus:

$$u_e(t) = \frac{1}{\sqrt{T}} \exp - \left(\frac{t}{T} \right)^2 . \quad (136)$$

If we take the interval to the e^{-1} point for duration and bandwidth, the time-bandwidth product of the signal is TW . We assume that TW is adequately large. We want to find an expression for the phase characteristics $\varphi(t)$ and $\Theta(f)$ which when associated with $u_e(t)$ and $U_m(f)$, respectively will make a Fourier pair. As the first step, we determine the relation between t and λ by use of Eq. (126). We have

$$\frac{1}{T} \int \exp -2 \left(\frac{t}{T} \right)^2 dt = \frac{1}{W} \int \exp -2 \left(\frac{\lambda}{W} \right)^2 d\lambda , \quad (137)$$

which yields immediately

$$\frac{t}{T} = \frac{\lambda}{W} . \quad (138)$$

From Eq. (138) above we find, by the methods of the last section, an expression for $\Theta(f)$ and $\varphi(t)$. We obtain

$$\Theta(f) = - \left[\pi TW \left(\frac{f}{W} \right)^2 + \Theta_o \right] \quad (139)$$

and

$$\varphi(t) = \pi TW \left(\frac{t}{T} \right)^2 + \varphi_o , \quad (140)$$

where Θ_o and φ_o are constants. We have now constructed the approximate Fourier pair

$$\frac{1}{\sqrt{W}} \exp - \left(\frac{f}{W} \right)^2 \exp -j \left[\pi TW \left(\frac{f}{W} \right)^2 + \Theta_o \right] \cong \mathcal{F} \left\{ \frac{1}{\sqrt{T}} \exp - \left(\frac{t}{T} \right)^2 \exp j \left[\pi TW \left(\frac{t}{T} \right)^2 + \varphi_o \right] \right\} . \quad (141)$$

The right side of Eq. (141) above has an exact Fourier transform which we may compute as a check on the approximate methods. For $TW = 10/\pi$ we have the following exact Fourier pair:

$$\begin{aligned} & \frac{\left(\frac{100}{101} \right)^{1/4}}{\sqrt{W}} \exp - \frac{100}{101} \left(\frac{f}{W} \right)^2 \exp -j \left[\frac{100}{101} \pi TW \left(\frac{f}{W} \right)^2 + \Theta_1 \right] \\ & = \mathcal{F} \left\{ \frac{1}{\sqrt{T}} \exp - \left(\frac{t}{T} \right)^2 \exp j \left[\pi TW \left(\frac{t}{T} \right)^2 + \varphi_1 \right] \right\}, \end{aligned} \quad (142)$$

which differs negligibly from the approximate pair, Eq. (141). Thus, good results are obtained here for $TW \approx 3$, which is in accord with our earlier statement. The signal $u(t)$ is

$$u(t) = \frac{1}{\sqrt{T}} \exp - \left(\frac{t}{T} \right)^2 \exp j \left[\pi TW \left(\frac{t}{T} \right)^2 + \varphi_o \right] . \quad (143)$$

We see that the signal and its approximate Fourier transform, Eq. (141), have quadratic phase, corresponding to a linear frequency sweep and to a linear group delay.

We may compute the two-dimensional signal correlation function for this linear FM Gaussian signal. We have

$$\chi(\tau, \nu) = \int_{-\infty}^{\infty} u(t) \bar{u}(t + \tau) \exp(-j2\pi \nu t) dt \quad (144)$$

We substitute $u(t)$ of Eq. (143) into Eq. (144) above and integrate and rearrange terms to obtain for $\chi(\tau, \nu)$

$$\chi(\tau, \nu) = \sqrt{\frac{\pi}{2}} \exp(j\pi \nu \tau) \exp \left[-\frac{1}{2} \frac{(\pi TW)^2}{1 + (\pi TW)^2} \left(\frac{\nu}{W} \right)^2 \right] \\ \times \exp - \frac{\left[\frac{\tau}{T} + \frac{(\pi TW)^2}{1 + (\pi TW)^2} \frac{\nu}{W} \right]^2}{2 \left[\frac{1}{1 + (\pi TW)^2} \right]} \quad (145)$$

When $\pi^2 T^2 W^2 \gg 1$

$$\chi(\tau, \nu) \cong \sqrt{\frac{\pi}{2}} \exp(j\pi \nu \tau) \exp \left[-\frac{1}{2} \left(\frac{\nu}{W} \right)^2 \right] \exp \left[-\frac{(\pi TW)^2}{2} \left(\frac{\tau}{T} + \frac{\nu}{W} \right)^2 \right]. \quad (146)$$

Notice that $\chi(\tau, 0)$ is approximately equal to the value required at the beginning of this example. For Eq. (146) above to hold, the TW product need not be very large.

Figure 25 shows a photograph of a model of the two-dimensional correlation function of the linear FM Gaussian signal. The profiles are taken vs. time at intervals in Doppler equal to 20 percent of the 3-db signal bandwidth. The interesting thing about this two-dimensional signal correlation function is that all profiles taken vs. time are Gaussian functions regardless of the value of Doppler shift ν , and, further, that the standard deviation or width of the function between e^{-1} points in the τ direction is constant. The function does not broaden (and degrade resolution) with Doppler shift. The effect of a Doppler shift is to attenuate the receiver output by $\exp - 1/2 (\nu/W)^2$, and to shift in time the position at which the peak value of the receiver output waveform occurs. The latter we should suspect from the linear FM discussion given previously. We see, further, that relaxing the requirement that the envelope be rectangular did, in this case, yield a smooth, non-oscillatory χ function.

Figures 26, 27 and 28 show photographs of waveforms in a pulse compression system which employs a linear FM Gaussian signal.* Figure 26 shows the Gaussian signal generated by applying a short pulse to a passive filter. Figure 27 shows the signal autocorrelation function. The time scales in Figs. 26 and 27 are the same. The time-bandwidth product (or compression ratio) is about 50. Notice that there are no sidelobes visible in the photograph of the autocorrelation function. Figure 28(a) through (f) shows the effect of a

*The experimental results are taken from Fowle et al., Ref. 13.

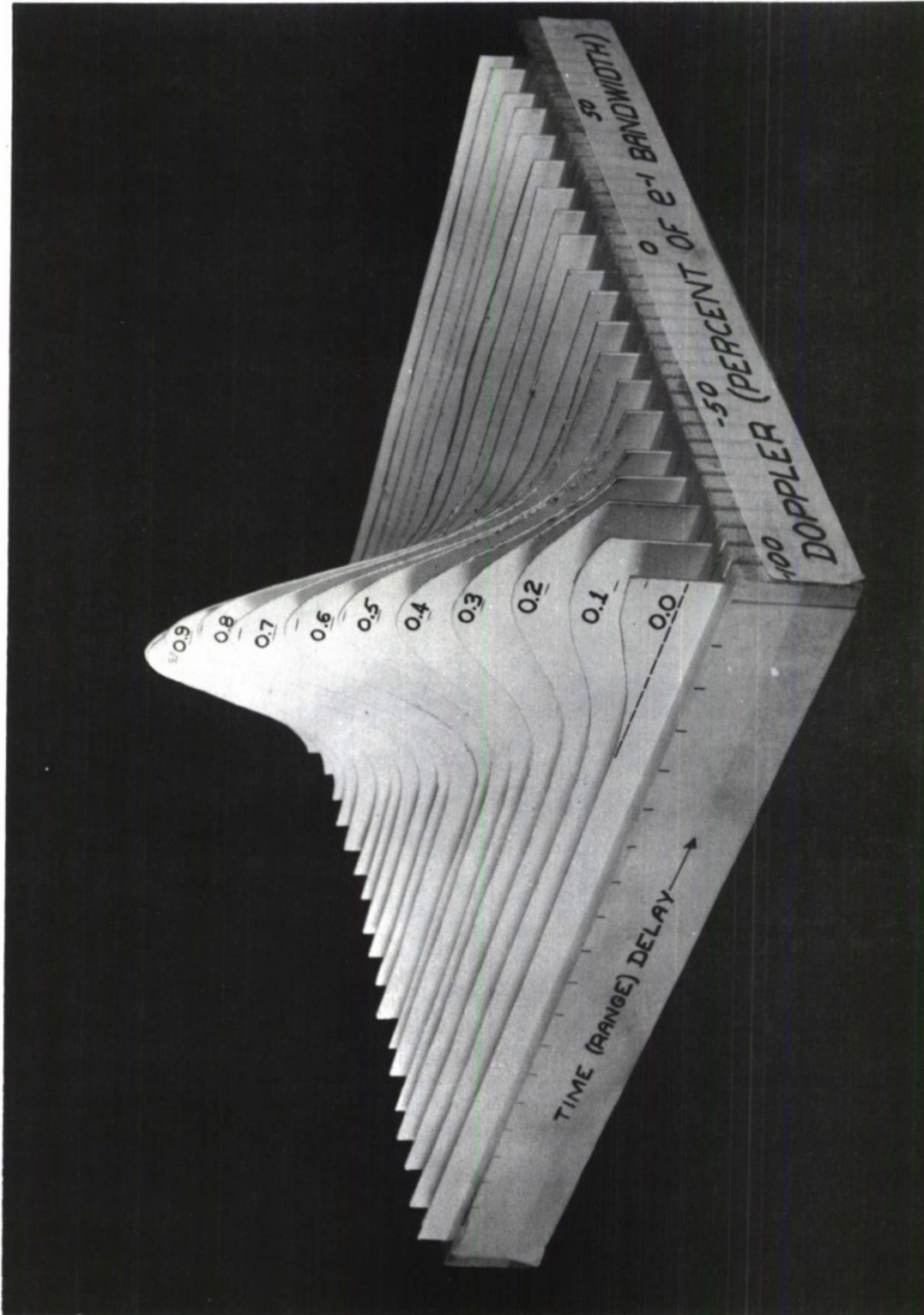


Fig. 25 Photograph of a model of the $|X|$ function of the linear FM Gaussian signal. (Taken from Fowle et al., Ref. 13, with permission.)

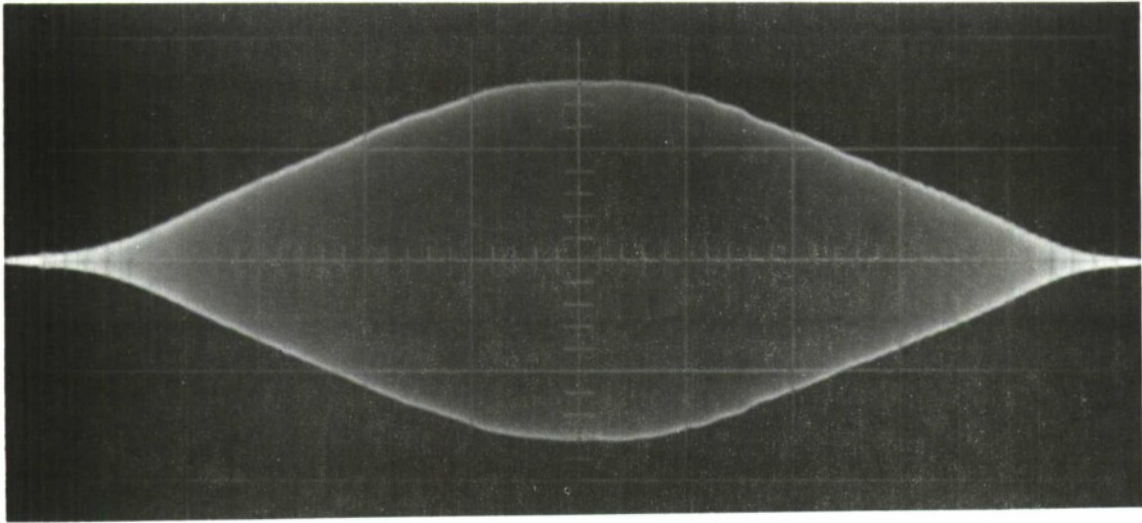


Fig. 26 Observed linear FM Gaussian signal generated by applying a short pulse to a linear filter. (Taken from Fowle et al, Ref. 13, with permission.)

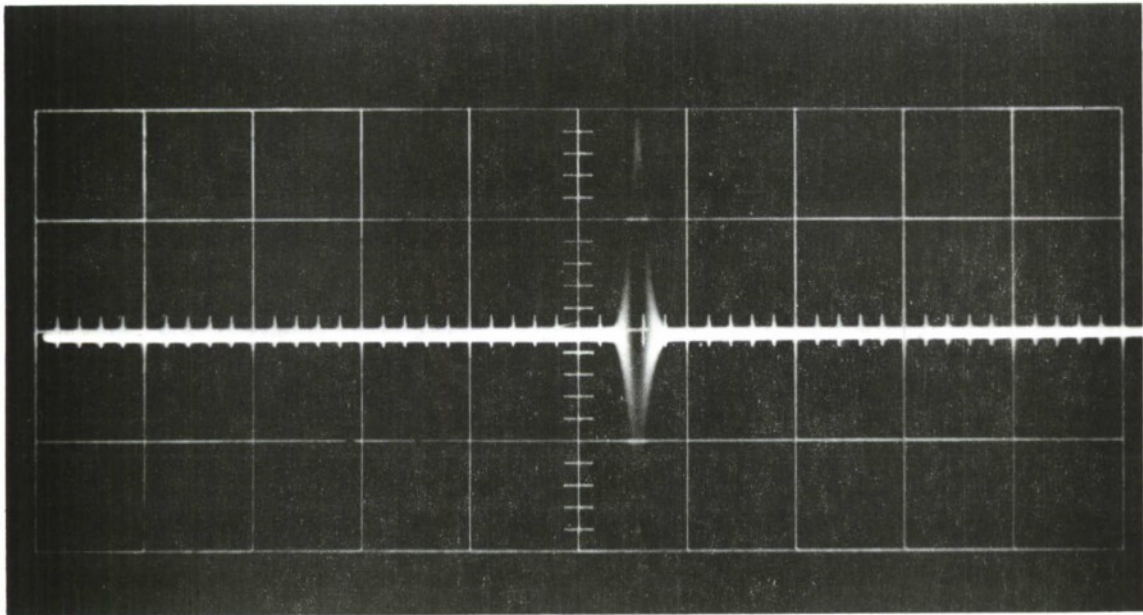


Fig. 27 Output waveform of the filter matched to the linear FM Gaussian signal when the signal has zero Doppler shift. (Taken from Fowle et al, Ref. 13, with permission.)

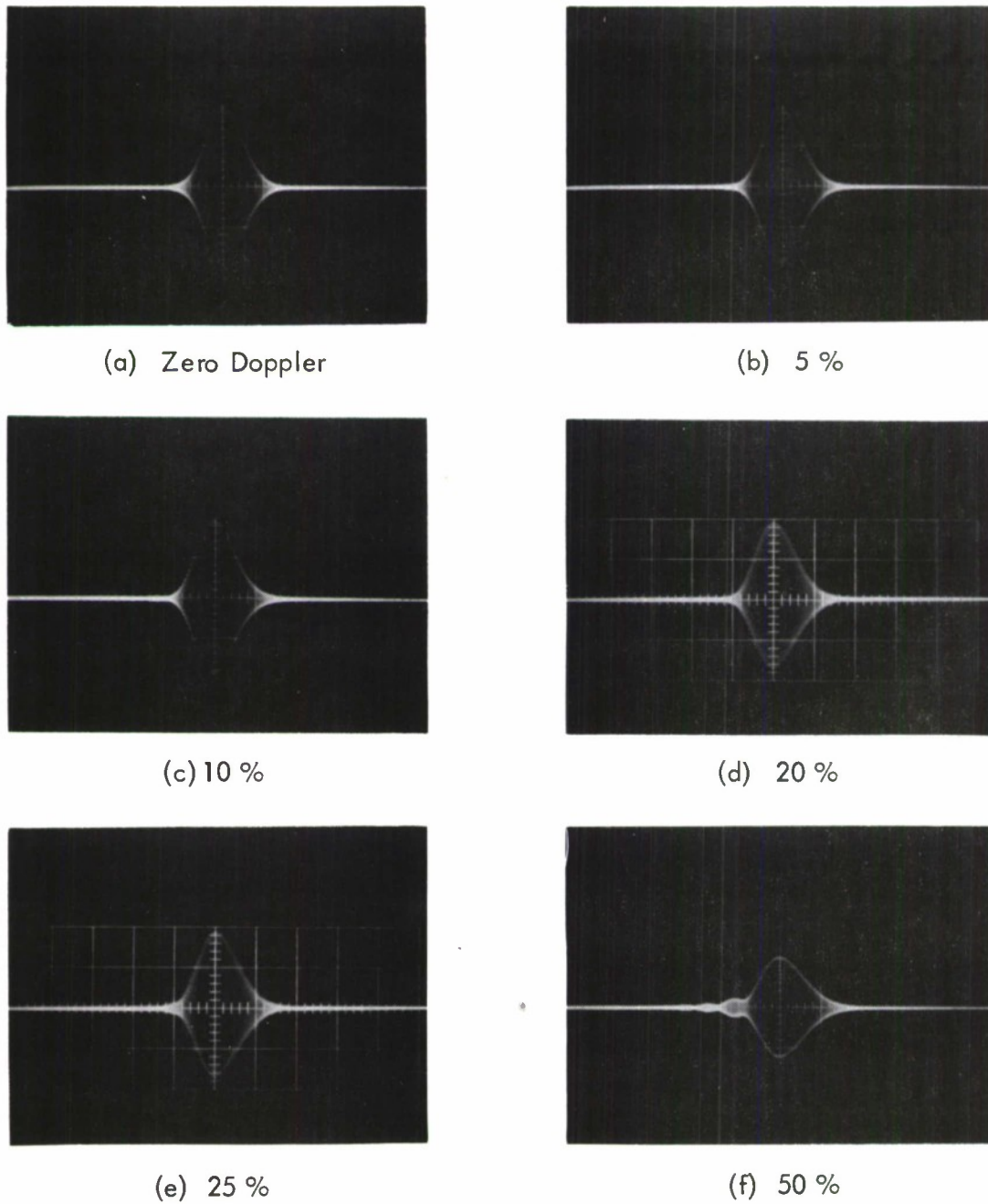


Fig. 28 Output waveform of the filter matched to the linear FM Gaussian signal when the signal has various Doppler shifts. Amount of Doppler shift is given as a percent of the 3-db signal bandwidth. (Taken from Fowle et al., Ref. 13, with permission.)

Doppler shift in the signal on the shape of the matched filter output waveform. (The time shift of the peak caused by the Doppler shift has been suppressed in the photographs.) The shape of the receiver output waveform does not change appreciably for Doppler shifts of up to 25 percent of the signal bandwidth; the sidelobes remain low. The shape of the output waveform changes considerably in Fig. 28(f) for a Doppler shift of 50 percent of the signal bandwidth, but this is due to the details of the equipment used.

3.11 Design of Phase-modulated Signals with Two-dimensional Correlation Functions of the Thumbtack Shape*

So far in this chapter we have discussed a variety of phase-modulated signals, most of which have been useful over a (relatively) narrow range of Doppler frequency shifts. If the signal χ function were sharply peaked at the origin and low elsewhere in the time-Doppler plane, it would be possible to locate a signal echo accurately in time and frequency and hence, permit simultaneous measurement of target range and radial velocity. In this section we will discuss a particular class of signals whose χ functions are sharply peaked at the origin and which have, approximately, the shape of a thumbtack with its point up.

To begin our discussion, let us represent the signal correlation function in terms of $u(t)$. We have

$$\chi(\tau, \nu) = \int_{-\infty}^{\infty} u(t) \bar{u}(t + \tau) \exp(-j2\pi \nu t) dt \quad (147)$$

*The material in this section is taken from Fowle, Ref. 33.

To place the phase modulation in evidence, we substitute $u_e(t) e^{j\varphi(t)}$ for $u(t)$ in Eq. (147).

$$\chi(\tau, \nu) = \int_{-\infty}^{\infty} u_e(t) u_e(t + \tau) \exp -j[2\pi\nu t - \varphi(t) + \varphi(t + \tau)] dt \quad (148)$$

Now let us evaluate the integral in Eq. (148) above by the method of stationary phase. For a given Doppler shift, ν , and time shift, τ , the argument of the exponential is stationary when its derivative is zero, that is, when

$$\frac{d}{dt} [2\pi\nu t - \varphi(t) + \varphi(t + \tau)] = 0 \quad (149)$$

The stationary point is given by the value of t which satisfies the equation

$$2\pi\nu - \varphi'(t) + \varphi'(t + \tau) = 0 \quad (150)$$

Assume Eq. (150) above is satisfied for $t = t_s$. The instantaneous frequency, $f(t)$, is related to $\varphi'(t)$ by the relation

$$2\pi f(t) = \varphi'(t) \quad (151)$$

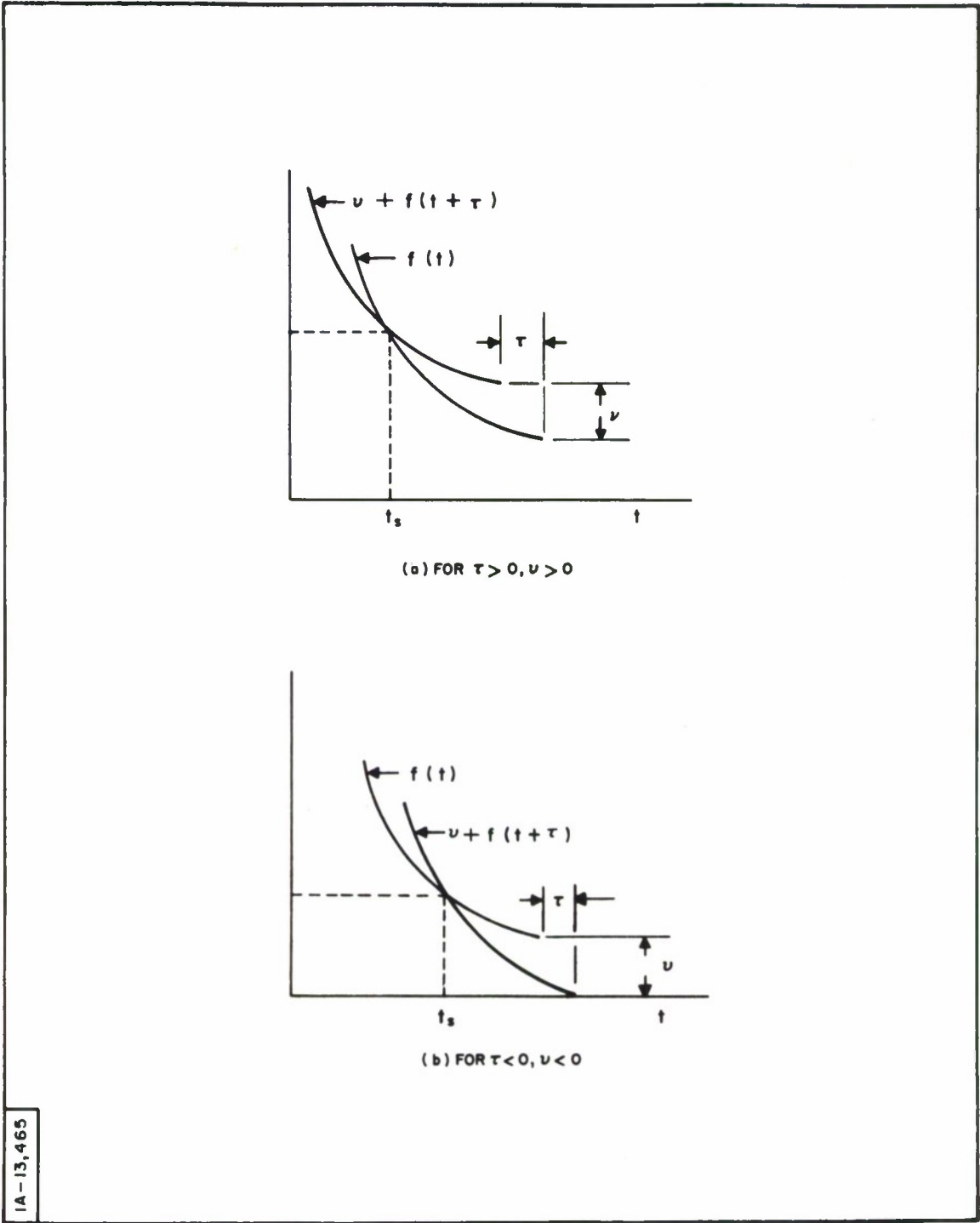
In terms of the frequency, $f(t)$, Eq. (150) above becomes

$$\nu + f(t_s + \tau) - f(t_s) = 0 \quad (152)$$

If the frequency sweep is unidirectional with time, we have the situation illustrated in Fig. 29. In the figure the solution of Eq. (152) for t_s is indicated graphically. By inspection of Fig. 29, one can see how the stationary point, t_s , moves with time shift, τ , and Doppler shift, ν . In Fig. 29(a), where ν and τ are both greater than zero, and in Fig. 29(b), where ν and τ are both less than zero, a stationary point exists. For values of τ and ν in the first and third quadrants of the τ, ν plane, where a stationary point exists, the integral which gives $\chi(\tau, \nu)$ will tend to have non-zero value. In the second and fourth quadrants a stationary point does not exist, as shown in Fig. 30, and the integral which gives $\chi(\tau, \nu)$ will tend to have zero value. Where a stationary point exists, we can evaluate the integral for $\chi(\tau, \nu)$, Eq. (148), by the method of stationary phase described in an earlier section. We obtain for $\chi(\tau, \nu)$

$$\chi(\tau, \nu) \cong \begin{cases} \sqrt{2\pi} \frac{u_e(t_s) u_e(t_s + \tau)}{\sqrt{|\beta''(t_s)|}} \exp j[2\pi \nu t_s - \varphi(t_s) + \varphi(t_s + \tau) \pm \frac{\pi}{4}] & \text{for } \nu, \tau > 0 \\ & \text{and } \nu, \tau < 0 \\ 0 & \text{, otherwise} \end{cases} \quad (153)$$

where $\beta(t) = 2\pi \nu t - \varphi(t) + \varphi(t + \tau)$ and $\beta''(t)$ is the second derivative with respect to time. We take + for $\beta''(t_s) > 0$ and - for $\beta''(t_s) < 0$. There are two objectives at this point in our development. First we want to determine what kind of phase modulation we should use to make $\chi(\tau, \nu)$ small in the regions of the τ, φ plane where it has value. Second, since the total volume under $|\chi(\tau, \varphi)|^2$ is constrained, to make $\chi(\tau, \nu)$ as small as possible everywhere in the τ, φ plane away from the origin, we should probably try

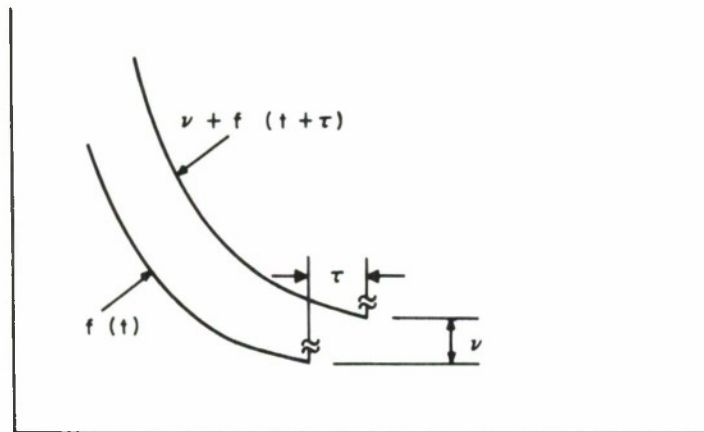


(a) FOR $\tau > 0, \nu > 0$

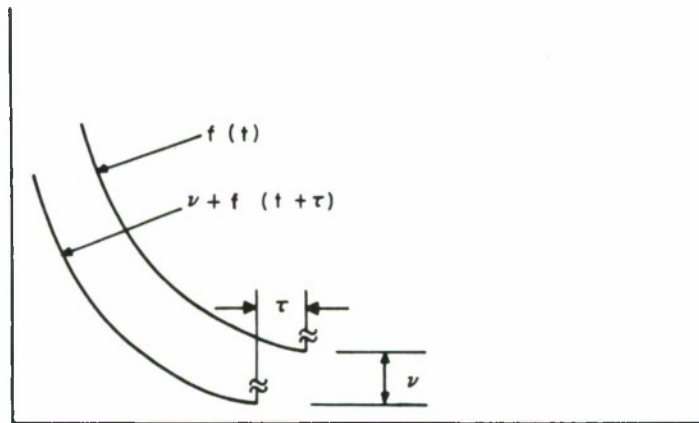
(b) FOR $\tau < 0, \nu < 0$

IA-13,465

Fig. 29 Solution of Eq. (152) for t_s , illustrated graphically. (a) for $\tau > 0, \nu > 0$; (b) for $\tau < 0, \nu < 0$.



(a) FOR $\tau < 0, \nu > 0$



(b) FOR $\tau > 0, \nu < 0$

IA-13,466

Fig. 30 Solution of Eq. (152) for t_s , illustrated graphically. (a) for $\tau < 0, \nu > 0$; (b) for $\tau > 0, \nu < 0$.

to spread the volume out uniformly rather than let it concentrate in the first and third quadrants.

The latter problem has a simple solution, so let us consider it first. We can cause $\chi(\tau, \nu)$ to have value in the second and fourth quadrants by re-designing the shape of the frequency sweep so that a stationary point exists for values of τ and ν in those quadrants. A frequency sweep which does this is illustrated in Fig. 31 for two of the four quadrants. The frequency sweep shown first decreases and then increases; a sweep which first increased and then decreased would do quite as well. The frequency sweep shown in Fig. 31 is an even function about its center; it does not have to be even, but there is probably no reason why it should not be. Let us consider, then, that for our purpose the frequency sweep is an even function. Now $\chi(\tau, \nu)$ has a stationary point in all four quadrants everywhere, except on the ν axis; with the surface $|\chi|$ more nearly uniform, it can be lower and still satisfy the volume constraint on $|\chi(\tau, \nu)|^2$.

We have the first problem yet to answer: What should the nature of the phase modulation be to cause $\chi(\tau, \nu)$ to be small in the regions where it has value? First we note that the stationary phase solution for $\chi(\tau, \nu)$ now applies everywhere except near the origin and on the ν axis. We have

$$\chi(\tau, \nu) \cong \sqrt{2\pi} \frac{u_e(t_s) u_e(t_s + \tau)}{\sqrt{|\beta''(t_s)|}} \exp j \left[\beta(t_s) \pm \frac{\pi}{4} \right] \quad (154)$$

We have hypothesized that the product of the envelopes is to be slowly varying; the envelope product cannot, therefore, be manipulated to make $\chi(\tau, \nu)$ small. The exponential has a modulus of unity. Clearly if $\chi(\tau, \nu)$ is to be small, the function $|\beta''(t_s)|$ must be large for every t_s . Let us see how this may be done. We have for $\beta(t)$

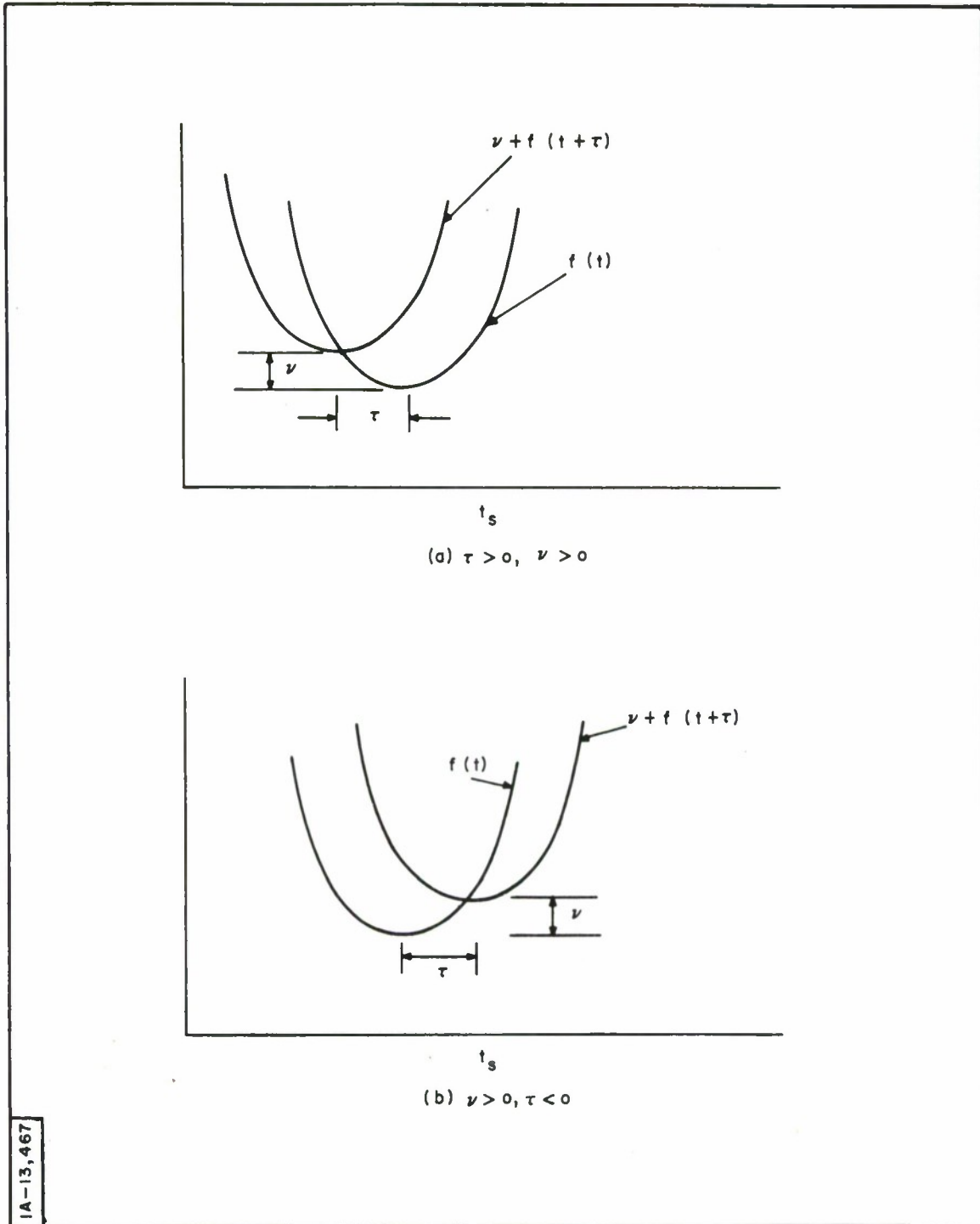


Fig. 31 Solution of Eq. (152) for a symmetrical frequency sweep. (a) $\tau > 0, \nu > 0$; (b) $\nu > 0, \tau < 0$.

$$\beta(t) = 2\pi \nu t + \varphi(t + \tau) - \varphi(t) \quad . \quad (155)$$

By differentiating Eq. (155) twice with respect to t and substituting $t = t_s$ we obtain

$$\beta''(t_s) = \varphi''(t_s + \tau) - \varphi''(t_s) \quad . \quad (156)$$

In Eq. (156) above let us expand $\varphi''(t + \tau)$ in a Taylor's series about $t = t_s$. We obtain

$$\begin{aligned} \beta''(t_s) &= \varphi''(t_s) + \varphi'''(t_s) \tau + \frac{\varphi^{IV}(t_s)}{2!} \tau^2 + \dots - \varphi''(t_s) \\ &= \varphi'''(t_s) \tau + \frac{\varphi^{IV}(t_s)}{2!} \tau^2 + \dots \quad . \quad (157) \end{aligned}$$

In terms of the instantaneous frequency $f(t)$, $\beta''(t_s)$ becomes

$$\beta''(t_s) = 2\pi \left[f''(t_s) \tau + \frac{f'''(t_s)}{2!} \tau^2 + \dots \right] \quad . \quad (158)$$

Equation (158) states that before $|\beta''(t_s)|$ can begin to be large, the frequency sweep must have a non-zero second derivative. Vee-shaped linear frequency sweeps, for example, will not do, because the second derivative is zero. At least a quadratic frequency sweep is required before $\beta''(t_s)$ can be large and $\chi(\tau, \nu)$ therefore small. The existence, in the frequency sweep, of derivatives higher than the second will help make $\beta''(t_s)$ even larger and χ even smaller.

Let us recapitulate our progress up to this point. We first make the frequency sweep bi-directional, that is, a downward sweep followed by an upward sweep (or vice versa) to cause the χ function to have some value in all four quadrants of the τ, ν plane so that the volume under $|\chi|^2$ would be spread over all four quadrants. Next we saw that to make the χ function small away from the origin, the second and higher derivatives of the frequency sweep should be large. No stationary point exists, however, in the integral of Eq. (148) for points on the ν axis, and we ask how the χ function may be controlled there. With $\tau = 0$ in Eq. (148), we see that $\chi(0, \nu)$ is given by the Fourier transform of the square of the signal envelope, $u_e(t)$. Given a desired shape for $\chi(0, \nu)$, one may then compute the required signal envelope shape. We have thus determined one method of constructing a signal so that its two-dimensional correlation function will be sharply peaked at the origin of the τ, ν plane and low elsewhere.

The facts that we have deduced about the characteristics necessary to the frequency sweep of a signal to cause its χ function to assume the thumbtack shape confirm our experience and extend our ideas. For example, the χ -function modulus has been given by Miedema^[54] for a signal with a vee-shaped linear frequency sweep. Figure 32 shows the envelope and frequency versus time of

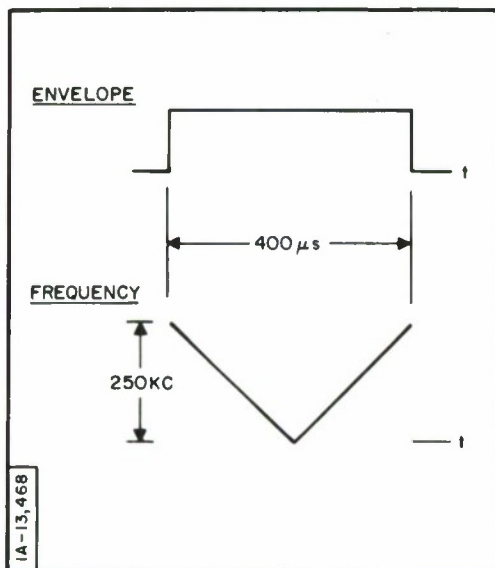


Fig. 32 Envelope and frequency sweep of the vee-shaped linear FM signal.

the signal, and Fig. 33 shows a photograph of a model of the χ function of the signal in the region near the origin of the τ, ν plane. The shape is not very much like that of a thumbtack and indeed, according to our argument it should not be.

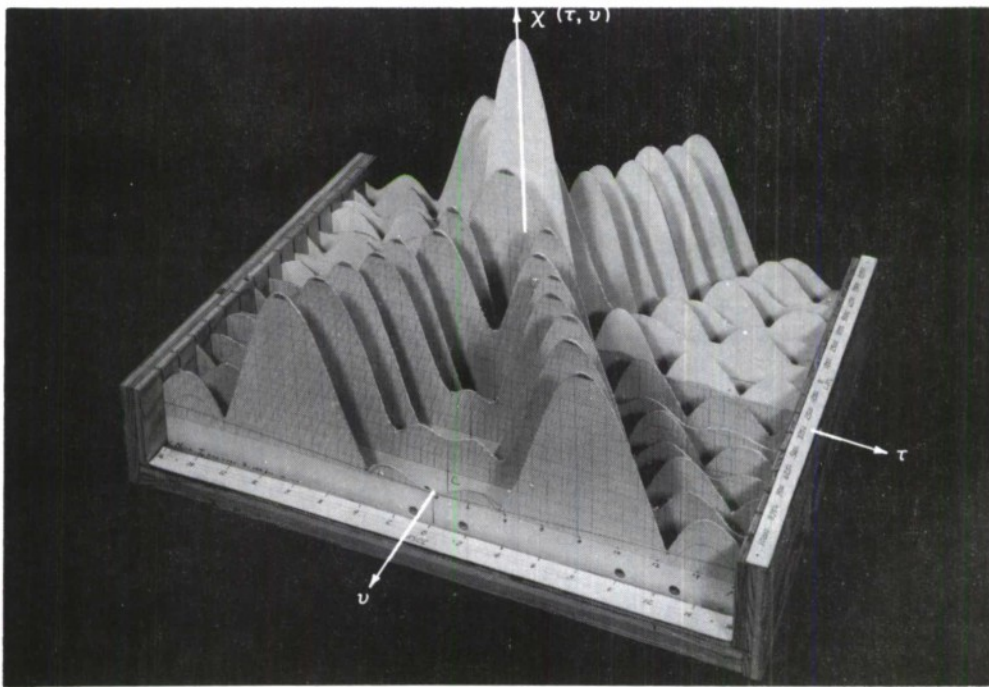


Fig. 33 $|\chi|$ function of the vee-notch linear FM signal of Fig. 32. Region shown is near the origin of the τ, ν plane. (Photo courtesy of Western Electric Company and H. Miedema, of Bell Telephone Laboratories.)

In Fig. 34 we have the envelope and instantaneous frequency vs. time for a quadratic FM signal.* Figure 35, from Miedema,^[54] shows a photograph of a model of the χ function of the signal, again in the vicinity of the origin. Notice that the χ function of the quadratic FM signal is much closer to the desired thumbtack shape, as our argument above says it should be. The

*The quadratic FM signal was proposed independently by Richman, Ref. 35 and by Callahan, Ref. 36.

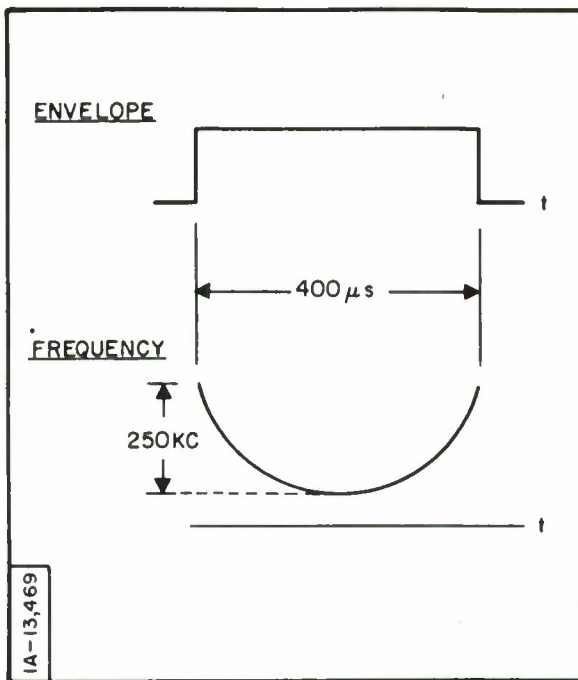


Fig. 34 Envelope and frequency sweep of a quadratic FM signal.

shape in Fig. 35 is a dramatic improvement over that of the χ function of the vee-notch FM signal of Fig. 33. The envelope shape of both the vee-notch FM signal and the quadratic FM signal is rectangular. Smoother signal envelopes would no doubt lead to smoother χ functions. However, a smooth envelope would not eliminate the very high ridges in the χ function of the vee-notch FM signal.

χ functions of signals with frequency sweeps of higher power than quadratic have not, to the author's knowledge, been computed, although there is no practical reason why they cannot be. The stationary phase argument given above indicates that such signals should have χ functions which are better approximations to the thumbtack shape than the quadratic FM signal.

It is interesting, at this point, to inquire whether there are other types of signals that have χ functions of the general thumbtack shape. We

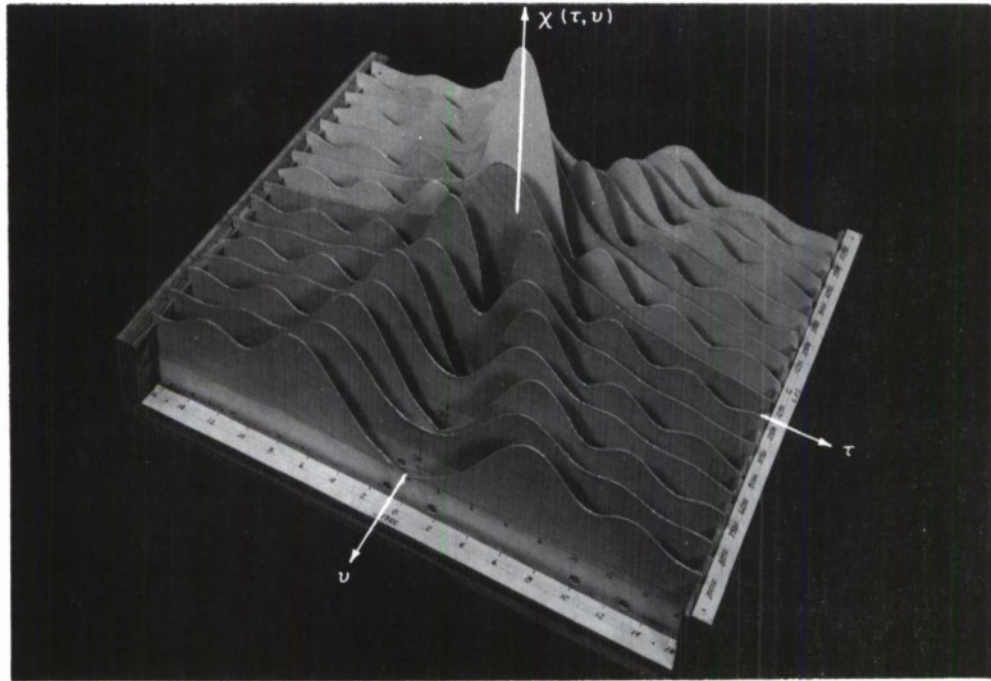


Fig. 35 $|\chi|$ function of the quadratic FM signal of Fig. 33. Region shown is near the origin of the τ, ν plane. (Photo courtesy of Western Electric Company and H. Miedema, of Bell Telephone Laboratories.)

recall that it was noted in Section 2.0 that if a signal gives a certain χ function, then its Fourier transform, if taken for the signal, yields the same χ function but rotated 90° in the τ, ν plane. A signal with a symmetrical envelope and symmetrical frequency sweep has a Fourier transform with a highly structured modulus and a phase which alternates between zero and π . In short, the Fourier transform, taken as the signal, is an amplitude-modulated phase-reversal signal. Or to put it another way, certain phase-reversal signals also have χ functions which approximate the thumbtack shape. Figure 36, for example, shows another photograph of the model of the χ function of the 13-code, phase-reversal signal. Note the similarity between the shape of the χ function of the 13-code signal and that of the χ function of the vee-notch FM signal.

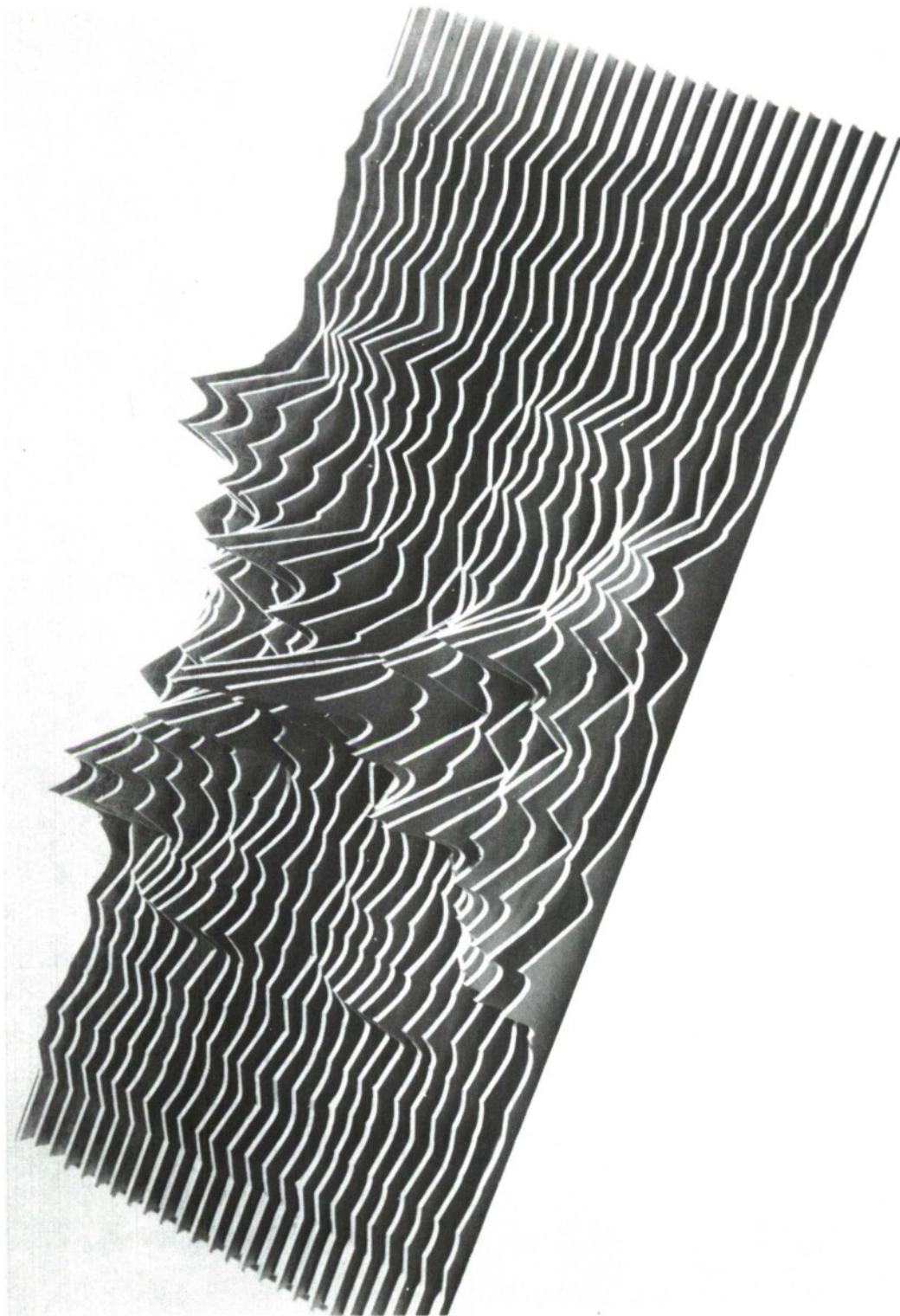


Fig. 36 The two-dimensional correlation function of the 13-code signal. Profiles are taken vs. time at intervals of $1/4 \Delta$ in Doppler, where Δ is the duration of the signal. (Taken from Key et al., Ref. 31, with permission.)

In the next section we shall discuss a procedure for the design of phase-reversal signals which have χ functions of the general thumbtack shape but which have smoother skirts than the χ function of the 13-code signal.

3.12 Amplitude-modulated, Phase-reversal Signals with χ functions of the Thumbtack Shape*

In the last section we saw that signals of large time-bandwidth product with smoothly varying envelopes and symmetrical, highly curved frequency sweeps had χ functions of the general thumbtack shape. The Fourier transform of such a signal has a highly structured modulus and a phase which changes by π radians at points in frequency where the modulus is zero. Thus we see that we can get a thumbtack χ function by transmitting certain kinds of amplitude-modulated, phase-reversal signals. Since the phase-reversal signal is attractive because of the relative ease with which it can be generated and received (see Section 4.0), it seems worthwhile to explore the matter further. Earlier in Section 3.0 we considered the problem of designing phase-reversal signals to have χ functions of useful shape in a narrow Doppler region on either side of the time axis. In that case we had to worry only about choosing codes that had good autocorrelation functions. Here we have the problem of choosing codes that have good two-dimensional properties. The problem seems very difficult. How do we proceed?

An ingenious method of approach has been invented by Lerner. [37]
To explain Lerner's method, let us for the moment assume that we have a signal which consists of a periodic sequence of numbers. The periodic function has, of course, a line spectrum. The χ function associated with such a periodic

* The material in this section is taken from Lerner, Ref. 37.

sequence must be zero except for values of Doppler shift equal to multiples of the line spacing, and it must be zero except for values of time equal to multiples of the space in time between the members of the sequence. The χ function of such a periodic sequence thus has value only at lattice points in the τ, ν plane, and, of course, it is periodic in both time and Doppler. The value the χ function has will be a maximum for values of τ and ν equal to multiples of the period of the sequence in time and frequency, respectively. The values χ has in between must, by Theorem 13 of Section 2.0, be less than the maximum values. For our purpose here, an ideal sequence would have a ψ function (i. e., $|\chi|^2$) whose values at the lattice points would be uniform and, of course, small compared to the maximum values.

The next step is to truncate the periodic sequence (which we tentatively took for the signal at the beginning of this discussion) in time and to truncate its spectrum in frequency. The χ function of the sequence after truncation in time is given by the convolution in the Doppler direction of the χ function of the periodic sequence with the χ function of the time-truncating function. The χ function following frequency truncation, analogously, is given by the convolution in the time direction of the χ function of the time-truncated sequence with the χ function of the spectrum-truncating function. This is the statement of Theorem 11 of Section 2.0 for Θ functions, and the same theorem also holds for χ functions. Quite obviously, if the function used for time truncation is chosen so that its χ function has an extent in Doppler less than or about equal to the spacing in Doppler of the lines of the χ function of the periodic sequence, then the χ function of the truncated sequence will be at least as low, relatively, in regions away from the maximum values as was the χ function of the sequence before truncation. Analogously, the spectrum-truncating function should be chosen to have a χ function with an extent in time less than or about equal to

the spacing in time of the lines of the χ function of the sequence. Thus, if the truncations are done carefully, the space between the lines of the χ function of the periodic sequence is filled in (by the convolution processes) without raising the level of the χ function away from the origin in the τ, ν plane relative to the maximum value. The signal that one transmits is the time- and frequency-truncated sequence.

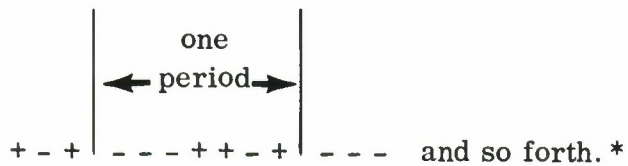
To implement the design procedure we have given above, we need periodic sequences which have χ functions that are uniformly low away from the periodic lattice points. Useful periodic sequences are the so-called maximal length, binary shift register sequences (abbreviated to M-sequences) which have been studied by Zierler^[26] and used by Lerner and others in the design of signals. In the material which follows in this section we will discuss a method of generation of M-sequences, give a few of their properties, and calculate their χ functions. Finally, we will give an example of a signal derived from an M-sequence and give its χ function.

An M-sequence is a set of plus and minus ones (x_p) such that for all p the next member of the sequence is given by the product

$$x_{p+1} = x_p^{y_1} x_{p-1}^{y_2} x_{p-2}^{y_3} \dots x_{p-n+1}^{y_n} \quad (159)$$

in which the numbers y_k are either one or zero. With a set of y 's and an initial set of x 's, Eq. (159) generates a sequence (x_p) which, after an initial transient, is periodic. The period of the sequence is at most $2^n - 1$. For a given n there is always at least one sequence of maximal length.

For example, if we take $n = 3$, $y_1 = 0$, $y_2 = 1$, $y_3 = 1$, and $x_p = -1$, $x_{p-1} = -1$, $x_{p-2} = 1$, the sequence one obtains (which has length 7) is



Some of the properties of M-sequences as given by Lerner are of interest here. They are as follows:

(1) The algebraic sum of the x 's taken over a period P is minus one. That is

$$\sum_p x_p = -1 \quad . \quad (160)$$

(2) The product of two M-sequences one of which is a translate of the other is itself a translate of the same sequence. That is

$$(x_p x_{p+k}) = (x_{p+h}) \quad , \quad k \neq 0 \text{ mod } P \quad . \quad (161)$$

(3) The autocorrelation function of a sequence (x_p) has a period P . At the origin its value is P , elsewhere in the period it is (-1) . That is

$$\begin{aligned} \sum x_p x_{p+k} &= P \quad , \quad k = 0 \text{ mod } P \\ &= -1 \quad , \quad k \neq 0 \text{ mod } P \quad . \end{aligned} \quad (162)$$

* The seven-bit sequence marked off constitutes one period; by accident it turns out to be the 7th order Barker code (see Table 1, Section 3.0).

(4) The Fourier transform of the periodic sequence (x) is another periodic sequence of complex numbers (X) with period P . The zero order term and those which occur at multiples of the period have magnitude one. The other terms all have magnitude of $\sqrt{P+1}$. That is

$$X_m = \sum_p x_p e^{j \frac{2\pi}{P} pm}$$

$$|X_m|^2 = 1, \quad m = 0 \pmod{P}$$

$$= P+1; \quad m \neq 0 \pmod{P} \quad . \quad (163)$$

Now we are in a position to compute the analog of the χ function, b_{ks} , for the M-sequence which we take as a_n . We have

$$b_{ks} = \sum_n a_n \bar{a}_{n+k} e^{j \frac{2\pi}{P} ns} \quad . \quad (164)$$

Here k and s are parameters of the two-dimensional sequence analogous to the variables τ and ν , respectively. The a_n are real, of course, and using Property (2) above, Eq. (164) becomes

$$b_{ks} = \sum_n a_{n+h} e^{j \frac{2\pi}{P} ns}, \quad k \neq 0 \pmod{P} \quad . \quad (165)$$

But the right side of Eq. (165) gives the Fourier coefficients of the sequence a_n shifted by h . Use of the shifting rule of Fourier Series on Eq. (165) gives

$$b_{ks} = A_s e^{-j \frac{2\pi}{P} hs}, \quad k \neq 0 \pmod{P} \quad (166)$$

Also

$$b_{ks} = \sum_n e^{j \frac{2\pi}{P} ns}, \quad k = 0 \pmod{P} \quad (167)$$

We represent the squared moduli of the b_{ks} , the ambiguity function of the M-sequence, by C_{ks} . Using Eqs. (163), (166), (167) and the relation

$$\sum_{n=1}^P \exp\left(j \frac{2\pi}{P} n\right) = 0, \text{ we obtain for } C_{ks}$$

$$\left. \begin{aligned} C_{ks} &= P^2, \quad k, s = 00 \pmod{P} \\ &= 0, \quad k=0 \pmod{P}, \quad s \neq 0 \pmod{P} \\ &= 1, \quad k \neq 0 \pmod{P}, \quad s = 0 \pmod{P} \\ &= P + 1, \quad \text{elsewhere} \end{aligned} \right\} \quad (168)$$

The ambiguity function for an M-sequence of length 7 is sketched in Fig. 37.

Now let us consider a signal consisting of very narrow pulses with complex magnitudes $a_n(t)$. Let the period be of duration T_1 and the interval between pulses T_1/P . The ambiguity function $\chi(\tau, \nu)$ will look like C_{ks}

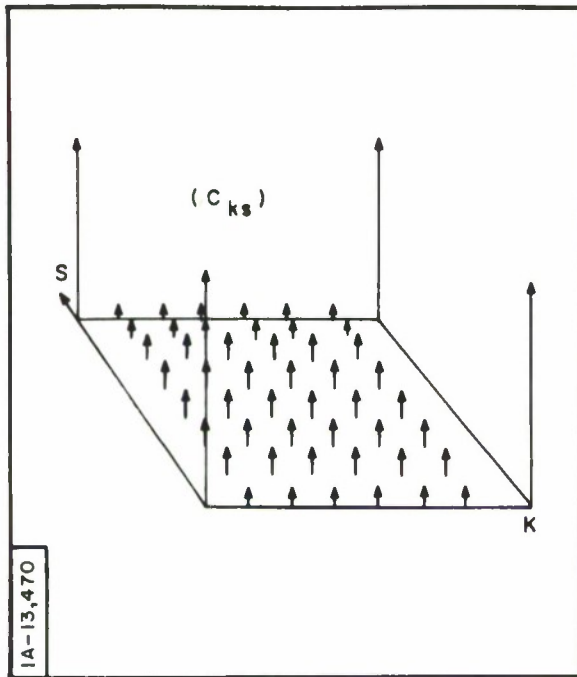


Fig. 37 The ambiguity function of a 7-digit M-sequence. (Taken from Lerner, Ref. 37, with permission.)

where the intervals in k correspond to T_1/P in τ , and the intervals in s correspond to $1/T_1$ in ν . We now truncate this sequence in time by $h(t)$ where

$$h(t) = \frac{\sin \pi t/T_1}{\pi t/T_1} \quad (169)$$

The χ function corresponding to $h(t)$ has an extent of roughly $1/T_1$ in the ν direction, which is equal to the spacing of the lines of the χ function of the M-sequence in Doppler. Next we truncate the function in frequency by $g(f)$ where

$$g(f) = \frac{\sin \pi T_1 f/P}{\pi T_1 f/P} \quad (170)$$

The χ function associated with $g(f)$ has a duration of about T_1/P , the line spacing in the τ direction. The $|\chi|$ function of the time- and frequency-truncated 7-digit M-sequence is shown in Fig. 38. Notice in our example that the time duration of the signal is approximately T_1 , and the bandwidth P/T_1 . The time-bandwidth product, TW , is then

$$TW = P \quad (171)$$

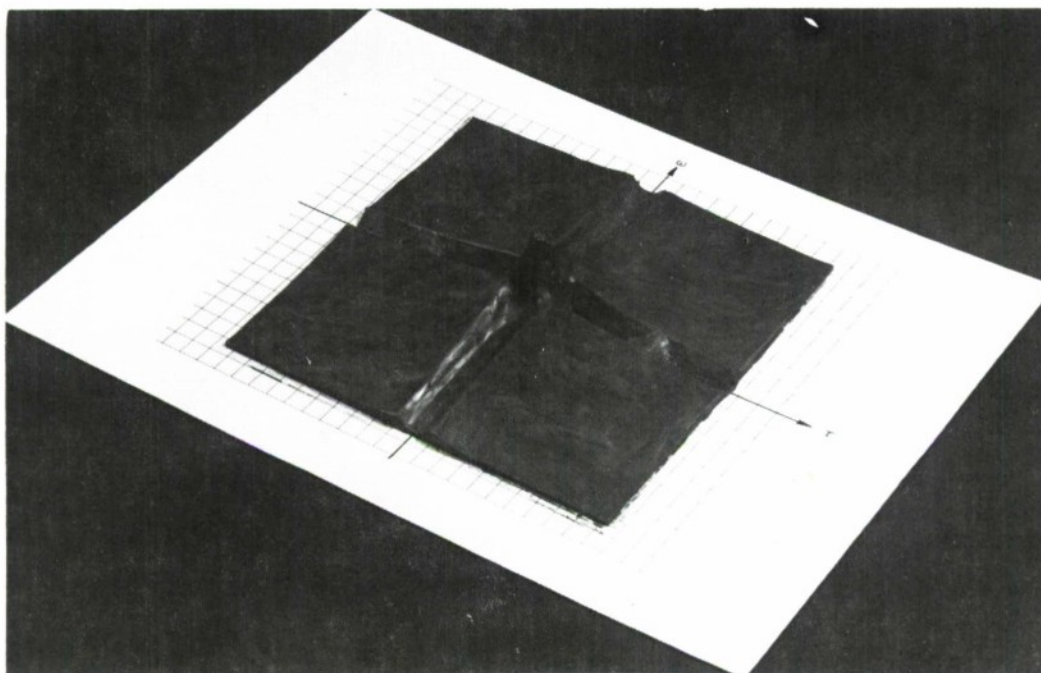


Fig. 38 $|\chi|$ function of the truncated 7-digit M-sequence. (Taken from Lerner, Ref. 37, with permission.)

The truncation has been designed so as to keep the relative levels of the peak and the skirts the same as those of the line function C_{ks} of Eq. (168). In the ambiguity function of Fig. 38, the peak-to-skirt ratio is approximately $P^2/P+1$. For the χ function, the ratio is $\sqrt{P^2/P+1}$. For long sequences, the skirts

of the χ function are below the peak by about \sqrt{P} , where P is the time-bandwidth product. It should be emphasized that when the $a_n(t)$ are given by the M-sequence, their values will be plus or minus one. The signal after truncation will be an amplitude-modulated, phase-reversal signal. When the $a_n(t)$ are complex (for example, if they are taken as the Fourier transform of an M-sequence), the phase of the resulting signal will, of course, be given by the phase angle of the $a_n(t)$.

Other truncations more conservative of time and bandwidth than those used here are discussed by Lerner.

3.13 Amplitude-modulated, Phase-reversal Signals With Circularly Symmetric χ Functions*

We shall now discuss a class of ambiguity functions that have the property that their moduli are functions of $\tau^2 + \nu^2$ only. A more general formulation would recognize the fact that a change of time scale $t' = at$, where a is a constant, maps the circles $\tau^2 + \nu^2 = \text{constant}$ into the ellipses $\tau'^2/a^2 + a^2\nu^2 = \text{constant}$, but this perspective would encumber the notation without particularly clarifying the discussion.

We consider the function

$$\Theta(\tau, \nu) = \chi(\tau, \nu) e^{-j\pi\tau\nu}, \quad (172)$$

the modulus of which is $|\chi(\tau, \nu)|$.

*This section, which depends on Klauder, Ref. 38, and on Wilcox, Ref. 16, was written by J. A. Sheehan.

Then a necessary and sufficient condition that $\Theta(\tau, \nu)$ should be a function of $\tau^2 + \nu^2$ only is that it should satisfy the differential equation

$$\nu \frac{\partial \Theta}{\partial \tau} - \tau \frac{\partial \Theta}{\partial \nu} = 0 \quad . \quad (173)$$

It can be shown that this equation for $\Theta(\tau, \nu)$ reduces to the following one for $u(t)$:

$$\frac{d^2 u(t)}{dt^2} - t^2 u(t) + \lambda u(t) = 0 \quad , \quad (174)$$

where λ is an arbitrary parameter. It can further be shown that the only values of λ which yield solutions $u(t)$ which are finite-energy waveforms are the odd integers, and we have the result that any solution of

$$\frac{d^2 u(t)}{dt^2} - t^2 u(t) + (2n + 1) u(t) = 0 \quad (175)$$

will produce an ambiguity function with a radially symmetric modulus.

The solutions of Eq. (175) are the Hermite functions

$$u_n(t) = e^{-t^2/2} H_n(t) \quad ,$$

where $H_n(t)$ is the n th Hermite polynomial

$$H_n(t) = (-1)^n e^{t^2} \frac{d^n e^{-t^2}}{dt^n} \quad .$$

The Θ function of Eq. (172) is, within a suitable normalizing factor,

$$\Theta(\tau, \nu) = L_n \left(\frac{\tau^2 + \nu^2}{2} \right) e^{-\frac{\tau^2 + \nu^2}{4}}, \quad (176)$$

where $L_n(x)$ is the Laguerre polynomial,

$$L_n(x) = e^x \frac{d^n}{dx^n} (x^n e^{-x})$$

It is important to note the fact that the Hermite functions solve a specific problem, that is, that the $\Theta(\tau, \nu)$ of Eq. (172) shall be radially symmetric. The discussion here does not preclude the possibility that other functions exist which have χ or Θ functions which have radially symmetric moduli.*

Figures 39(a) and 39(b) illustrate the 10th order Hermite function and its associated autocorrelation function, respectively, both of which are even functions. A view of the 10th order ambiguity surface is given in Fig. 40. With the type of ambiguity function shown in Fig. 40, there is no correlation of range and Doppler measurements, and both may be accurately measured simultaneously. The difficulty with the signal of Fig. 39(a) and its ambiguity function of Fig. 40 is that it is suitable for general use only with isolated targets according to the discussion in Section 2.0.

* This is one aspect of a more general situation: Statements relating to uniqueness, realizability, etc. of the complex function $\chi(\tau, \nu)$ are relatively easy to make; it has not yet been possible to establish analogous statements for $|\chi(\tau, \nu)|$.

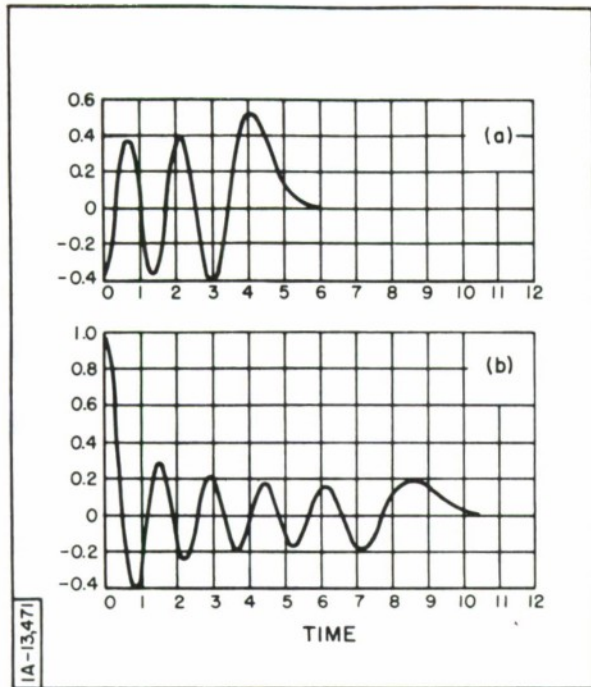
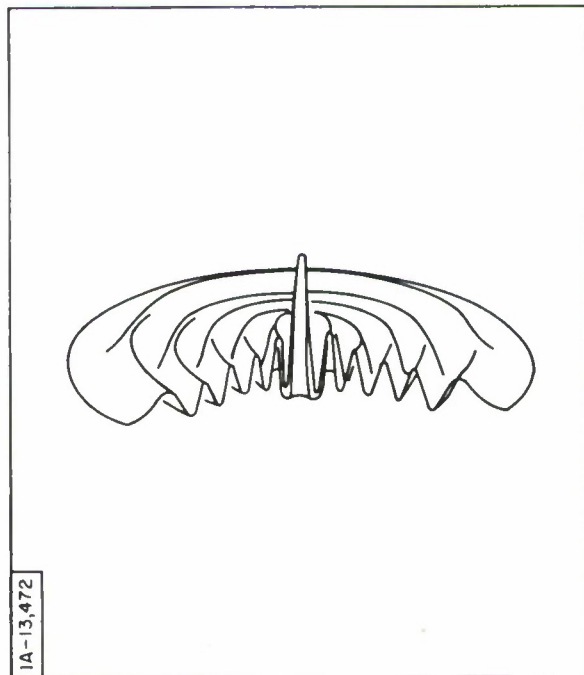


Fig. 39 (a) Envelope of 10th order Hermite function signal for positive time (envelope is an even function about the origin); (b) a radial section of the envelope of the two-dimensional correlation function of the signal of part (a). (Taken from Klouder, Ref. 38, with permission.)

Fig. 40 The radially symmetric two-dimensional correlation function associated with the 10th order Hermite function signal. (Taken from Klouder, Ref. 38, with permission.)



3.14 Pulse Burst Signals

According to the discussion in Section 2.0, the pulse burst signal has a χ function which has a shape that is useful when one wants to resolve (i. e. , detect) a large number of nearby objects and, at the same time, measure with high accuracy both the range and Doppler shift parameters of the objects. When the number of pulses in the burst is large, the peaks of the χ function near the origin of the τ, ν plane are nearly the same size, and in the presence of noise the measurements of range and Doppler are somewhat ambiguous (i. e. , which peak corresponds to true range and Doppler ?). When the ambiguity is objectionable, it may be removed by operation of the radar in different modes (perhaps by transmitting different signals) or by making measurements with a second radar, etc. The virtue of the χ function of the simple pulse burst signal is that it is identically zero in certain regions of the τ, ν plane. One way to make a χ function identically zero in regions of the time-Doppler plane is to make the signal identically zero at regularly spaced intervals in time (and, of course, non-zero in between). In this section we will augment the discussion of simple pulse burst signals given in Section 2.0. By "simple," we mean that the pulses in the burst are all at the same frequency and equally spaced in time. In the two sections that follow we will discuss pulse burst signals other than the simple kind.

It is interesting to apply Lerner's method, discussed earlier, to the problem of designing a pulse burst signal. We will take as a preliminary signal a periodic train of impulses and compute the associated χ function. Then we will see how one may truncate the train of impulses in time and frequency in such a way as to make the χ function assume a desirable shape and at the same time give a signal which can be transmitted.

Let the train of impulses be denoted by $u_1(t)$ thus,

$$u_1(t) = \sum_{n=-\infty}^{\infty} \delta(t - n\Delta) \quad , \quad (177)$$

where $\delta(t)$ is the unit impulse function. The two-dimensional correlation function, $\chi(\tau, \nu)$, is given by

$$\begin{aligned} \chi_1(\tau, \nu) &= \int_{-\infty}^{\infty} u_1(t) \bar{u}_1(t + \tau) e^{-j2\pi\nu t} dt \\ &= \sum_n \sum_m \int_{-\infty}^{\infty} \delta(t - n\Delta) \delta(t + \tau - m\Delta) e^{-j2\pi\nu t} dt \quad . \quad (178) \end{aligned}$$

Equation (178) may be written

$$\chi_1(\tau, \nu) = \sum_n \sum_m e^{-j2\pi\nu n\Delta} \delta[\tau - (m - n)\Delta] \quad . \quad (179)$$

$\chi_1(\tau, \nu)$ is, of course, periodic in both the τ and ν directions. The period in the τ direction is Δ ; we can see the shape of $\chi(\tau, \nu)$, then, by restricting $|\tau| \leq \Delta/2$, which requires that $m = n$ in Eq. (179). With $m = n$, the double sum in Eq. (179) becomes a single sum on n which may be evaluated to give for $\chi_1(\tau, \nu)$

$$\chi_1(\tau, \nu) = \frac{1}{\Delta} \sum_{p=-\infty}^{\infty} \delta\left(\nu - \frac{p}{\Delta}\right) \delta(\tau) \quad , \quad (180)$$

where it is understood that $|\tau| \leq \Delta/2$. The χ function of the train of impulses [Eq. (180)] is thus seen to be an array of impulses of uniform weight regularly spaced at intervals of $1/\Delta$ in the ν direction on lines which are themselves equally spaced by Δ in the τ direction. There is a clear space around the impulse at the origin of the τ, ν plane which is of extent Δ in time by $1/\Delta$ in Doppler frequency. The area of the clear space is unity. The point of the truncation process which follows is to create a signal which can be transmitted while at the same time keeping the spaces between the peaks of the χ function as clear as possible. We consider two truncation procedures out of the many that are possible. The first will give a very good χ function but yields a signal not economical of time or bandwidth. The second yields a convenient signal but a less attractive χ function.

Theorem 11 of Section 2.0 states that if $u_1(t)$ corresponds to $\chi_1(\tau, \nu)$ and if $u_2(t)$ corresponds to $\chi_2(\tau, \nu)$, then $u_3(t) = u_1(t) u_2(t)$ corresponds to $\chi_3(\tau, \nu)$ where

$$\chi_3(\tau, \nu) = \int_{-\infty}^{\infty} \chi_1(\tau, \mu) \chi_2(\tau, \nu - \mu) d\mu \quad . \quad (181)$$

The χ function of the product of two time functions is thus given by the convolution in the ν direction of the χ functions of the two time functions. We want to have the space between successive peaks in the ν direction as clear as possible, so we will want to convolve with the bed-of-spikes χ function, $\chi_1(\tau, \nu)$, a χ function, $\chi_2(\tau, \nu)$, which is narrow in the ν direction compared to $1/\Delta$. As a first example we let the time-truncating function, $u_2(t)$, be

$$u_2(t) = \frac{\sin \pi t/T}{\pi t/T} \quad , \quad (182)$$

where $T \gg \Delta$. The χ function of this function is given by Eq. (59) if signal and transform are interchanged. The effect of the truncation on the signal is sketched in Fig. 41, and the χ function which results from the convolution in the ν direction is sketched in Fig. 42.

We now consider the problem of the truncation of the spectrum of the impulse train signal. By Theorem 11 of Section 2.0, if $U_3(f)$ corresponds to $\chi_3(\tau, \nu)$ and $U_4(f)$ to $\chi_4(\tau, \nu)$, then $U_5(f) = U_3(f) U_4(f)$ corresponds to $\chi_5(\tau, \nu)$, where

$$\chi_5(\tau, \nu) = \int_{-\infty}^{\infty} \chi_3(t, \nu) \chi_4(\tau - t, \nu) dt \quad . \quad (183)$$

In keeping with our choice of $u_2(t)$, Eq. (182), we choose for $U_4(f)$

$$U_4(f) = \frac{\sin \pi f / F}{\pi f / F} \quad , \quad (184)$$

where $1/F \ll \Delta$. The χ function corresponding to the time- and frequency-truncated impulse train is shown in Fig. 43; the corresponding signal is sketched in Fig. 44.

The more usual pulse burst signal is obtained by truncation in time by a rectangular function and truncation in frequency by a $\sin y/y$ function. The resulting signal consists of a finite number of pulses of uniform amplitude. We take for $u'_2(t)$

$$u'_2(t) = \begin{cases} 1 & , \quad -\frac{T}{2} \leq t \leq \frac{T}{2} \\ 0 & , \quad \text{elsewhere} \end{cases} \quad . \quad (185)$$

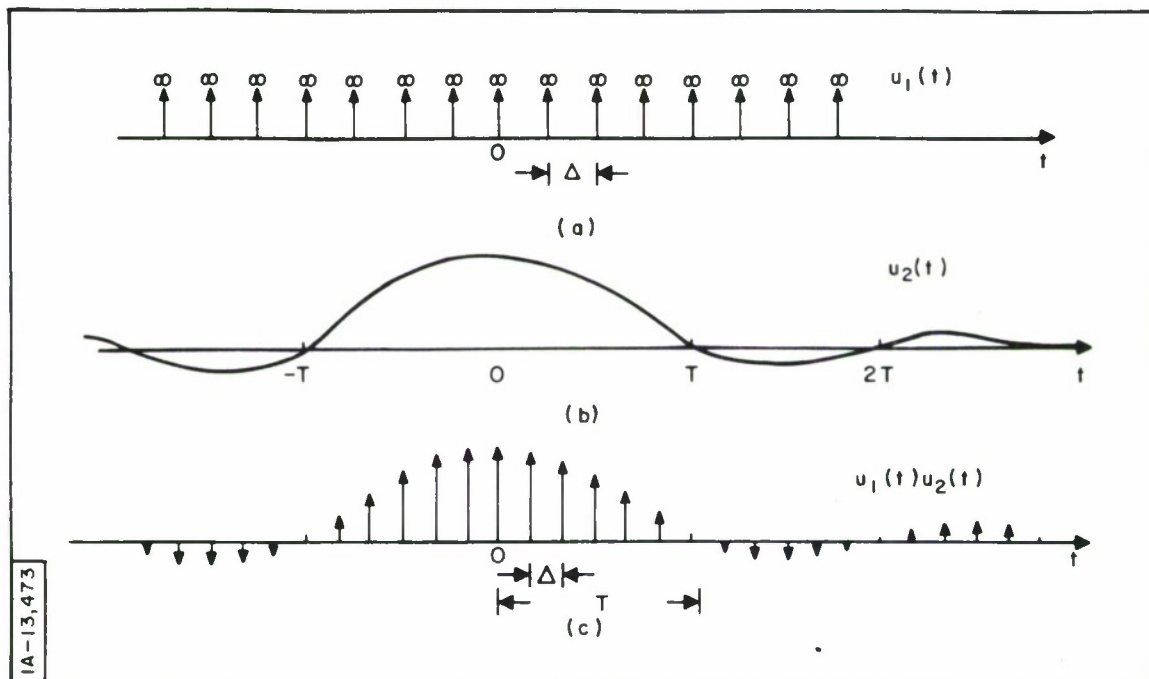


Fig. 41 The time truncation of the periodic impulse train. (a) The periodic train of impulses; (b) the $(\sin \pi t/T) (\pi t/T)$ truncating function; (c) time-truncated train of impulses. (Weight of impulse is indicated by height.)

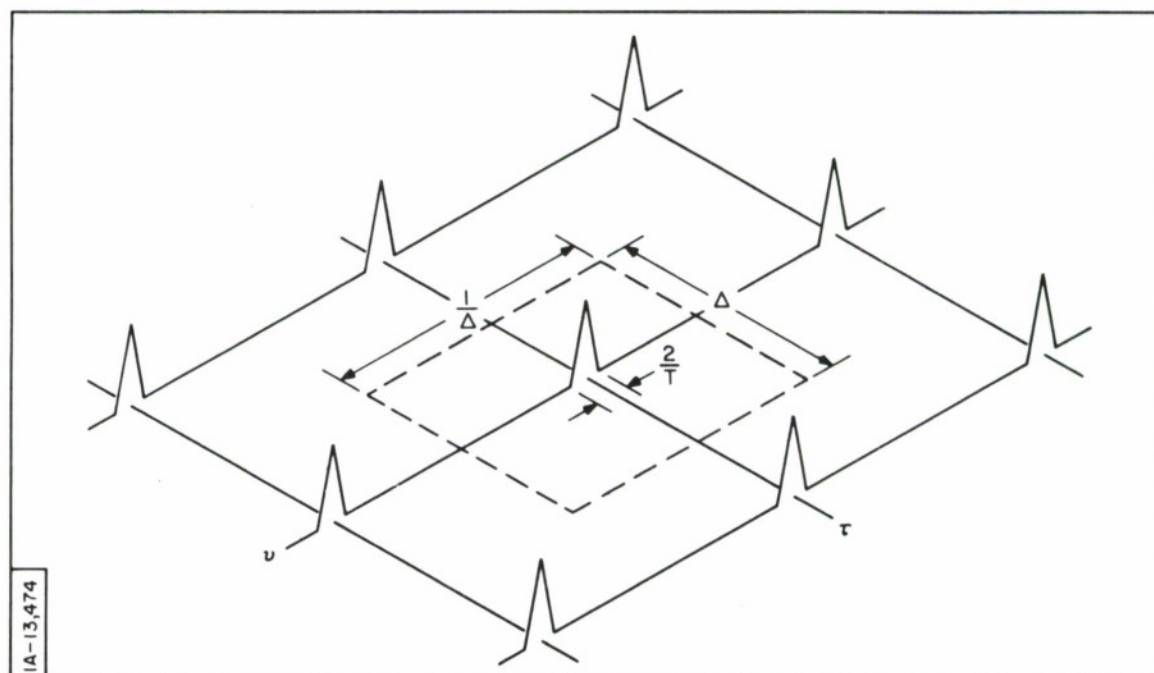


Fig. 42 Central region of the χ function of the impulse train after truncation in time by the $(\sin \pi t/T) (\pi t/T)$ function.

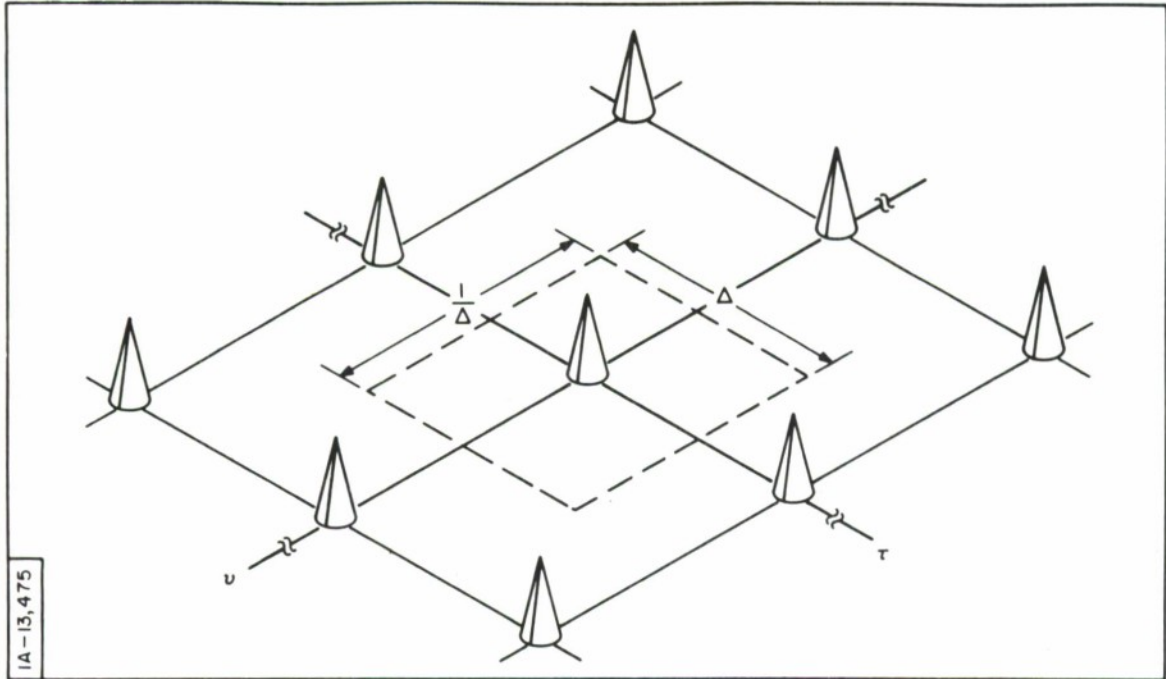


Fig. 43 Central region of the χ function of the periodic impulse train after truncation in time and frequency by siny/y functions.

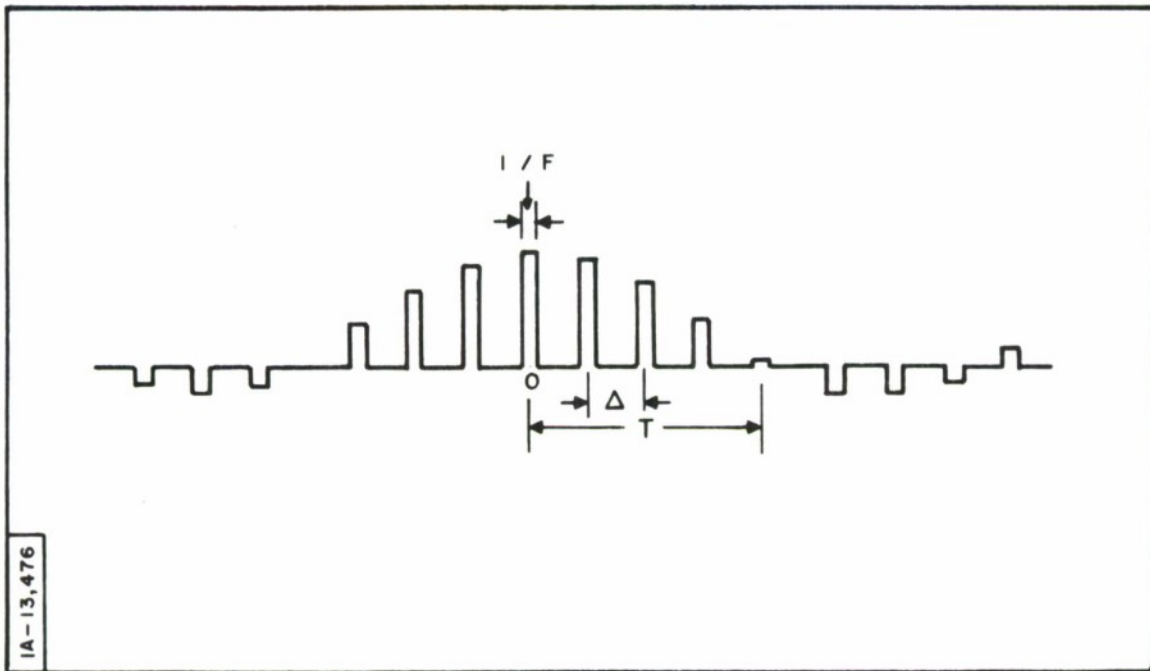


Fig. 44 Sketch of the pulse-train signal after siny/y time and frequency truncations.

and for $U_4'(f)$

$$U_4'(f) = \frac{\sin \pi f / F}{\pi f / F} \quad (186)$$

The χ function which results and the corresponding signal are shown in Figs. 45 and 46 respectively.

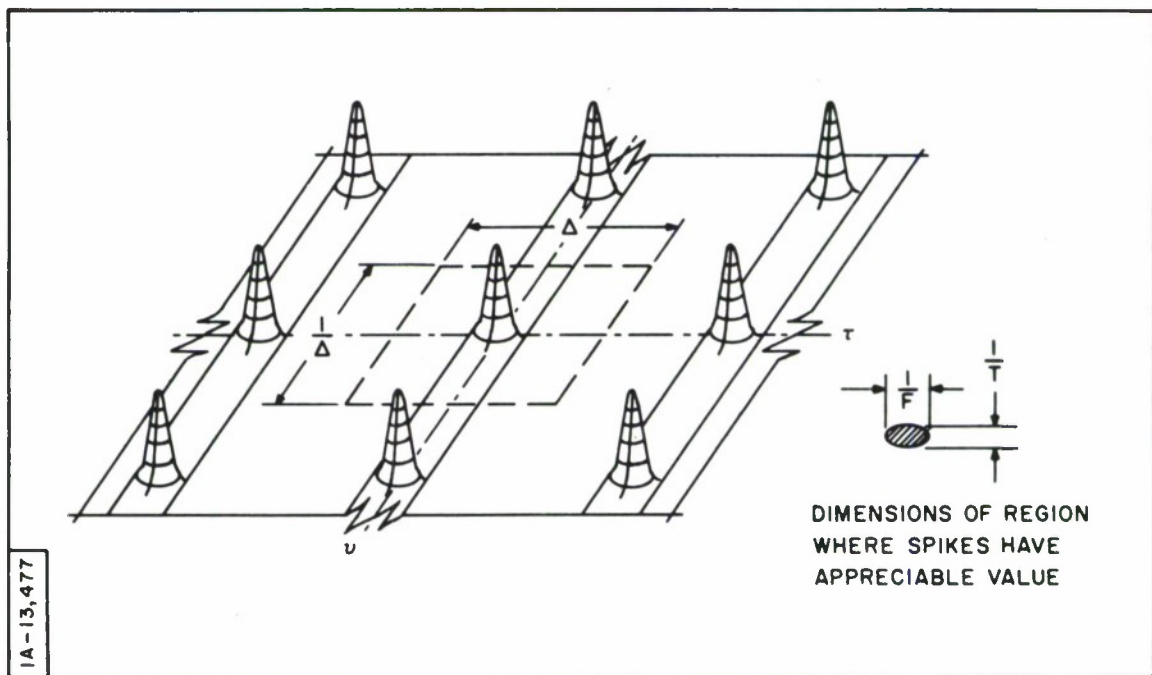


Fig. 45 Sketch of the central region of the χ function corresponding to rectangular time truncation and $\sin y/y$ spectrum truncation.

Optimal use of the pulse burst, as explained in Section 2.0, requires that the repetition interval, Δ , of the pulse train be adjusted to correspond to the extent in time of echoes from objects in the beam of the radar, and that the carrier frequency be low enough so that the extent of the echoes in Doppler fit into the interval $1/\Delta$. For example, with $\Delta = 12 \mu\text{sec}$ (corresponding to a

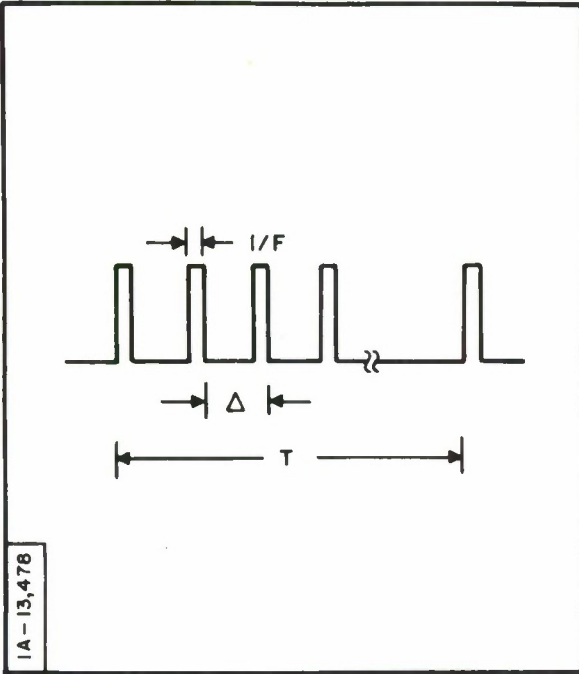


Fig. 46 Sketch of the impulse-train signal after rectangular time truncation and $\sin y/y$ spectrum truncation.

group of targets extending over a one-mile interval) and a carrier frequency of 1000 Mcps, we calculate the allowable spread of target radial velocities, δV_R , as follows.

$$\delta f_{\text{Doppler}} = \frac{2\delta V_R}{C} f_{\text{carrier}} = \frac{1}{\Delta}$$

$$\begin{aligned} \delta V_R &= \frac{C}{2f_c \Delta} \\ &= \frac{3 \times 10^8}{2 \times 10^9 \times 12 \times 10^{-6}} = 12.5 \times 10^3 \frac{\text{meters}}{\text{sec}} \\ &= 6.8 \text{ nautical miles/sec} \end{aligned}$$

If the targets extended over a two-mile range interval, and if the total spread of velocities was 6.8 nautical miles/sec, quite obviously the carrier frequency would have to be set at 500 Mcps and so forth.

The question which occurs naturally at this point is this: What can be done to eliminate fold-overs in the Doppler direction when the radar carrier frequency is fixed and cannot be lowered? For this problem one would like a χ function with an unambiguous clear space around the origin with an area greater than unity. It does not appear, however, that such a χ function is possible.* When the time-Doppler area occupied by the expected target complex cannot be scaled to unity, it should be clear that the pulse burst signal loses much of its attractiveness. It is possible, of course, to modify the pulse burst signal to reduce the amplitude of certain spikes of the χ function by changing the carrier frequency from pulse to pulse within the burst or by jittering the interval between pulses. But the thing that makes the simple pulse burst signal attractive is, as we have said, that its χ function is identically zero in regions. Jittering the carrier frequency or the repetition interval suppresses certain of the spikes (sometimes called "ambiguities") at cost of giving the χ function non-zero value in regions where it was zero and, hence, impairs the multiple target capacity of the radar. If estimates of both range and velocity are required and if the area of the target space cannot be scaled to unity, then there are two alternatives. First, signals with χ functions of the thumbtack shape can be used and the pedestal made low enough (by increasing the TW product of the signal) to reduce the interference as defined in Section 2.0 to an acceptably low level for detection and parameter estimation. Second, the objects can be

*See Kailath, Ref. 39.

resolved in range only by signals with χ functions having the shape of thin ridges. True range and radial velocity of the objects can then be determined from range rate and apparent range measurements.

The repetition interval of the pulse burst signal can be jittered to cause the associated χ function to assume, approximately, the thumbtack shape in a strip. Alternatively, the carrier frequency of a pulse burst signal can be jittered to make the associated χ function assume, effectively, the shape of a thin ridge. Pulse burst signals with jittered repetition intervals and carrier frequencies will be considered in the next two sections.

3.15 Pulse Burst Signals with Non-uniform Repetition Intervals

The χ function of the simple pulse burst signal, as we have seen, consists of a two-dimensional array of spikes, but when the objects in the beam of the radar have an extent of less than Δ in range and $1/\Delta$ in Doppler (area less than one), the large number of spikes causes no trouble. The details of the target complex may be seen clearly (i. e., there are no fold-overs, etc.). When the area of the target space is greater than unity, however, if the pulse burst signal is to be used at all, some means must be found to suppress at least some of the spikes of the χ function away from the origin. The spikes or "ambiguities" or "sidelobes" in range may be suppressed by a variety of methods. First, the phase of successive pulses might be stepped according to a suitable code, such as a Barker code or an M-sequence. Second, the carrier frequency could be changed from pulse to pulse to reduce the sidelobe level of the χ function. A third method of reducing the range sidelobes is to make the time interval between successive pulses non-uniform. The latter method is our subject here.

Figure 47(a) shows a simple pulse burst signal consisting of five pulses, and 47(b) shows its autocorrelation function. In Fig. 48(a) the signal is modified in a simple way: each successive interval between pulses is increased beyond the preceding one by a pulse width. Figure 48(b) shows the associated autocorrelation function. All of the sidelobes have been reduced to unit height. The χ function of the signal is particularly easy to visualize. The χ function vs. ν for a given shift τ is actually the Fourier transform of the product of the signal with a replica of itself shifted by τ . When the pulse burst is arranged like that of Fig. 48(a) for values of τ greater than a pulse width, at the most only two pairs of pulses overlap partially and only single pairs of pulses overlap completely. The product in the latter case is a rectangular pulse. The χ function divided by δ , the pulse duration, vs. Doppler for that τ then has the form $(\sin \pi \delta \nu) / \pi \delta \nu$; the maximum value, which occurs at $\nu = 0$, is one. It appears to be generally true that for $|\tau| > \delta$ the height of the χ function in the plane has a maximum value of one. For $|\tau| < \delta$ the χ function is of course different, because the product function looks like the signal which consists of five pulses. The peak value of the χ function, normalized with respect to δ , occurs at $\tau = \nu = 0$ and is equal to the number of pulses, 5 in this case. A sketch of the χ function of a signal constructed in the same way as that of Fig. 48(a) is shown in Fig. 49. Within the Doppler interval, $\pm 1/2 \Delta$ average on either side of the τ axis, the χ function has roughly the thumb-tack shape.

Other methods of staggering the pulses of a burst to suppress sidelobes have been investigated extensively by Resnick; [40] the reader desiring more information is referred to his report.

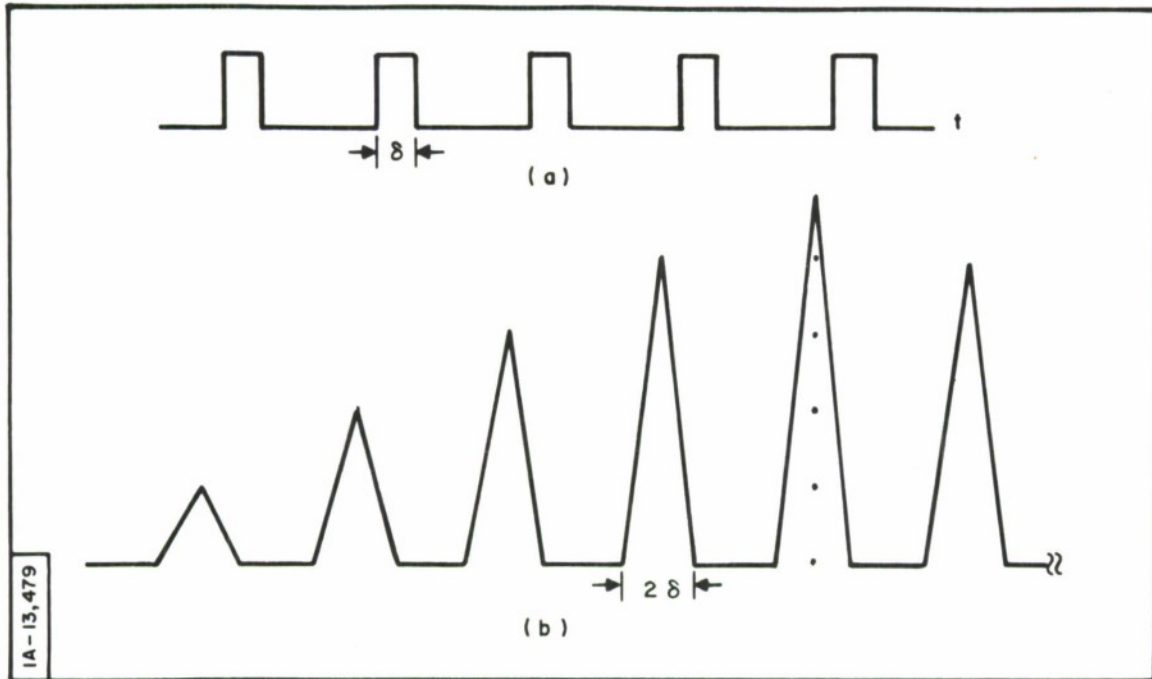


Fig. 47 (a) A simple pulse-burst signal; (b) the autocorrelation function of (a).

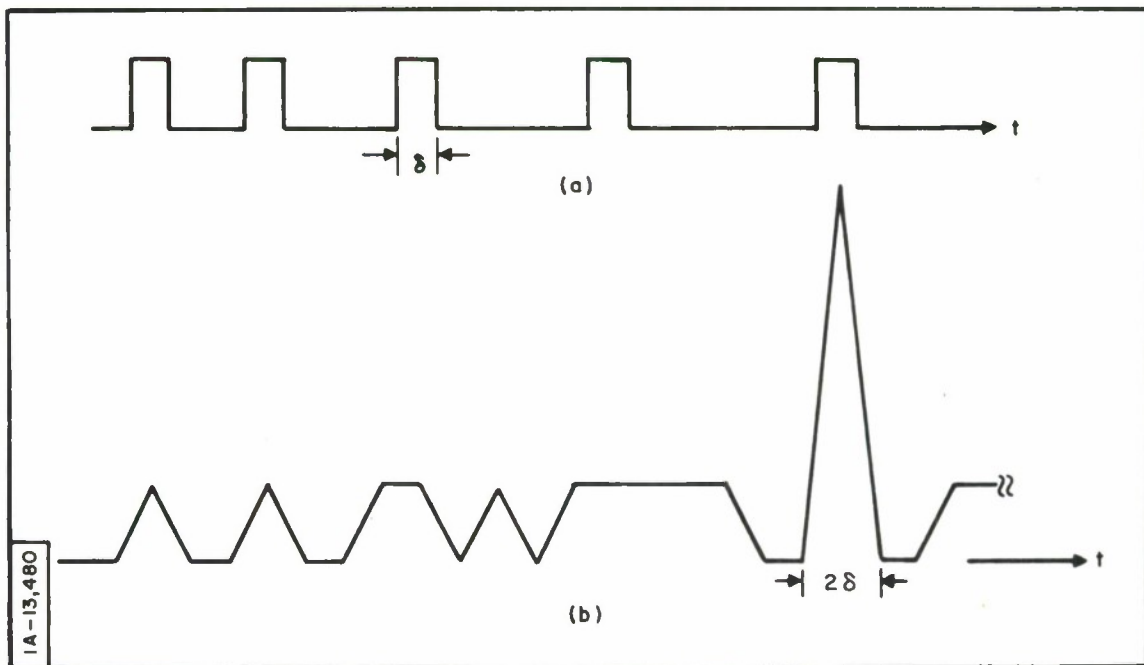


Fig. 48 (a) A pulse-burst signal with non-uniform pulse spacing; (b) the autocorrelation function of (a).

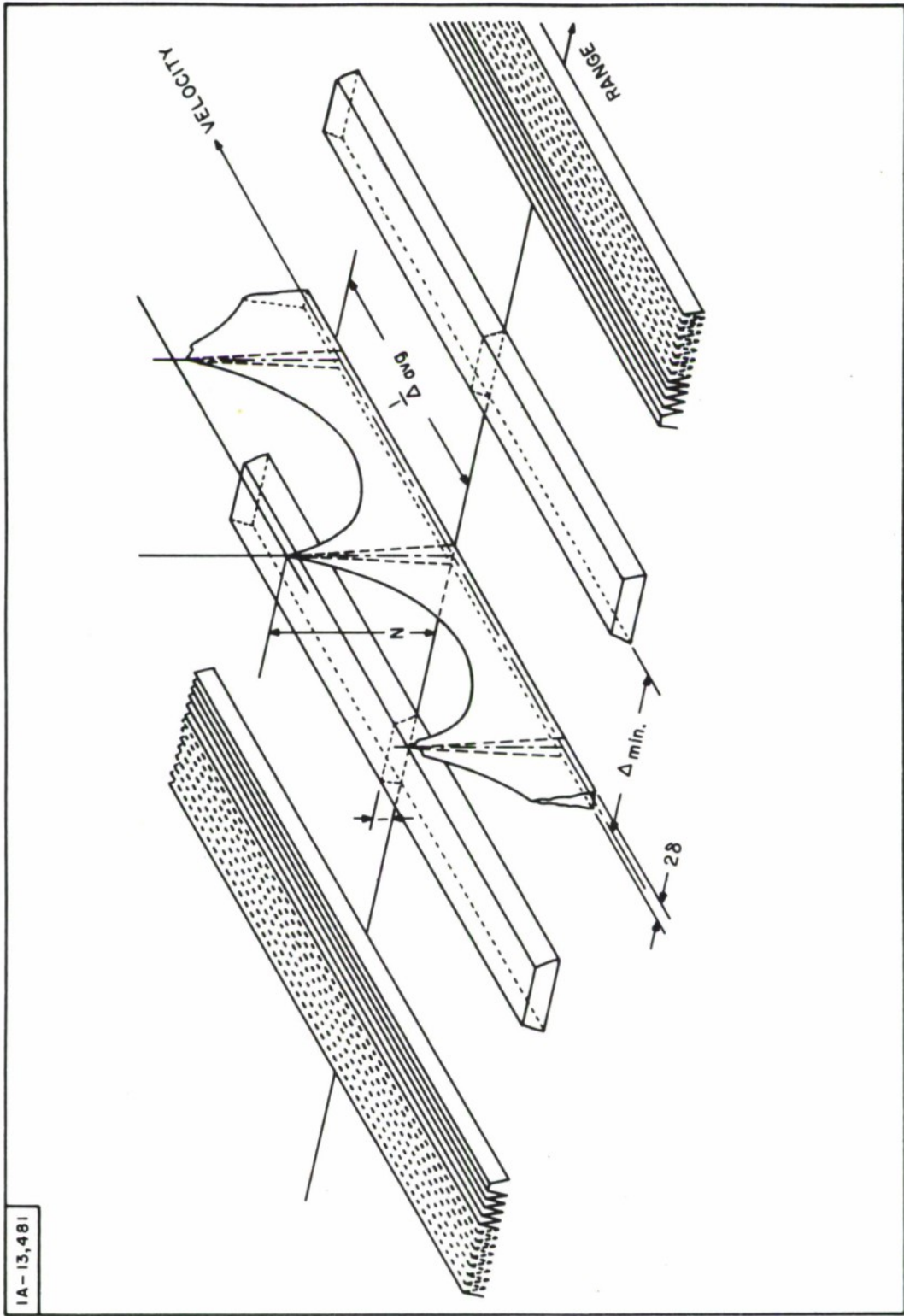


Fig. 49 Envelope of the two-dimensional correlation function for a non-uniformly spaced pulse train of N pulses. The χ function is normalized with respect to δ , the duration of the individual pulses. (Taken from Resnick, Ref. 40, with permission.)

IA-13,481

3.16 Pulse Burst Signals with Jittered Carrier Frequency*

If the successive pulses in a burst of pulses are designed so that their spectra do not overlap significantly, the sidelobes of the autocorrelation function of the signal will be quite small. The sidelobes will remain small for values of Doppler shift up to the minimum spacing in frequency between the spectra of the pulses. Let us compute the χ function of a pulse burst signal in the vicinity of the origin of the τ, ν plane. For convenience let us consider that the pulses of the signal $s(t)$ are uniformly spaced in time by Δ and that the carrier frequency increases by the fixed amount f_s on successive pulses. We have for $s_c(t)$, the exponential form of $s(t)$

$$\begin{aligned} s_c(t) &= \sum_{n=-N}^N a(t - n\Delta) e^{j2\pi(f_o + nf_s)t} \\ &= e^{j2\pi f_o t} \sum_{n=-N}^N a(t - n\Delta) e^{j2\pi n f_s t} \end{aligned} \quad (187)$$

The χ function of $s(t)$ is

$$\begin{aligned} \chi(\tau, \nu) &= \sum_{m=-N}^N \sum_{n=-N}^N \int_{-\infty}^{\infty} a(t - n\Delta) a(t + \tau - m\Delta) e^{j2\pi n f_s t} e^{-j2\pi m f_s (t + \tau)} \\ &\quad \times e^{-j2\pi \nu t} dt \end{aligned}$$

*This section is based upon an unpublished manuscript of R. Price, MIT Lincoln Laboratory.

$$\chi(\tau, \nu) = \sum_m \sum_n e^{-j2\pi m f_s \tau} \int_{-\infty}^{\infty} a(t - n\Delta) a(t + \tau - m\Delta) e^{-j2\pi f_s t(m-n)} e^{-j2\pi \nu t} dt \quad (188)$$

Let us assume that $a(t)$ is substantially zero for $|t| > \delta/2$, where $\delta \ll \Delta$. Then the central peak of $\chi(\tau, \nu)$ will occur for $|\tau| < \delta$. For the integral to have value for $|\tau| < \delta/2$, we must have $m = n$. Then Eq. (188) becomes

$$\chi_o(\tau, \nu) = \sum_{n=-N}^N e^{-j2\pi n f_s \tau} \int_{-\infty}^{\infty} a(t - n\Delta) a(t + \tau - n\Delta) e^{-j2\pi \nu t} dt, \quad (189)$$

where the subscript "o" indicates that the expression is for the region near the origin. We set $t' = t - n\Delta$ in Eq. (189) to obtain

$$\chi_o(\tau, \nu) = \chi_a(\tau, \nu) \sum_{n=-N}^N e^{-j2\pi n(f_s \tau + \Delta \nu)}, \quad (190)$$

where $\chi_a(\tau, \nu)$ is the χ function associated with the envelope of the individual pulses, $a(t)$. The sum on n in Eq. (190) may be written in closed form, and $\chi_o(\tau, \nu)$ becomes

$$\chi_o(\tau, \nu) = \chi_a(\tau, \nu) \frac{\sin \pi (2N + 1) (f_s \tau + \Delta \nu)}{\sin \pi (f_s \tau + \Delta \nu)}. \quad (191)$$

To interpret Eq. (191), first consider the case when the frequency step $f_s = 0$. Then the factor which multiplies $\chi_a(\tau, \nu)$ is a function of ν only. For N large, the factor is essentially a sampling function with a sampling interval of $1/\Delta$ as sketched in Fig. 50. As f_s is increased from zero, the peaks of the sampling factor in Eq. (191) are inclined at an angle to the τ and ν axes. The maxima occur when

$$f_s \tau + \Delta \nu = \pm k, \quad k = 0, 1, 2, \dots \quad (192)$$

The tangent of the angle of the ridge is given by the derivative

$$\frac{d\nu}{d\tau} = \frac{f_s}{\Delta} \quad (193)$$

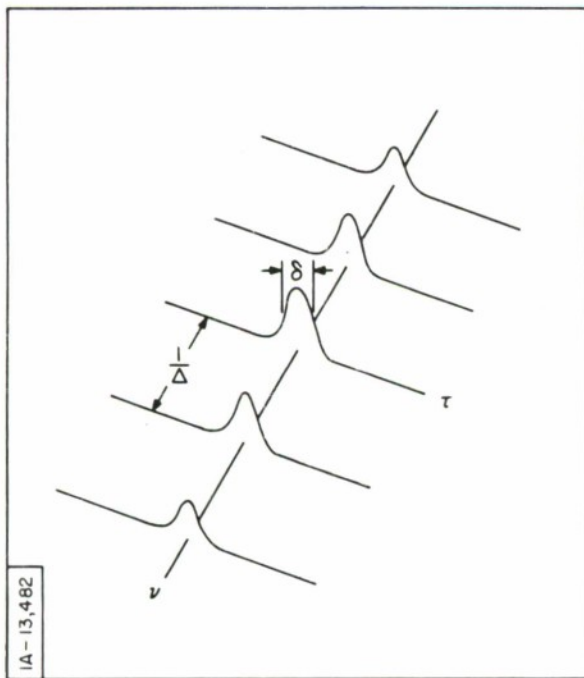


Fig. 50 Sketch of the χ function of a simple pulse-burst signal in a strip in the Doppler direction.

The situation which occurs for $f_s \neq 0$ is sketched in Fig. 51. When the frequency step, f_s , is made large compared to $1/\delta$ to suppress sidelobes, a cut through the surface in the τ direction sketched in Fig. 51 will have the character shown in Fig. 52. As the Doppler shift is allowed to increase or decrease, the pattern of spikes in Fig. 52 will move to the right or left. The width of the lines in the τ direction is about $1/[(2N + 1)f_s]$, which is the reciprocal of the total bandwidth used in the signal. If the Doppler shift of the signal has been determined by some other means, and if the range to the target is known to within the ambiguity spacing $1/f_s$, then range can be measured with an accuracy commensurate with the total bandwidth, $1/(2N + 1)f_s$. Otherwise it will not be possible to make use of the fine structure of Fig. 52. One would then probably take the envelope of the lines, and accuracy in the measurement of range would be that corresponding to the bandwidth of a single pulse, $1/\delta$. Without prior knowledge of Doppler and approximate range, we have, effectively, the χ function of a single pulse of the burst. However, provided that the target is not larger than the interval between ambiguities, $1/f_s$, the range resolution of the signal corresponds to the full bandwidth, $1/(2N + 1)f_s$. To make use of this resolving power, it is not necessary to have prior knowledge of either Doppler or range. The target must not, of course, have too large a spread of Doppler in its echo or obvious difficulties will arise.

What is gained by using the stepped frequency pulse burst instead of a single short pulse? Clearly, one gain is in signal energy. Assuming that the radar transmitter is peak power limited, the energy received from the burst signal echo is greater than that received from a single pulse by a factor equal to the number of pulses in the burst. Bandwidth is traded in this case for signal energy and, hence, for detection. In addition, with the stepped frequency pulse burst one may achieve high resolution over a limited range interval.

Fig. 51 Sketch of the χ function of a pulse-burst signal whose frequency increases by f_s on successive pulses.

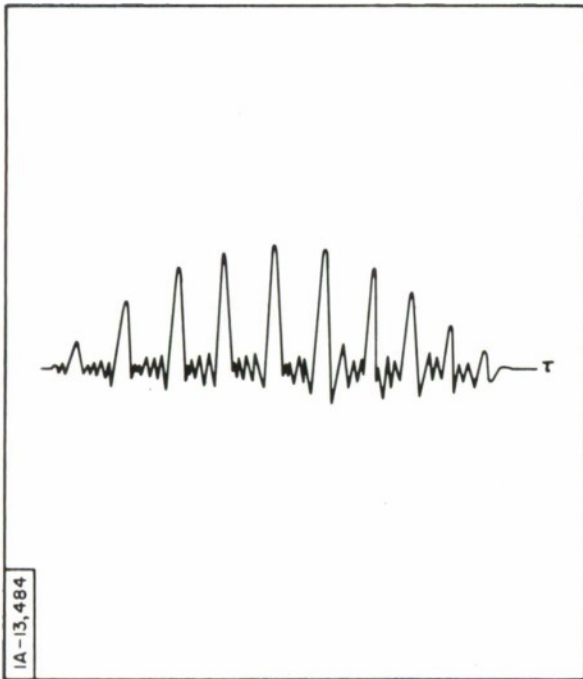
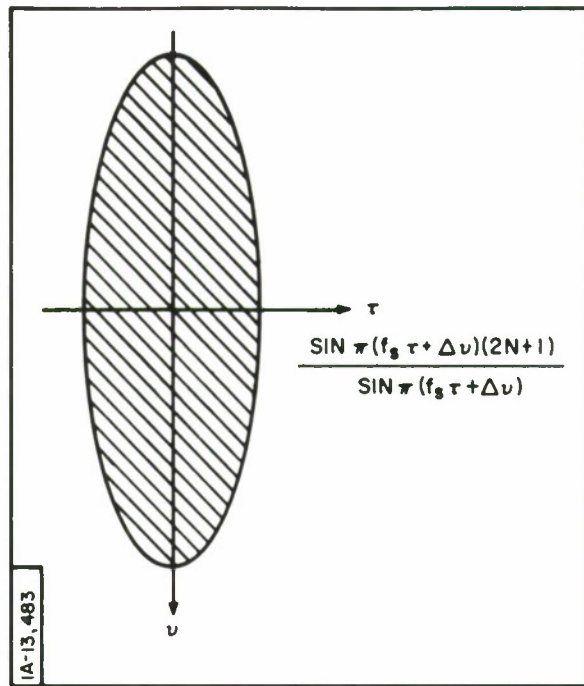
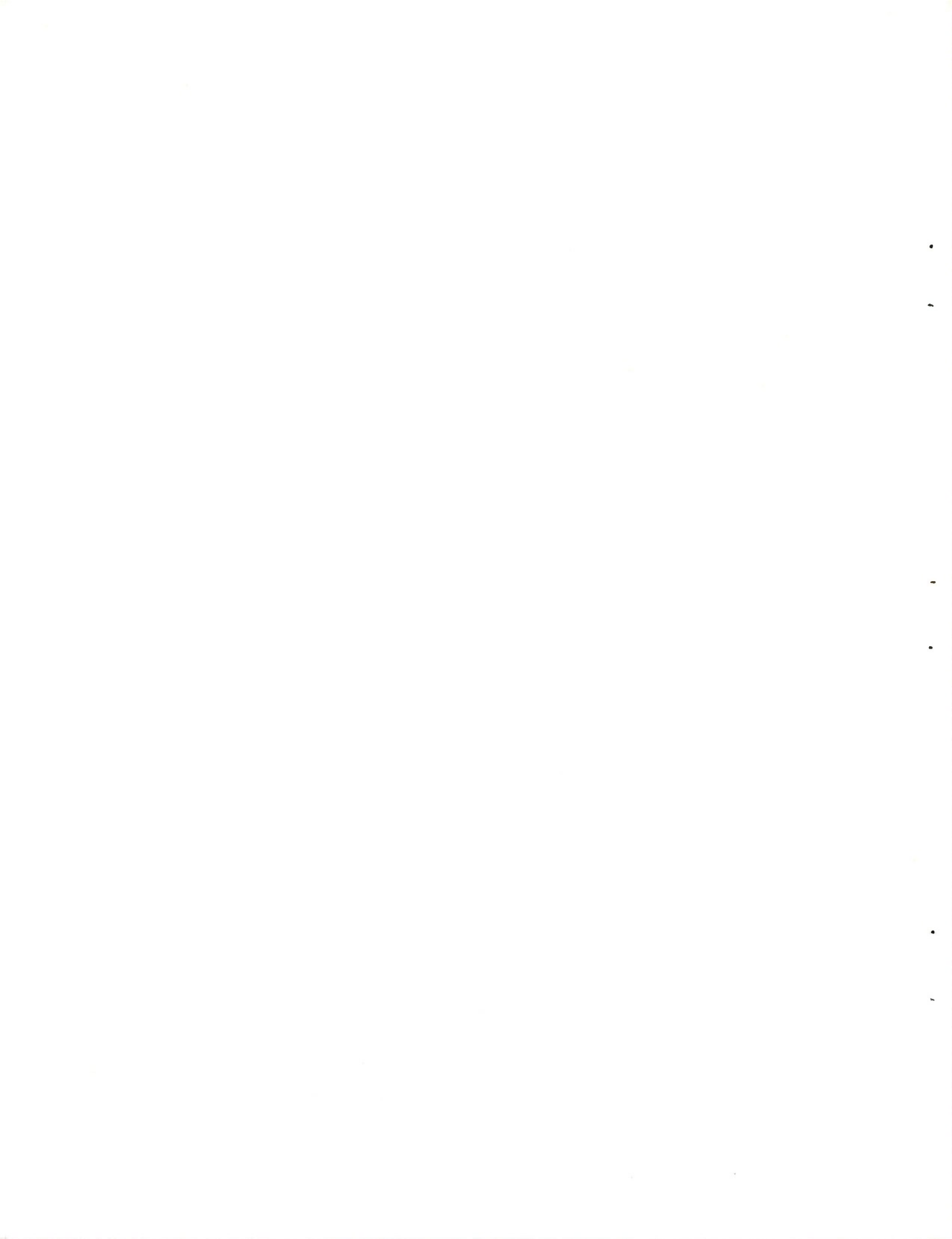


Fig. 52 Sketch of a cross section in the τ direction of the χ function of Fig. 51.

How does the stepped frequency pulse burst signal compare to the simple constant frequency pulse burst? Clearly, at the expense of bandwidth, the stepped frequency pulse burst gives a χ function that can have low sidelobes along the τ axis and high resolution in a limited region; the comparable constant frequency pulse burst has large sidelobes. On the other hand, the constant frequency pulse burst permits resolution in Doppler proportional to the reciprocal of the total time duration of the burst, while the stepped frequency pulse burst has a Doppler resolution proportional only to the reciprocal of the duration of one pulse of the burst.

How does the stepped frequency pulse burst signal compare to the non-uniformly spaced pulse burst? With the latter, one gets essentially the Doppler resolution which goes with the duration of the burst; the price paid for Doppler resolution in this case is the presence of skirts in the χ function which, while low, extend over the entire useful region of the τ, ν plane. The presence of the skirts, of course, impairs the multiple target capacity of the signal, as described in Section 2.0.



4.0 TECHNIQUES

4.1 Introduction

In Section 2.0 we discussed signals from the standpoint of the signal ambiguity functions and the effect of the ambiguity function shape upon the accuracy of parameter estimation and upon the multiple target capacity of the radar. In Section 3.0 we discussed signals in terms of the modulation the signal contained and the kinds of ambiguity function shapes which were achievable with particular types of modulation. In this section we will discuss some of the techniques available for generating and receiving the types of signals described earlier. The subject of techniques is central to the question of signal selection. One will certainly tend to use signals that are supported by well-developed techniques, and tend to avoid signals not thus supported unless time and resources are available to develop techniques. The subject is thus clearly important, but it is also the most difficult to discuss. A great deal of development work is presently going on in many places, and consequently, remarks made about the state-of-the-art in techniques soon will be obsolete. There is also the problem of security classification; new developments in techniques frequently arise in connection with military equipment and are thus more likely to have a security classification. The above problems, together with a space limitation, preclude a complete treatment of the subject of techniques here. We will, instead, try to stress some fundamental aspects and then refer the reader to the literature for further details.

In this section we will briefly consider the kinds of waveforms discussed in Section 3.0 and discuss in general the ways in which such signals may be generated and received. Then we will discuss the technique of sideband exchange which, for certain types of waveforms, makes it possible to use as a

matched filter the filter initially used to generate the waveform. Following that, we will discuss some aspects of lumped constant filters, ultrasonic delay lines, and tapped delay lines.

4.2 General

Here we will list the waveforms considered in Section 3.0 and tabulate for each waveform the most attractive techniques for generation and reception. Some techniques are well developed; others are less so. It is useful at this point again to call attention to the fact that when it is desired only to achieve a certain χ function shape, one can transmit the signal which gives the χ function or the Fourier transform of the signal. When the Fourier transform is taken for the signal, the χ function has the same shape but is rotated in the τ, ν plane by 90° .

It is convenient for purposes of classification to distinguish between two methods of synthesis of a device to generate a signal: frequency domain and time domain. The distinction is a usual and obvious one. When the synthesis has as its object the realization of a filter with a frequency response equal to the Fourier transform of the signal, we will say that frequency domain synthesis is employed. Alternatively, when the design proceeds directly in the time domain to produce a device the impulse response of which is the signal, we will say time domain synthesis is employed.

A. Uni-directional frequency-modulated signals with smooth envelopes

(The Fourier transform of such a signal has a smooth modulus and a group delay characteristic which varies in a unidirectional way with frequency.)

- (1) Frequency domain realization requires a device with a dispersive group delay characteristic such as one of the following:

- (a) lumped constant, electric networks,
- (b) waveguides in the vicinity of the cut-off frequency,
- (c) ultrasonic delay lines.

(2) Time domain realization:

- (a) tapped delay lines,
- (b) non-linear means such as variable frequency oscillators.

B. Symmetrical FM signals with smooth symmetrical envelopes (The Fourier transform of such signals has a highly structured modulus and a phase which is either zero or π radians. Clearly the same χ function, rotated by 90° , could be obtained by transmitting the Fourier transform of the symmetrical FM signal, in this case, an amplitude-modulated, phase-reversal signal.)

(1) Frequency domain realization:

- (a) filter with highly structured frequency response modulus and a phase of zero or π radians. This could be a difficult synthesis job.

(2) Time domain realization:

- (a) tapped delay line,
- (b) non-linear means such as a variable frequency oscillator.

C. Amplitude-modulated, phase-reversal signals (The Fourier transform of Category "B" above)

(1) Frequency domain realization (spectral modulus smooth and symmetrical, group time delay):

- (a) lumped constant filters.

(2) Time domain realization:

(a) tapped delay lines.

D. Time-limited, constant amplitude, phase-reversal signals

(1) Frequency domain realization is apparently, in many cases, unattractive.

(2) Time domain realization:

(a) tapped delay lines.

E. Pulse burst signals including simple bursts, jittered p. r. f. bursts, jittered frequency burst, bursts with complex modulation in the individual pulses

(1) Frequency domain realization:

(a) lumped constant filters (useful as a component of the overall filter).

(2) Time domain realization:

(a) tapped delay lines (useful for realizing the repetitive character of the burst).

4.3 Sideband Exchange

When the signal is generated by applying a pulse (effectively an impulse) to a linear filter, under certain circumstances the same filter may be used as a matched filter. It is useful to consider briefly the circumstances under which this may be done.

We recall that the matched filter to a signal has an impulse response which is a replica of the signal inverted in time. Quite obviously, then, when the signal is an even function of time about its midpoint, the filter used to generate the signal will serve directly as a matched filter.

We have a second example of a filter which serves to generate the signal and which also serves as a matched filter in the tapped delay line filter of Fig. 20. An impulse applied to terminal "a" in Fig. 20 produces the signal waveform at "b." When the impulse is applied at terminal "a'," the waveform at "b" is the signal inverted in time. Therefore, the filter is a matched filter for the signal when the signal is applied at terminal "a'."

Alternatively, if the signal could be inverted in time after generation, then the filter used to generate the signal would obviously serve as a matched filter. The signal may in effect be inverted in time by a modulation and filtering process which is called sideband exchange if it possesses certain characteristics: the signal envelope must be an even function of time about the midpoint of the signal, and the instantaneous frequency must be an odd function of time about the midpoint of the signal and about the carrier frequency. The sideband exchange process is illustrated in Fig. 53. In Fig. 53 the signal is shown with an even envelope and a linear downward frequency sweep of 2δ centered about f_0 . The frequency sweep does not, of course, have to be linear, but it must be an odd function. The signal is multiplied by a sine wave of frequency $2f_0$, and the sum component of the product, the upper sideband at $3f_0$, is selected by the first bandpass filter. Next follows multiplication by a sine wave of frequency $4f_0$; the difference component centered at f_0 is selected by a second bandpass filter. The frequency of the output waveform now increases with time as shown in the figure, and the waveform with which we began has been effectively reversed in time.

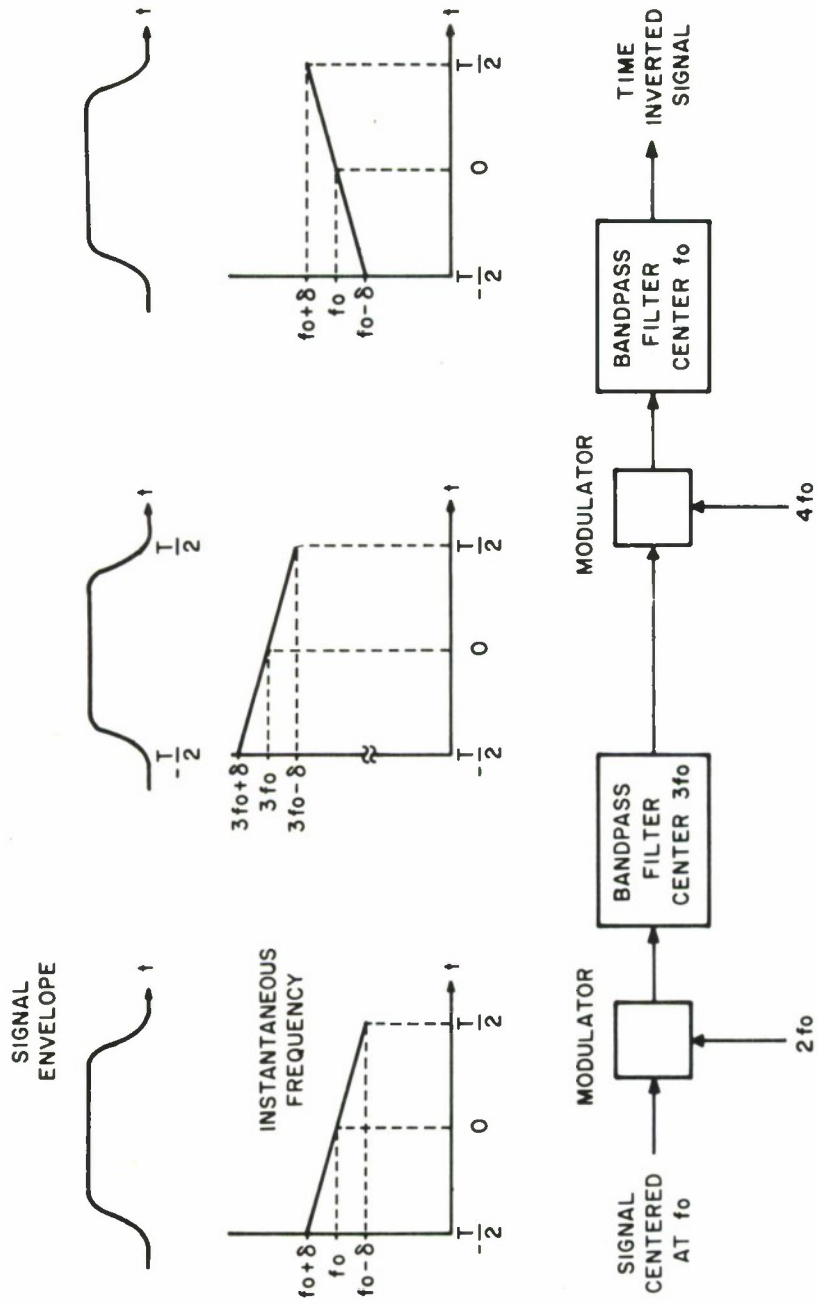


Fig. 53 Schematic to illustrate the process of sideband exchange.

Figure 54 illustrates by successive convolutions of spectra how such a signal as we have discussed might be transmitted and received in a radar. It may easily be shown that a narrow band signal which has an even envelope and an odd frequency sweep has a Fourier transform the modulus of which is even about the center frequency of the signal and the group delay of which is odd, as shown in Fig. 54(a). With this established, the rest of Fig. 54 is self explanatory.

4.4 Lumped-constant Filters

A filter, the impulse response of which is the signal, will usually consist of a number of parts arranged in cascade. A possible arrangement is shown in Fig. 55. In the figure, the first network serves to shape the modulus of the frequency response of the filter, and network number two equalizes the delay (or linearizes the phase) of network number one; network number three, an all-pass network, supplies the desired phase characteristic, and network number four corrects the overall frequency response modulus for errors caused by parasitic losses. For convenience in synthesis and construction, each block in Fig. 55 might well be further broken down into several blocks.

The parts of the filter will usually be specified by frequency response modulus and phase, and a first step in realizing the parts is that of finding arrangements of poles and zeros in the complex frequency plane which yield satisfactory approximations to the required j -axis characteristics. This is the so-called "approximation problem" in network synthesis. The techniques of handling the approximation problem are many and varied, and the interested reader is referred to the literature. [41, 42, 43] Perhaps the most common method of handling the approximation problem is that of trial and error. The trial and error method is much speeded by use of a digital computer programmed

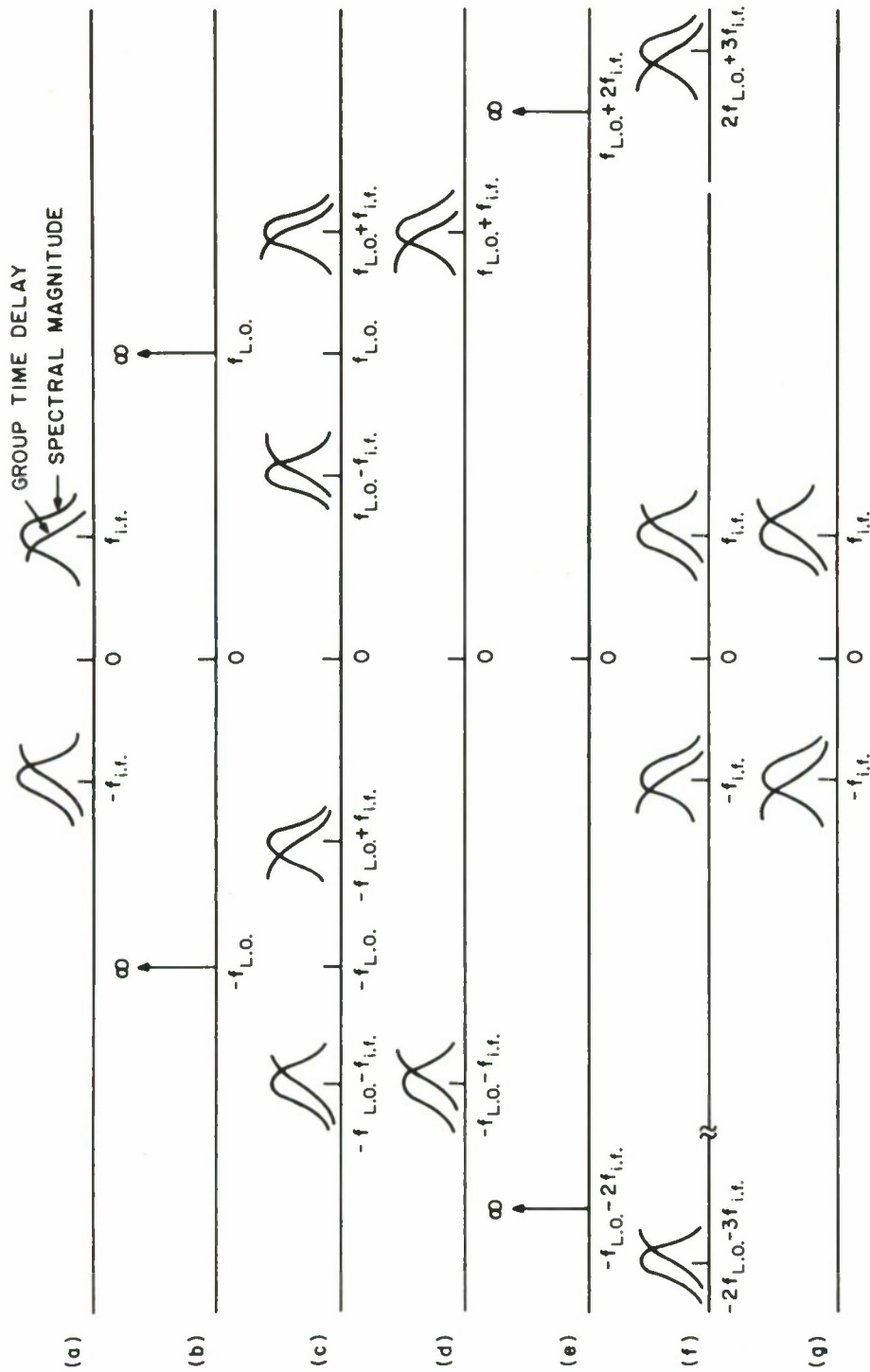


Fig. 54 Sketches illustrating the generation of a signal, its transmission and sideband exchange on reception. (a) The signal spectrum at i. f.; (b) spectrum of local oscillator in exciter; (c) effect of modulation, i. e., convolution of (a) with (b); (d) spectrum and group delay of radiated signal (lower sideband of (c) eliminated by filtering); (e) spectrum of oscillator in receiver; (f) convolution of (d) with (e); and (g) after low pass filtering of (f). The signal spectrum has been conjugated effectively; now the filter used to generate the signal in (a) is "matched" to the conjugated echo.

to give the j -axis modulus and phase associated with a set of poles and zeros. Here we will give some examples of frequency response characteristics and pole-zero configurations which approximately realize them. The circuit building block for all-pass network construction is the bridged-tee network. We will discuss some of the problems which arise in the construction and alignment of these networks.

Figure 56 shows a frequency response modulus and phase. The modulus is that associated with a single pole and the delay is constant (and hence, the phase is linear). Figure 57 shows an arrangement of poles and zeros which has approximately the frequency response characteristic shown in Fig. 56. The single pole on the real axis establishes the shape of the modulus of the transfer function frequency response. The other poles and zeros constitute an all-pass structure which linearizes the phase.

Figure 58 shows the frequency response characteristics of a bandpass filter with a maximally flat modulus and constant group delay (or linear phase). Figure 59 shows the pole-zero configuration which gives the frequency response of Fig. 58. The five poles on the semi-circular contour centered at $j\omega_0$ and the j -axis zero, together with their conjugates at negative frequency, give the modulus of the frequency response. The five poles are a low-pass Butterworth configuration reproduced about the center frequency, ω_0 . The unwanted weighting caused by the conjugate poles is approximately compensated for by the j -axis zero. The delay of the poles is made constant by the ten all-pass poles and zeros and their conjugates.

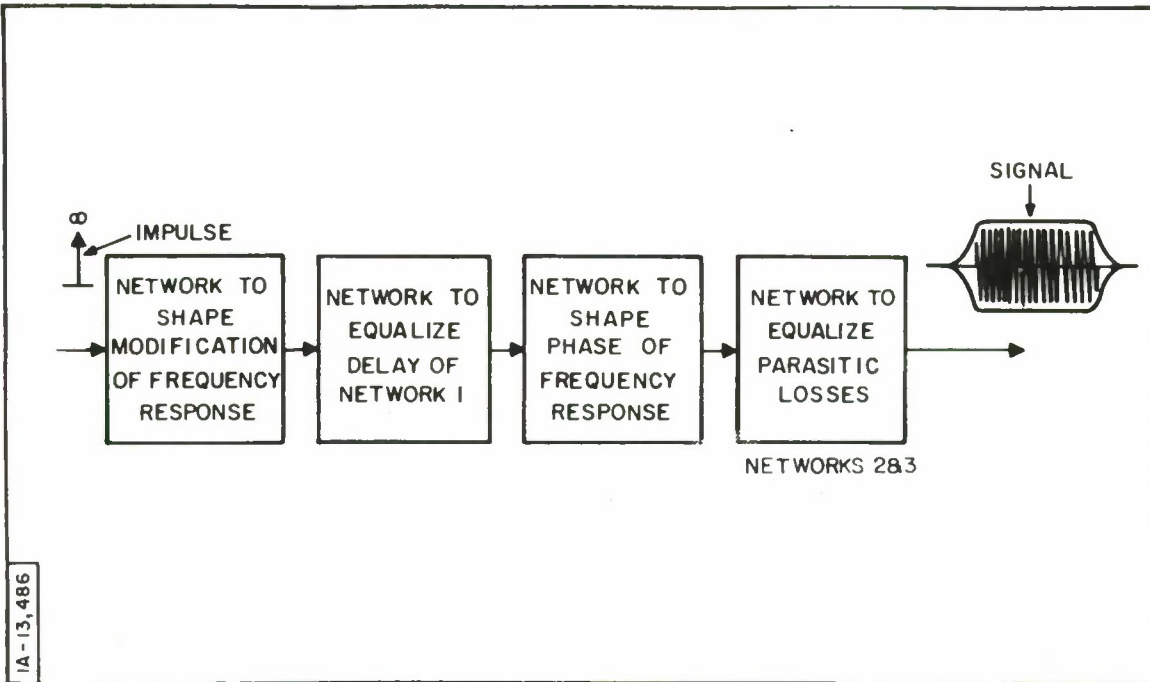


Fig. 55 A possible arrangement for realizing in the frequency domain a filter having an arbitrary frequency response.

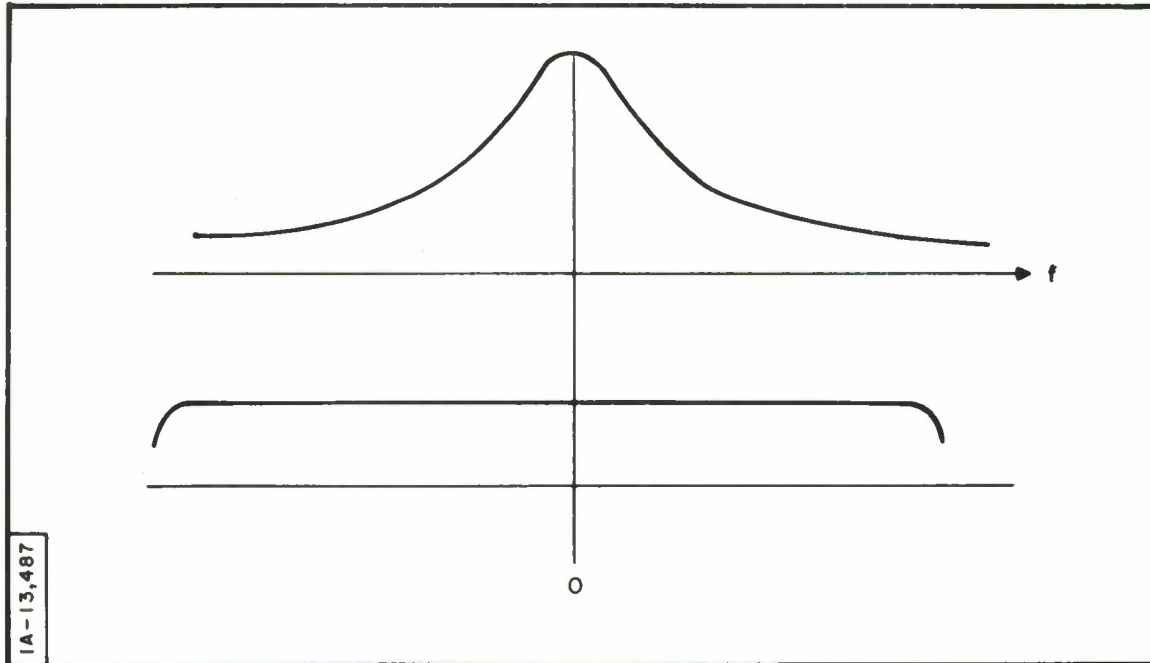
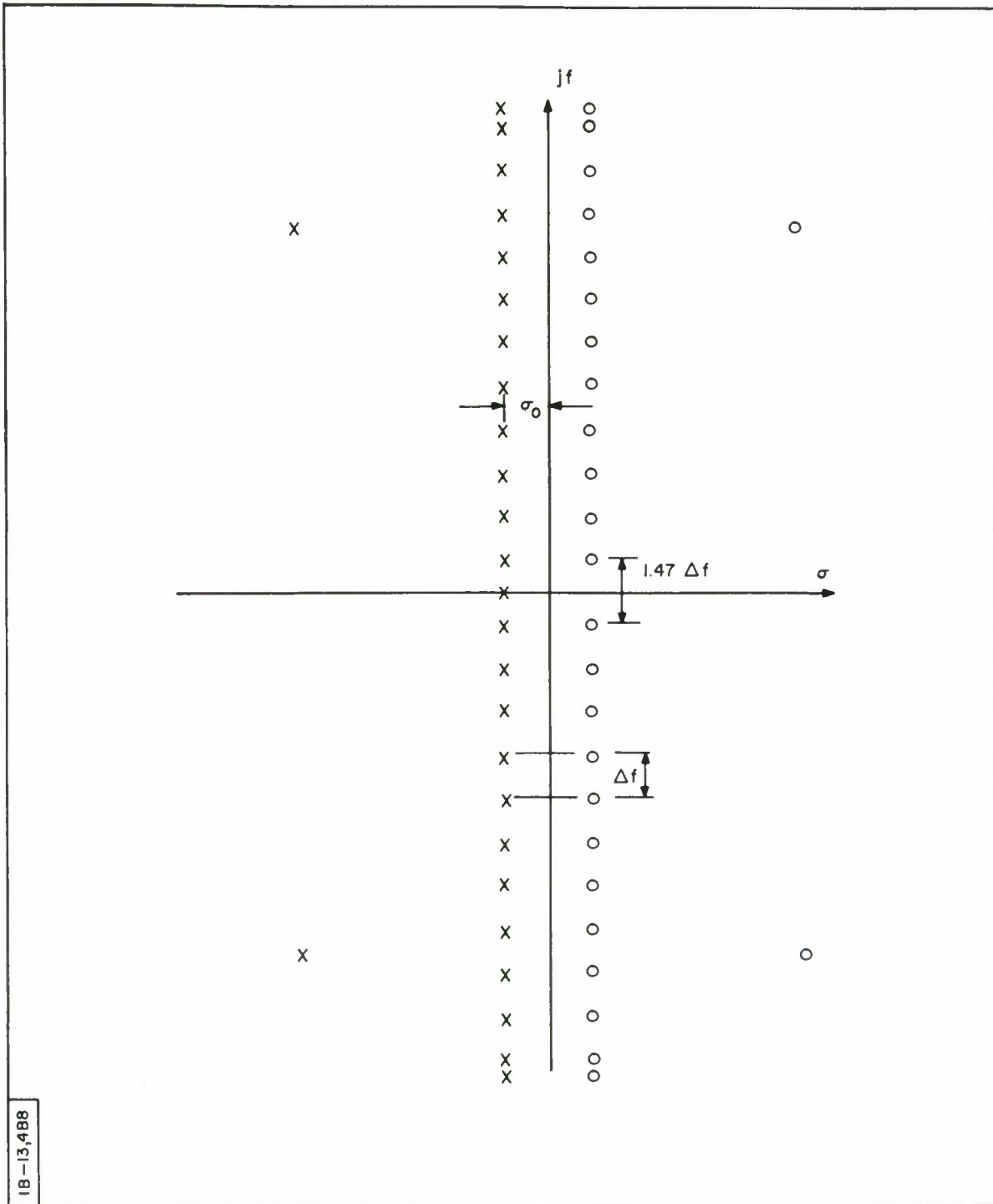


Fig. 56 Frequency response modulus (a) and group delay (b) of a linear phase, single-pole filter.



1B-13,4B8

Fig. 57 Pole-zero configuration which gives the frequency response of Fig. 56. Structure is all-pass except for the pole on the negative real axis. (Suggested by E. L. Key of The MITRE Corporation.)

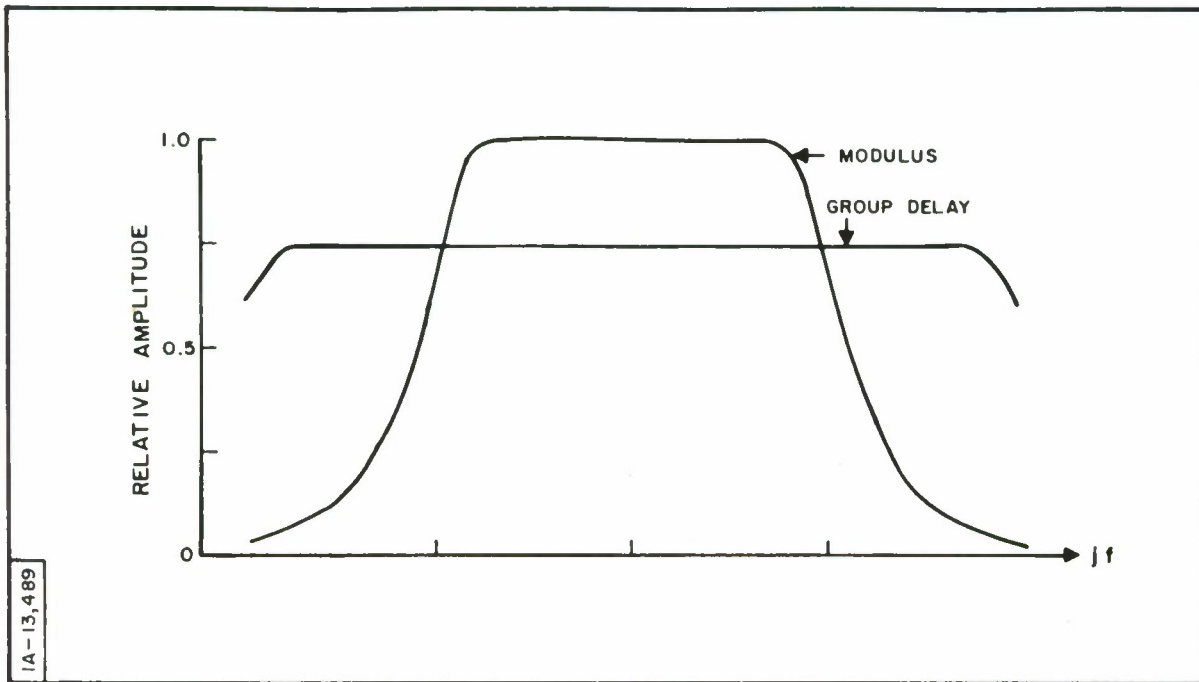
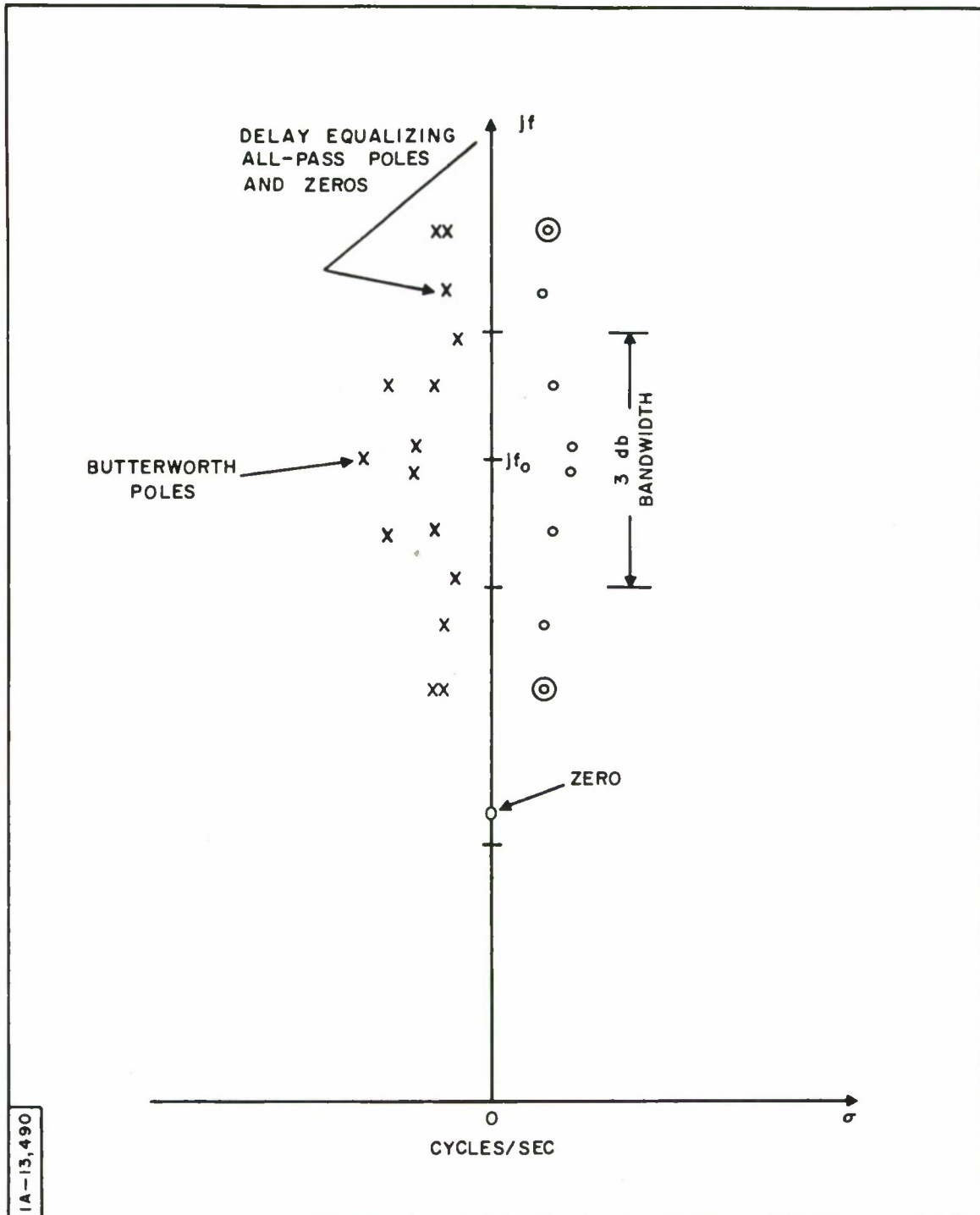


Fig. 58 The frequency response modulus and group time delay of a bandpass filter.

As a third example consider an all-pass network that has the group time delay characteristic, shown in Fig. 60, which closely approximates an inverse-tangent function. A pole-zero configuration which gives the inverse-tangent group delay is shown in Fig. 61. There are 38 positive frequency poles and zeros. Guillemin^[41] has shown that an indefinitely long array of poles equally spaced on a line parallel to the j axis has a group delay which goes very nearly as the inverse tangent near the end of the string. The 32 equally spaced poles and zeros give inverse tangent shape. The remaining 6 poles and zeros compensate for the truncation of the string.

One may proceed by any of a number of methods to synthesize networks having the required pattern of singularities, but, in general, it will be convenient to synthesize the networks in the manner in which they have been organized in Fig. 55, that is, realizing the amplitude-shaping networks and



IA-13,490

Fig. 59 Pole-zero configuration which gives the frequency response of Fig. 58. (Courtesy of R. D. Haggarty of The MITRE Corporation.)

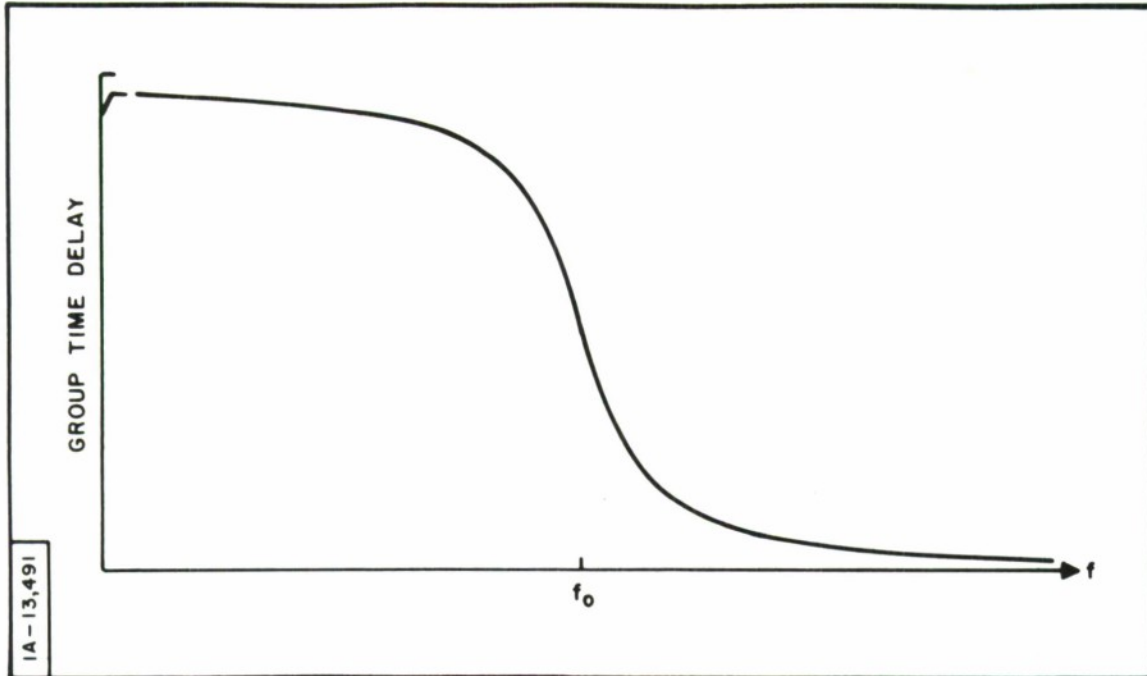


Fig. 60 Inverse-tangent group time delay characteristic.

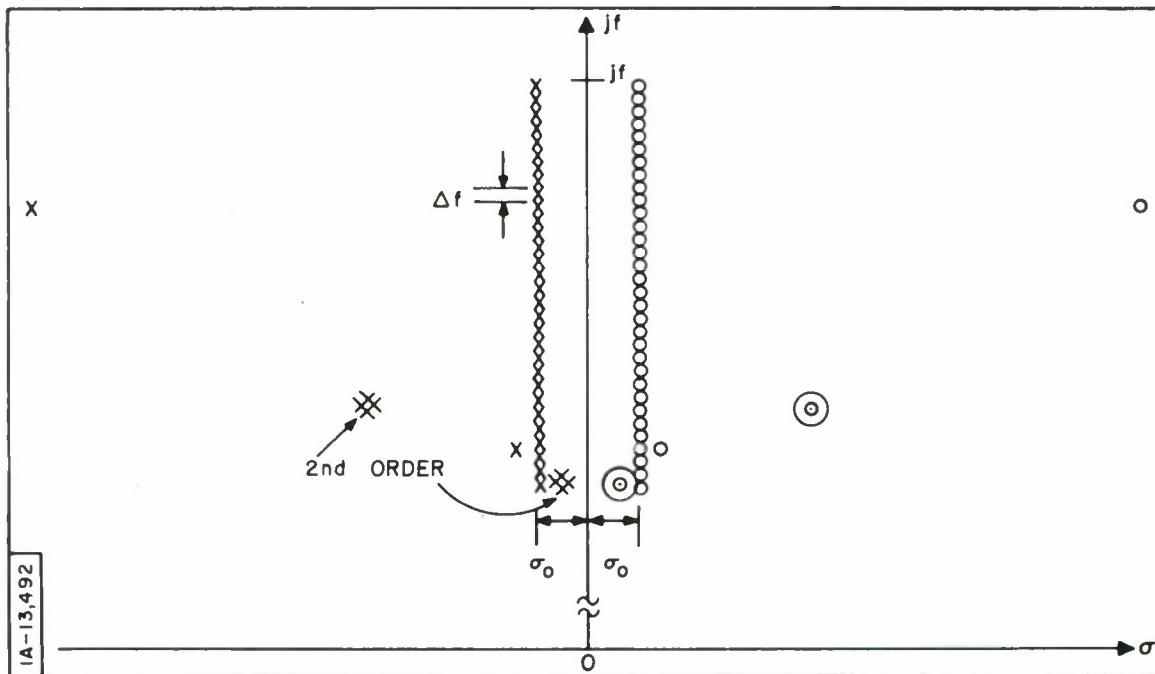


Fig. 61 The all-pass pole-zero arrangement whose delay approximates the inverse-tangent curve of Fig. 60.

delay equalizers separately. We will not discuss here the amplitude networks but will confine ourselves to some remarks regarding the realization of all-pass networks. All-pass transfer functions are of the form

$$F(s) = \frac{P(-s)}{P(s)} \quad , \quad (194)$$

where $P(s)$ is a polynomial in the complex-frequency variable s . The roots of $P(s)$ are all in the left half of the s plane. The roots may be real or, if complex, they must occur in complex-conjugate pairs; likewise, the roots of $P(-s)$ are in the right half s plane opposite the corresponding roots of $P(s)$. The polynomial $P(s)$ and likewise $P(-s)$ may then always be factored into a product of two types of factors: first order factors in s and quadratic factors, thus:

$$F(s) = \frac{(s - a_1)(s - a_2) \dots (s^2 - b_1 s + c_1)(s^2 - b_2 s + c_2) \dots}{(s + a_1)(s + a_2) \dots (s^2 + b_1 s + c_1)(s^2 + b_2 s + c_2) \dots} \quad . \quad (195)$$

Two types of networks suffice to realize any all-pass transfer function of the type shown by Eq. (195). They are $F_1(s)$ and $F_2(s)$, where

$$F_1(s) = \frac{s - a}{s + a} \quad (196)$$

and

$$F_2(s) = \frac{s^2 - bs + c}{s^2 + bs + c} \quad . \quad (197)$$

$F_1(s)$ and $F_2(s)$ may be realized as constant-resistance structures; such structures may be cascaded to produce over-all transfer functions of the form of Eq. (195).

Realization of transfer functions of the form of $F_1(s)$ and $F_2(s)$ as constant-resistance lattices and the equivalent bridge-tee networks is discussed by Bode, [44] Guillemin, [41] Van Valkenburg [42] and many others. We will outline the synthesis procedure for the transfer function $F_2(s)$ to set the stage for some remarks bearing on the construction of the physical networks, compensation for parasitic losses, and alignment procedures.

When the series and shunt arms, z_a and z_b respectively, of the lattices of Fig. 62 are reciprocal, the image impedance, Z_i , is

$$Z_i = \sqrt{z_a z_b} = 1 \quad , \quad (198)$$

and the transfer impedance, Z_T , is

$$Z_T = \frac{E_2}{I_1} = \frac{1 - z_a}{1 + z_a} \quad . \quad (199)$$

The all-pass quadratic transfer function may be written

$$Z_T = \frac{s^2 - \alpha s + 1}{s^2 + \alpha s + 1} = \frac{1 - \frac{\alpha s}{s^2 + 1}}{1 + \frac{\alpha s}{s^2 + 1}} \quad . \quad (200)$$

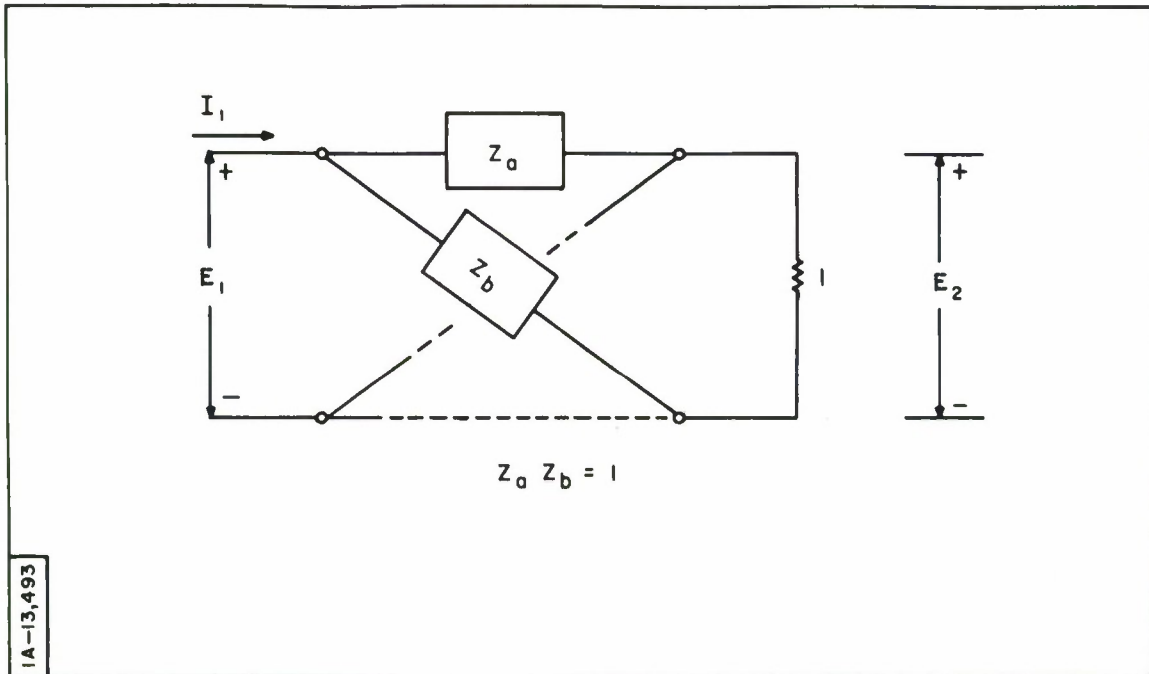


Fig. 62 The symmetrical constant-resistance lattice.

By comparison of Eqs. (199) and (200), we see that we may write

$$z_a = \frac{\alpha s}{s^2 + 1} = \frac{1}{\frac{1}{\alpha} s + \frac{1}{\alpha s}} \quad (201)$$

Therefore,

$$z_b = \frac{1}{\alpha} s + \frac{1}{\alpha s} \quad , \quad (202)$$

and we have the lattice of Fig. 63(a). But because of dissipation, z_a will assume the form

$$z_a = \frac{\alpha s}{s^2 + d_a s + 1} \quad , \quad (203)$$

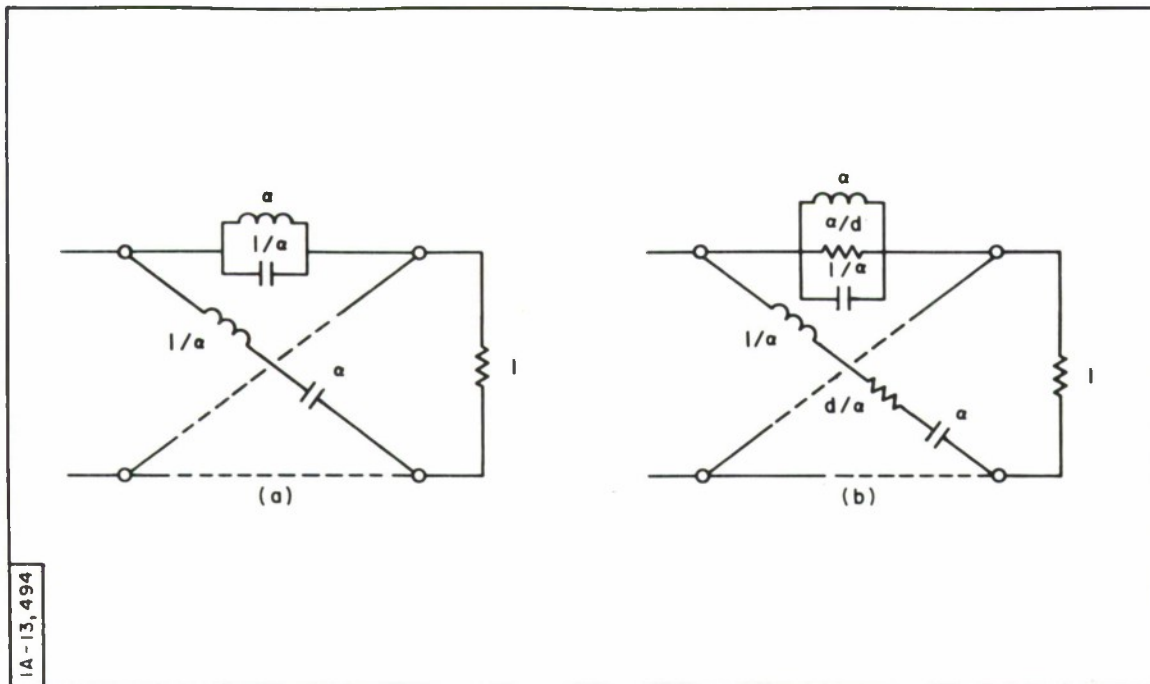


Fig. 63 (a) The all-pass, constant-resistance lattice; (b) the constant-resistance network of (a) with equalized parasitic losses.

where d_a may be shown to be $1/Q_a$, the "a" network quality factor. The shunt arm, z_b , likewise because of losses, will be

$$z_b = \frac{s^2 + d_b s + 1}{\alpha s} \quad , \quad (204)$$

and the lattice may be made constant-resistance if d_b is made to equal d_a . In other words, to obtain a constant-resistance lattice in the presence of parasitic losses, the losses in the series and shunt arms must be equalized. It is important that the networks be made constant-resistance, because success in cascading the networks and in obtaining the desired overall transfer function hinges on the termination of each network in its image impedance. With z_a given by Eq. (203), the expression for Z_T becomes

$$Z_T = \frac{s^2 - (\alpha - d)s + 1}{s^2 + (\alpha + d)s + 1} \quad (205)$$

The transfer function, with element losses, is no longer all-pass but has a notch near the critical frequency which, in this case, is one radian per second. The minimum value of Z_T occurs at about $s = j1$, where

$$|Z_T(j1)| = \frac{\alpha - d}{\alpha + d} = \frac{1 - \frac{d}{\alpha}}{1 + \frac{d}{\alpha}} \quad (206)$$

If the ratio d/α is of the order of 0.1, the minimum value of $|Z_T|$ is about 0.82, a loss of about 1.8 db.

The constant-resistance lattice with losses is shown in Fig. 63(b). The pole-zero patterns of the lattice with and without losses are shown in Fig. 64(a) and (b) respectively. Without losses, the singularities lie on the perimeter of the unit circle; zeros and poles are equidistant from both σ and $j\omega$ axes, as shown in Fig. 64(a). With losses, the singularities still lie on the unit circle, but all have been shifted to the left a distance equal to $d/2$. (The zeros move toward the $j\omega$ axis and up in frequency; the poles move away from the $j\omega$ axis and down in frequency.) When the angle between the real axis and a radial line drawn to the singularity is large, most of the motion of the singularities is toward or away from the $j\omega$ axis. The delay fillet due to the zero consequently gets narrower and higher, that due to the pole lower and broader, than in the lossless case; thus the motion of the pole tends to compensate for the motion of the zero, as far as the group delay is concerned.

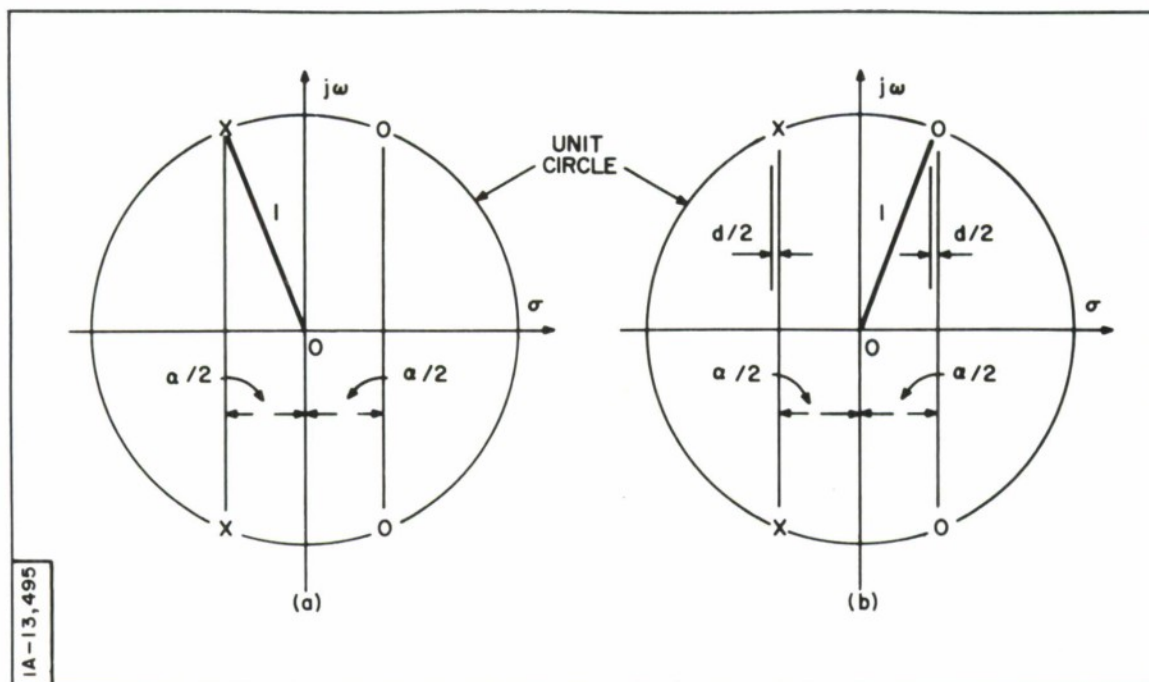


Fig. 64 Pole-zero plot of (a) all-pass constant-resistance network of Fig. 63 (a), and (b) loss-equalized, constant-resistance network of Fig. 63 (b).

Construction of the balanced network of Fig. 63(b) would prove awkward for a number of reasons, such as part tolerance requirements, requirement of a drive balanced to ground, lack of a common terminal for input and output, the problem of balancing strays to ground, and so forth. For construction, an unbalanced network is more convenient. The networks of Fig. 63 have a number of unbalanced equivalents; two possible such equivalents are shown in Fig. 65 with and without provision for losses. Networks of Fig. 65(a) and (c) serve for $\alpha < 1$; for $\alpha > 1$ the capacitor in the shunt arm becomes negative. Networks of parts (b) and (d) of Fig. 65 are for $\alpha > 1$. A unity coefficient of coupling is shown for the upper coil in the figure, but the circuit may be modified to account for couplings of less than unity if desired.

We will use the network type of Fig. 65(c) to illustrate some remarks on network construction and alignment. Figure 66 shows a single bridged-tee

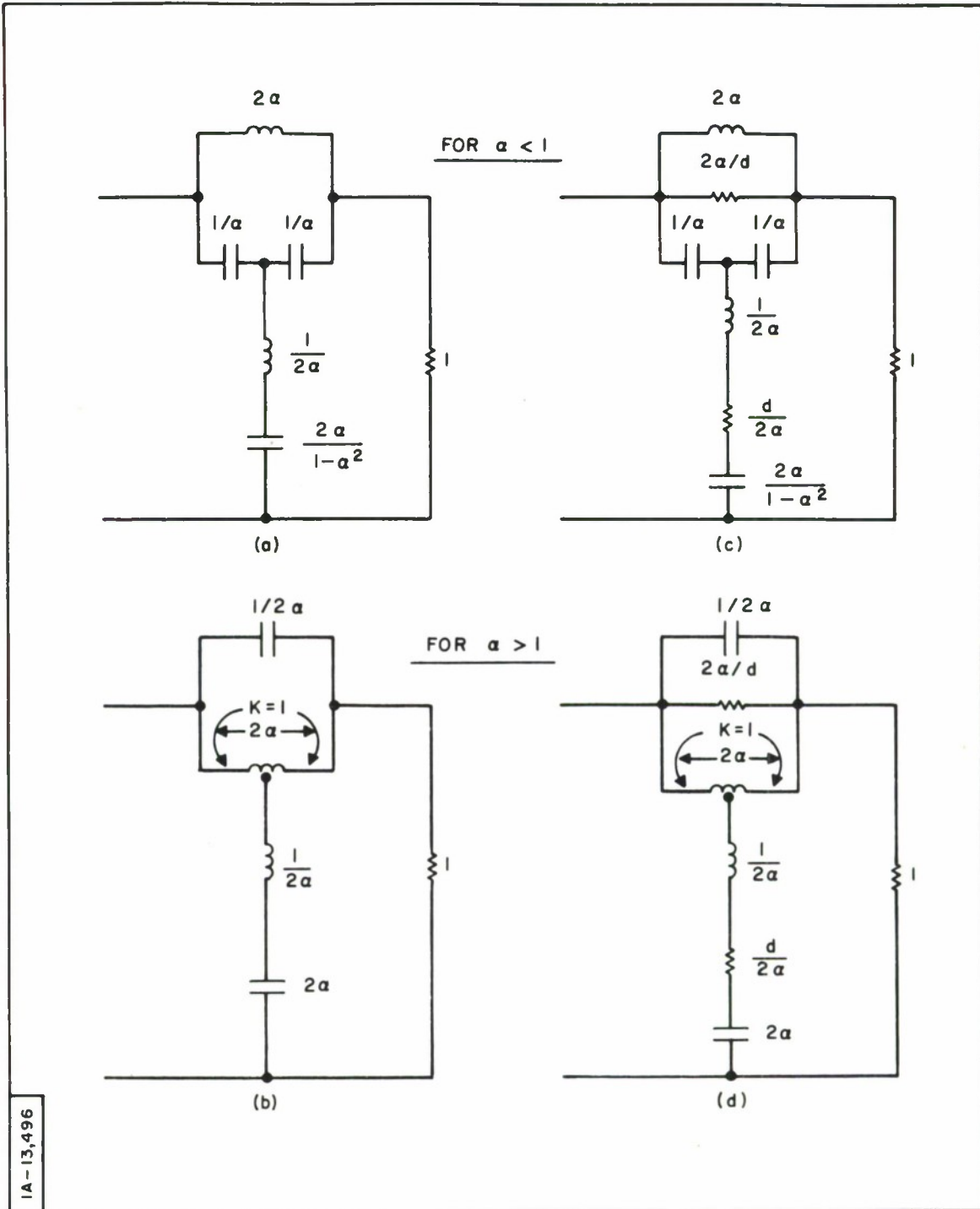


Fig. 65 (a) and (b) Unbalanced bridged-tee equivalents of the constant-resistance lattice of Fig. 63 (a); (c) and (d) Bridged-tee equivalents of lattice of Fig. 63 (b).

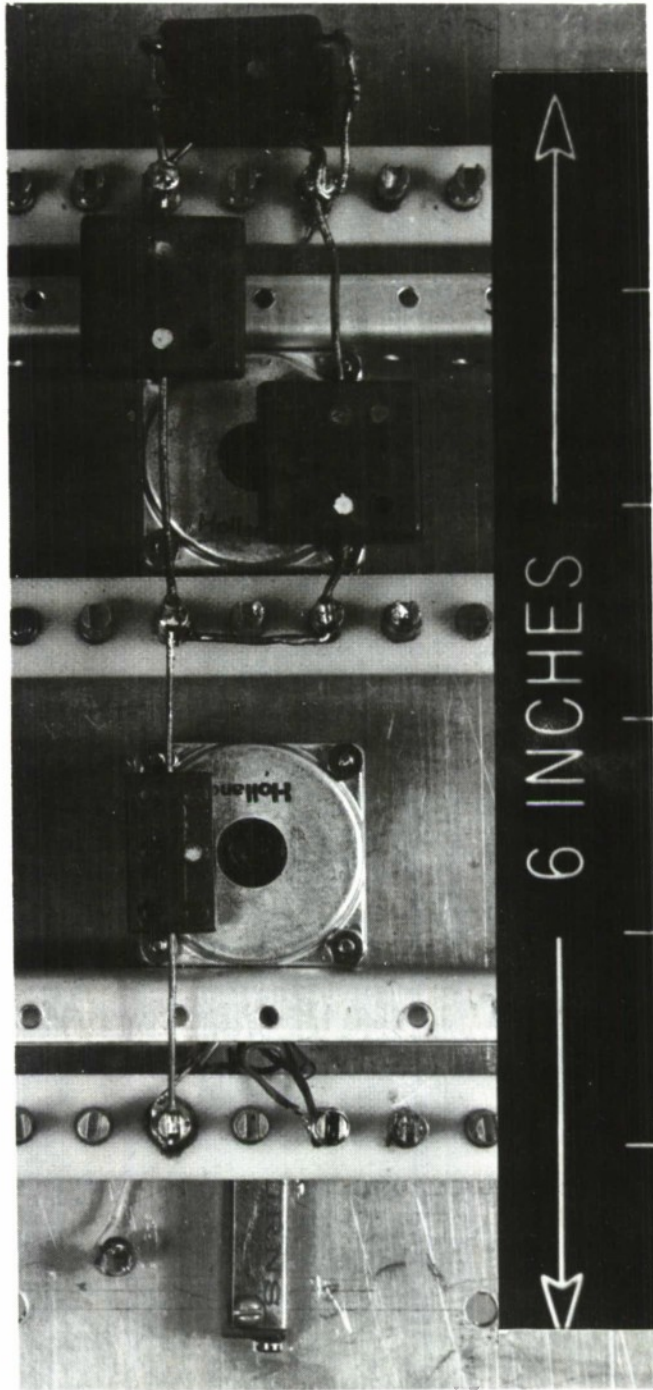
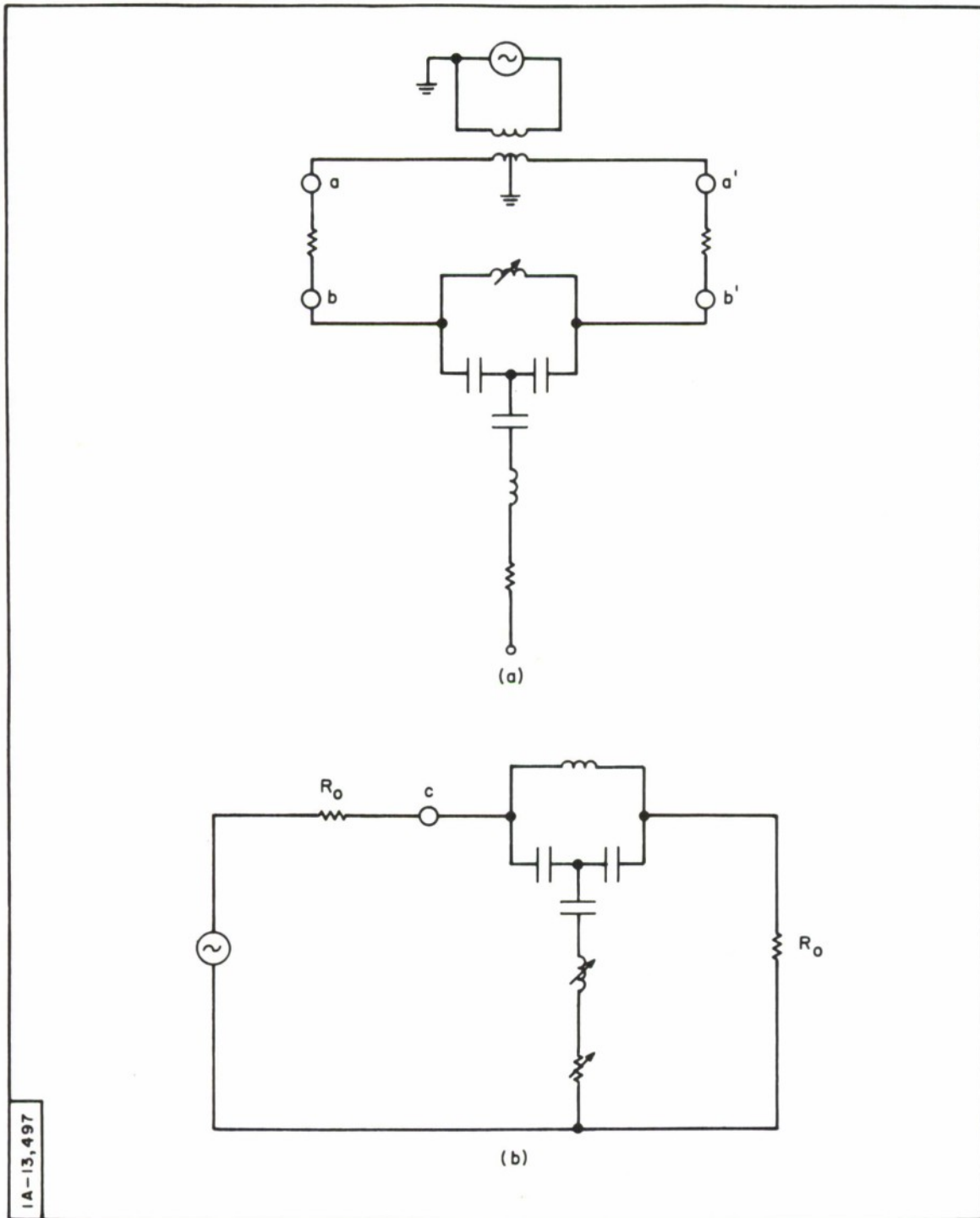


Fig. 66 Bridged-tee delay network of Fig. 65 (c).

network designed to operate at about 200 kc/sec. The inductors consist of a winding on a spool inside a ferrite cup-core which has, in the center, an air gap. A ferrite slug may be moved in the center to vary the dimensions of the air gap and hence the inductance. The capacitors are of the moulded, silvered mica type, and are within 1/2 percent of the calculated values. At the bottom of Fig. 66 may be seen protruding the end of a small adjustable resistor which is in the shunt arm and is used to introduce losses. The impedance level of the network shown is 200 ohms.

An alignment procedure which gives good results for the network of Fig. 66 is the following: First, the terminating resistor (not shown in the figure) is disconnected. Then a balanced voltage drive at the correct frequency is connected across the top tank circuit and, with the shunt arm effectively out of the circuit, the top inductor is adjusted to resonate the top tank. This procedure is illustrated in Fig. 67(a). When the tank in Fig. 67(a) is adjusted to resonance, the voltage from point "a" to ground will be in phase with the voltage from point "b" to ground. One may observe the voltages with a 2-channel oscilloscope and thus set the resonance very accurately. Observing the voltages at points "a" and "b" with the oscilloscope puts a few picofarads capacity from the points to ground. To preserve balance of the drive, the proper capacities are connected from points "a" and "b" to ground. Since the capacity from points "b" and "b'" to ground will appear across the tank, the tuning frequency must be adjusted so the circuit will resonate at the proper frequency with the drive removed. Next the balanced drive is removed, and the proper termination is connected across the output terminals of the network. A sweeping oscillator is connected to the input as shown in Fig. 67(b). The voltage from point "c" to ground is observed vs. frequency. The inductor and resistor in the shunt arm are alternately adjusted until the voltage at point "c" is constant over the band



IA-13,497

Fig. 67 Alignment of bridged-tee network; (a) method of setting frequency of top tank; (b) method of adjusting shunt elements.

of frequencies of interest. In this way, the network is made constant resistance. The bottom inductor obviously must initially have a higher quality factor, or "Q," than the top inductor; should it be otherwise, some damping must be put across the top tank before the top tank is tuned.

Figure 68 is a photograph of 10 networks in cascade mounted on an aluminum plate of dimensions 7 inches by 12 inches. Ten more networks are mounted on the other side of the plate. In this way, a great many networks may be assembled in a relatively small space.

4.5 Ultrasonic Delay Lines

Sonic waves propagate in solid cylindrical rods and ribbons in a number of ways. The waves can be longitudinal, shear, flexural, or torsional. There are an infinite number of modes by which waves of each type may propagate, and in nearly every case the velocity of propagation varies with frequency. Exceptions are the lowest torsional mode in a rod and the lowest shear mode in a strip, both of which have a nearly constant velocity of propagation, independent of frequency. The theory of the propagation of sinusoidal waves in infinitely long cylindrical bars was originally developed independently by Pochhammer^[45] and Chree.^[46] A summary is given by Love.^[47] One can make an electrical delay line utilizing the ultrasonic propagation effects by placing suitably designed electro-mechanical transducers on the ends of a cylindrical rod or ribbon. The transducers and the rod or ribbon must be of the proper size for the frequency employed, and the transducer must be designed to excite only the specific mode of propagation desired. A great deal of work aimed at the development of useful ultrasonic delay devices has been carried on at the Bell Telephone Laboratories.* Lines of constant delay have been constructed using

*A recent paper by May, Ref. 48, summarizes some of the Bell Laboratories work on ultrasonic delay lines.

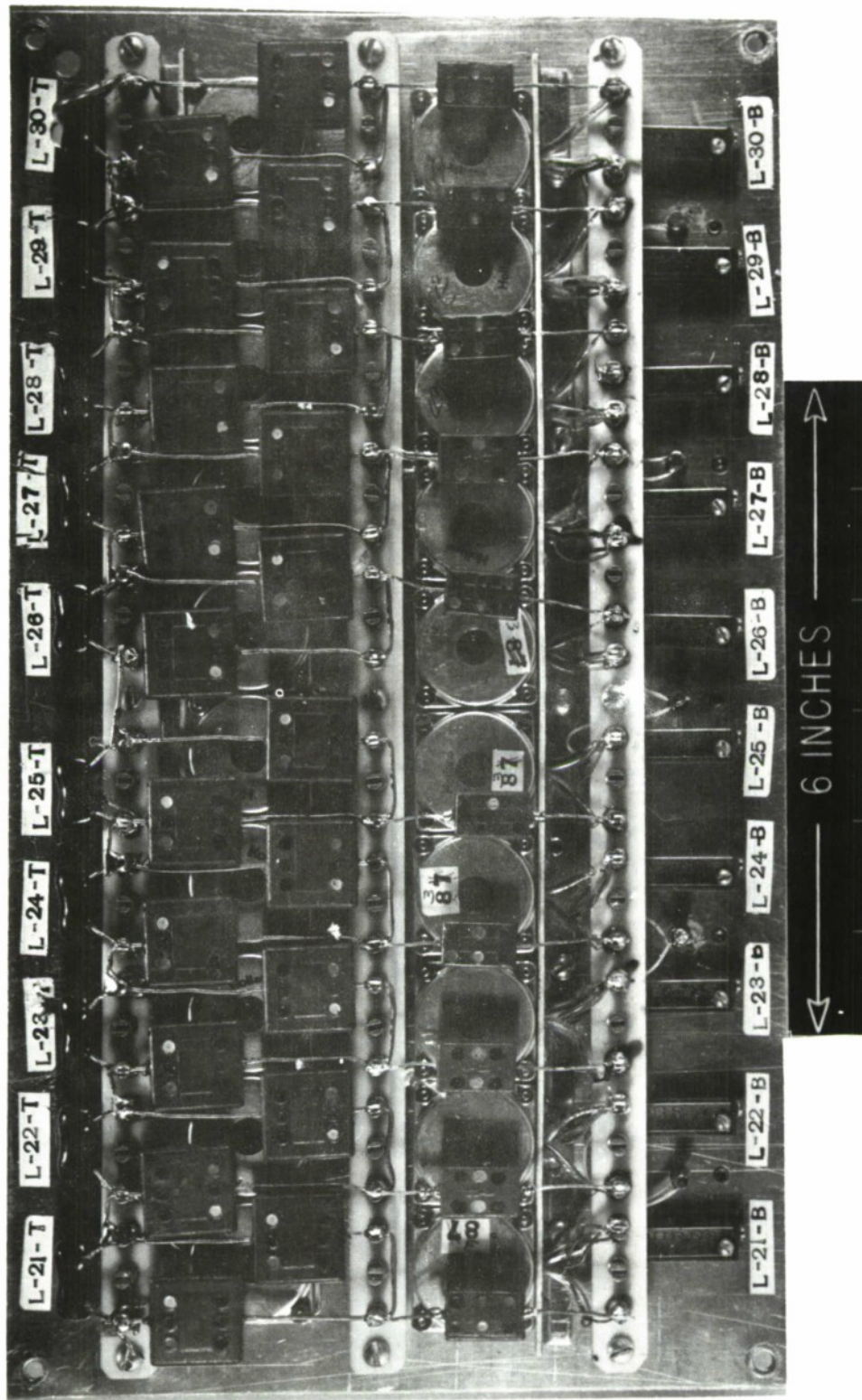


Fig. 68 Bridged-tee networks in cascade.

the lowest shear mode in an aluminum ribbon, [49] and dispersive delay lines have been realized by use of the first longitudinal mode in both cylindrical rods [50] and ribbons. [51] While both kinds of delay lines are potentially useful in the design of filters to generate and receive signals, we will confine our remarks here to the dispersive lines. Of the two shapes considered, rods and ribbons, apparently the ribbon is to be preferred because spurious responses are less troublesome with that shape.

Figure 69 shows the group time delay vs. frequency obtained by using the first longitudinal mode in an aluminum ribbon. V_s is the free space shear wave velocity (which for aluminum is 0.1259 inches/microsecond), L is the length, and h is the thickness of the ribbon.

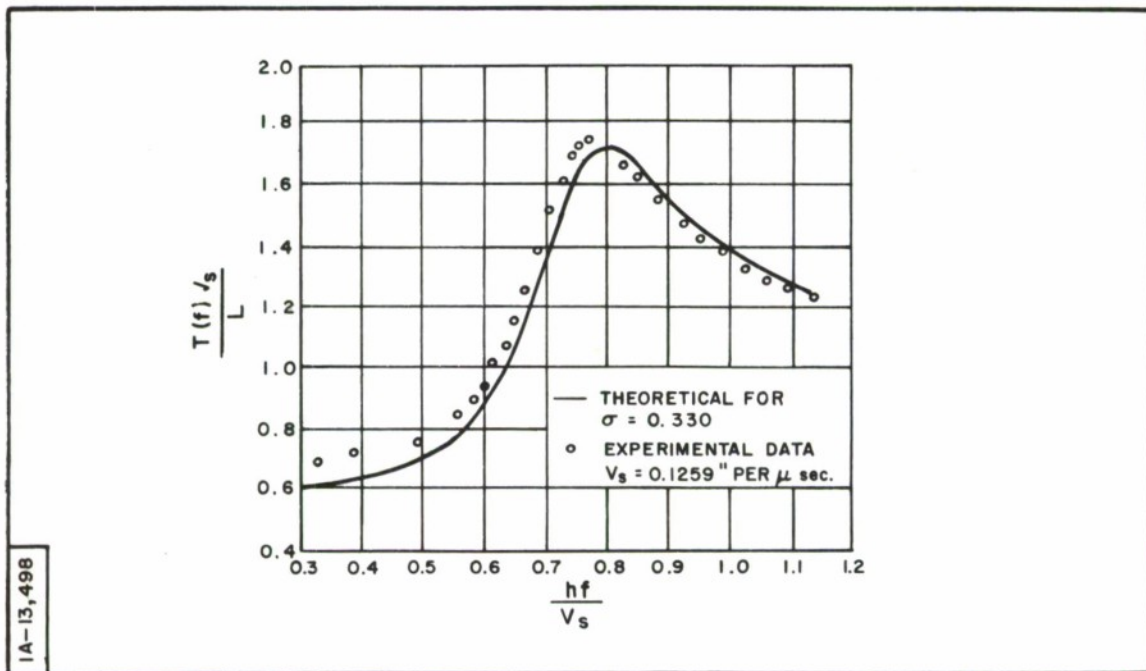


Fig. 69 Comparison of theoretical and experimental frequency dependence of delay for first longitudinal mode in a strip. (Taken from Meeker, Ref. 51, with permission.)

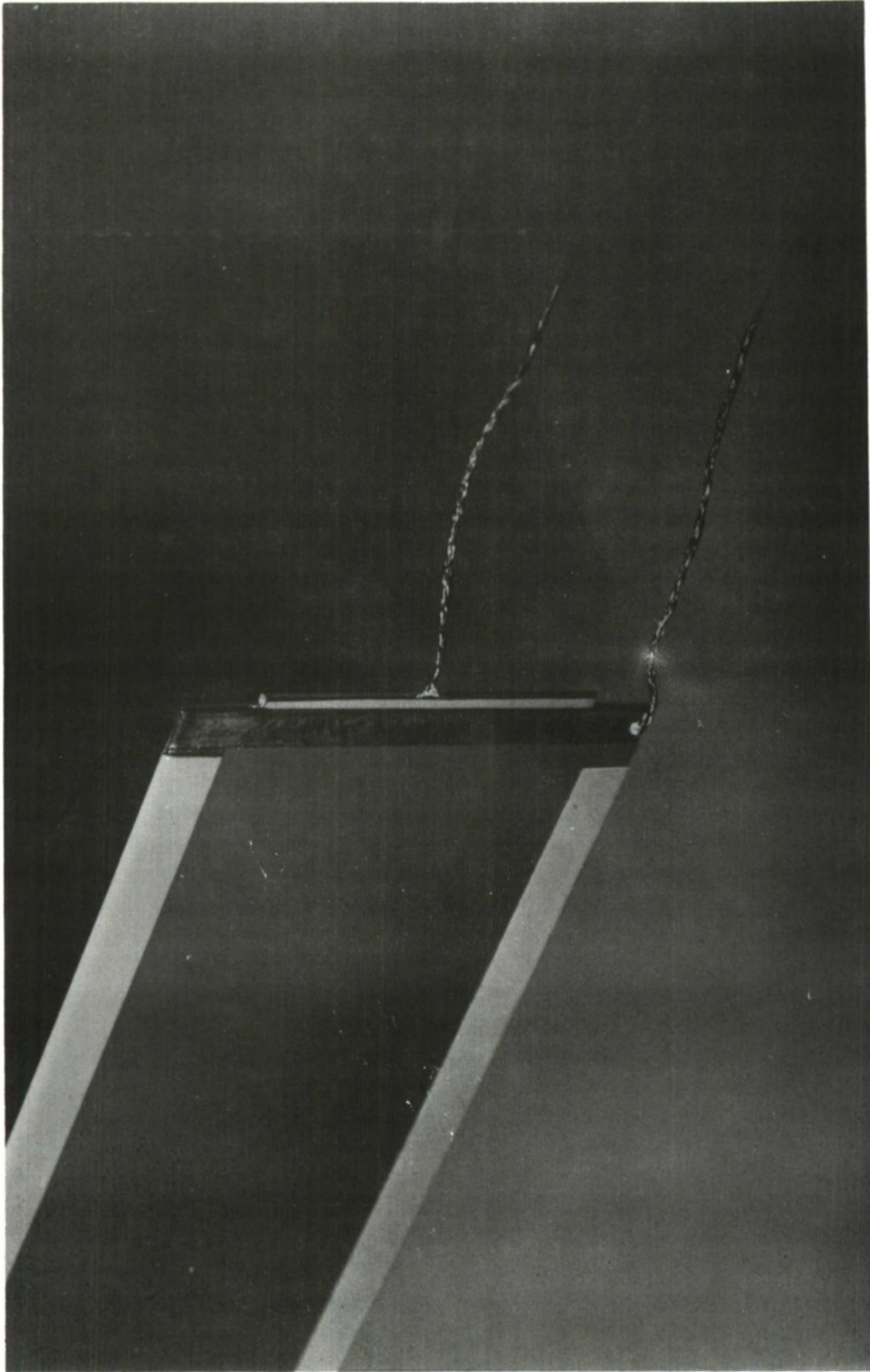


Fig. 70 Photograph of one end of a strip ultrasonic delay line showing the piezo-electric transducer. (Taken from Meeker, Ref. 51, with permission.)

Figure 70 shows how the transducers are affixed to the ends of the ribbon. It should be possible to use any one of a number of ceramic crystals for the transducers. Barium titanate has been used by Bell Laboratories. Other materials give broader or narrower pass-bands and higher or lower impedance levels.

Figure 71 shows the loss vs. frequency curve for the dispersive line when barium titanate transducers are employed. At midband the loss is about 13 db and it increases slightly on either side. The loss is almost entirely due to the transducers for lines of reasonable length.

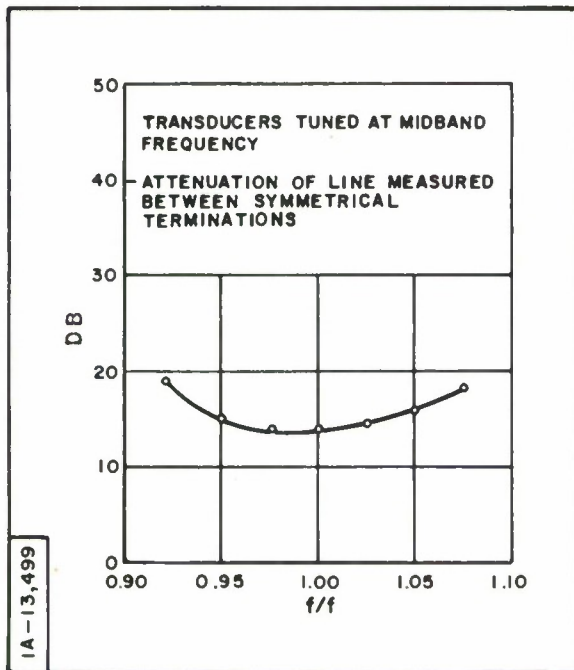


Fig. 71 Insertion loss for a typical dispersive longitudinal strip delay line with a center frequency of about 2 megacycles and a mid-band delay about one millisecond. (Taken from Meeker, Ref. 51, with permission.)

The line whose delay is shown in Fig. 69 may be used as it is or it may be used as a building block for the synthesis of other group delay curves.

Notice that the group delay curve of Fig. 69 has an inflection point at $hf/V_s \approx 0.68$. If the center frequency is taken at the inflection point, the group delay curve is a reasonable approximation to a straight line over an

interval equal to about 15 percent of the center frequency, and the device can be used as a component in the frequency domain realization of a filter designed to generate and receive linear FM signals.* An experimental line described by Meeker^[51] has the parameters given in Table 3.

Table 3

Center frequency	=	2 Mcps
Midband delay	=	1000 μ sec
Insertion loss	=	15 db
Change in delay (over 15% bandwidth)	=	400 μ sec
Discrimination to unwanted responses (over a 10% bandwidth)	=	40 db
Maximum departure from linearity (over 15% bandwidth)	=	12 μ sec

Figure 72 shows a photograph of an experimental Bell Laboratories ultrasonic delay line. The electrical matching networks may be seen near the ends of the aluminum ribbon. The top and bottom edges of the ribbon are covered with a tape which serves to absorb sonic waves that strike the edges of the line.

Let us consider how the delay line whose delay curve is given by Fig. 69 might be used in the synthesis of delay curves of other shapes. We view the elemental delay line and its delay curve of Fig. 69 as a building block;

*An ultrasonic delay line was used in the apparatus described in Ref. 13. System performance is shown in Figs. 26 through 28.

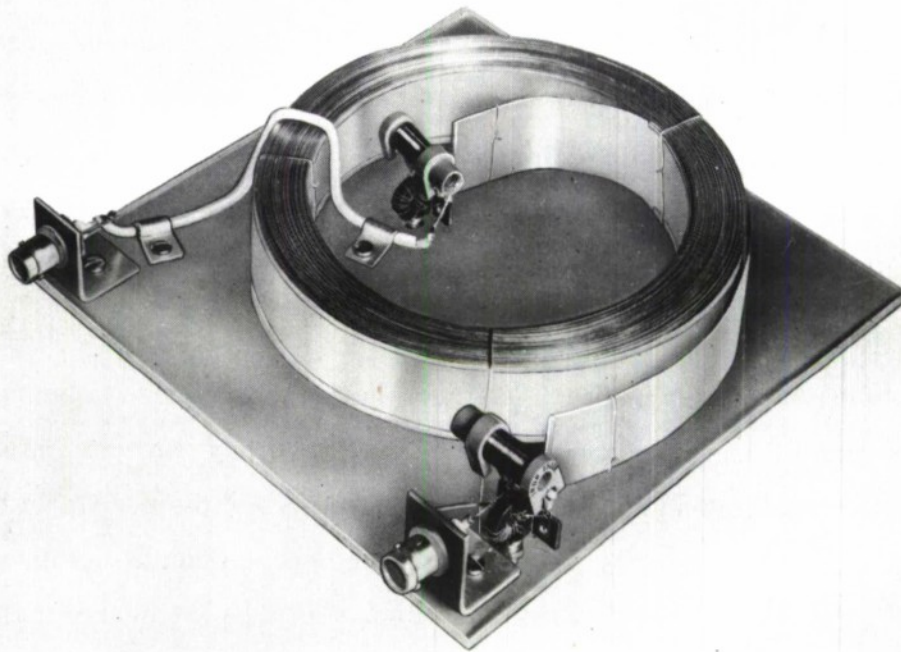


Fig. 72 Photograph of a strip ultrasonic delay line. The line contains 43 feet of strip and is mounted on 7-inch square plate. (Taken from Meitzler, Ref. 55, with permission.)

we can scale the delay by scaling the physical length of the ribbon, and shift the delay curve in the frequency direction by scaling the ribbon's thickness. Other delay curves can then be obtained by arranging delay lines of varying length and thickness in cascade. In order to realize a different delay curve one must first express the desired delay curve as a sum of appropriately weighted and frequency-shifted delays of the shape of Fig. 69. Fitch^[52] has reported a method of making such an expansion which uses the methods of linear programming. With ribbon lengths and thicknesses determined, the delay line is made as a single ribbon. With specially designed equipment the ribbon is rolled for length L_1 with appropriate thickness h_1 ; then the spacing of rolls is changed to h_2 and the ribbon is rolled for the appropriate length L_2 , and so on. When the rolling process is finished, a transducer is attached

to each end of the ribbon, and the delay line is complete. The measured loss and delay of such a delay line are smooth functions; apparently changing the thickness of the ribbon at points along its length does not cause noticeable reflections. Fitch also describes a chemical milling process in which the ribbons are withdrawn from an etchant at a non-uniform rate. In this way a continuous taper of the ribbon thickness can be achieved.

Fitch [52] describes the construction by the thickness tapering method of two ultrasonic lines with parabolic delay vs. frequency characteristics: one with delay that increases with increasing frequency, and the second with delay that decreases with increasing frequency. Other shapes can be achieved, particularly those that have a group delay that increases (or decreases) monotonically with frequency.

4.6 Tapped Delay Lines*

The technology of delay lines has developed enormously in recent years. Low-pass delay lines exist in distributed parameter form (e. g. delay cables) and as lumped element devices. Bandpass delay lines are available in the form of acoustic devices. All of the above types are commercially available and suitable for generating waveforms with duration-bandwidth products of several hundred. We will not try in this section to give a technical discussion on delay lines themselves. The subject is much too vast. Rather we will consider some ways in which delay lines can be used to generate and receive signals.

* An excellent discussion of the use of tapped delay lines in generating signals is given by Turin in Ref. 53.

As a first illustration of the use of tapped delay lines let us consider the low-pass, 13-code waveform of Fig. 19(a). We would like to use the tapped delay line in conjunction with a linear filter in such a way that the impulse response of the over-all device is the 13-code signal. Furthermore, for simplicity we would like the time delay between successive taps of the lines to be constant. The general filter configuration we have in mind is shown in Fig. 73. Just what the delay between successive taps should be we can deduce by

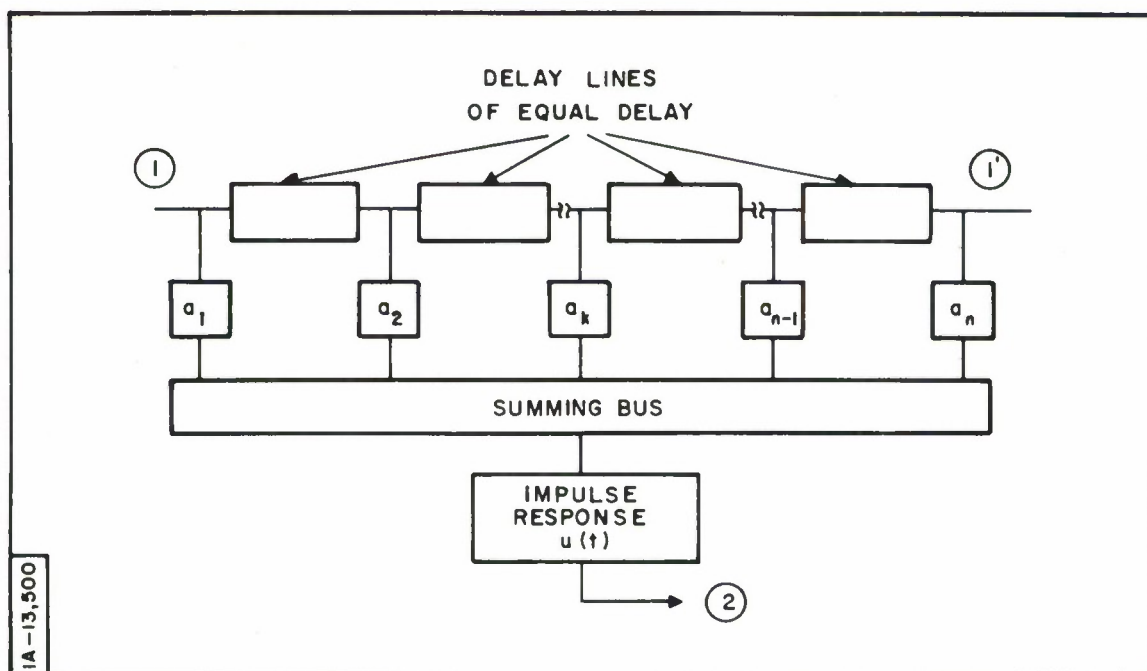


Fig. 73 Block diagram of a filter employing a tapped delay line.

two methods. First, inspection of the 13-code waveform shows that the shortest interval between alternations is T , and therefore, if the taps are to be uniform, the tap spacing should probably be T . Alternatively, inspection of the spectrum of the waveform Fig. 19(c) shows that its bandwidth, W , is approximately

$1/2T$ and that, therefore, in accordance with sampling theory, to describe the waveform we should take samples at intervals in time, Δt , given approximately by

$$\Delta t \cong \frac{1}{2W}$$

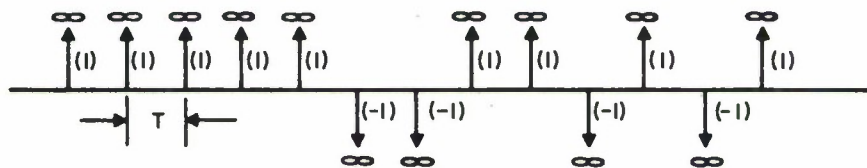
or

$$\Delta t \cong T \quad .$$

We next ask what the impulse response of the filter in Fig. 73 should be. An obvious choice for the impulse response, in this case, appears to be a rectangular pulse of duration T . Such a filter has a frequency response of the form $\sin \pi Tf / \pi Tf$.

With the weights, a_k , of the filter in Fig. 73 set to correspond to the values of the 13-code waveform taken at intervals of T , an impulse applied at the input terminal of the filter (terminal 1) will produce at the summing bus a train of impulses like that shown in Fig. 74(a). The response of the $\sin \pi Tf / \pi Tf$ filter, which appears at the output terminal of the filter (terminal 2), to the train of impulses is shown in Fig. 74(b). It is, not too surprisingly, the 13-code waveform. It is interesting to note that an impulse applied to terminal 1' of the filter in Fig. 73 produces at terminal 2 the 13-code waveform inverted in time, and that therefore, if the 13-code waveform is applied to terminal 1', the filter serves as a matched filter. This can be true of tapped delay line filters in general, as we shall see.

We have labored this example somewhat to stress the useful point that tapped delay line techniques of generating signals can be viewed as implementations of sampling notions.



(a) THE IMPULSE TRAIN ON THE SUMMING BUS WHICH RESULTS FROM APPLICATION OF AN IMPULSE TO TERMINAL 1 OF FIG. 73



(b) THE WAVEFORM AT THE OUTPUT OF THE FILTER OF FIG. 73 (TERMINAL 2)

IA-13,501

Fig. 74 Sketch to illustrate the method of generation of low-pass waveforms by use of tapped delay lines.

When signals are realized at bandpass by tapped delay line methods, the tap weighting required will be in general complex, corresponding to an amplitude and phase. A useful type of delay line for realizing signals at band pass is the magnetostrictive acoustic wire delay line developed at Lincoln Laboratory. The delay line and a matched filter system in which it is used is described by Lerner.^[54] The delay line consists of a thin rod of magnetic material to one end of which is affixed a ceramic piezo-electric crystal and acoustic transformer; around the rod center, tapped coils are placed at regular intervals to make the taps. Each tap has supplied a magnetic bias field. The arrangement is shown in Fig. 75. The ceramic transducer converts electrical signals to sound waves which travel along the rod. As the sound wave propagates along the rod, it alters the local magnetic properties, and the corresponding changes in flux due to the bias field induce voltages in the output coils. Plus or minus weights can be had from the opposite ends of the center-tapped output coil; changes in phase can be effected by moving the coil along the rod.

The configuration of the bandpass tapped delay line filter is the same as that of the low-pass device of Fig. 73 except that now, as noted above, the weights a_k are complex and the filter with impulse response $u(t)$ is at bandpass. If care is taken to make the elemental signal $u(t)$ have even symmetry about its center, then the signal generated by applying an impulse to terminal 1' is the inverted-time replica of the signal generated by applying an impulse to terminal 1. Lerner^[54] gives analysis of the delay line matched filter system and shows how the one delay line together with a suitable resistor matrix can make a matched filter not only to the signal but to the signal with a wide range of Doppler shifts as well. The interested reader is referred to the paper by Lerner.

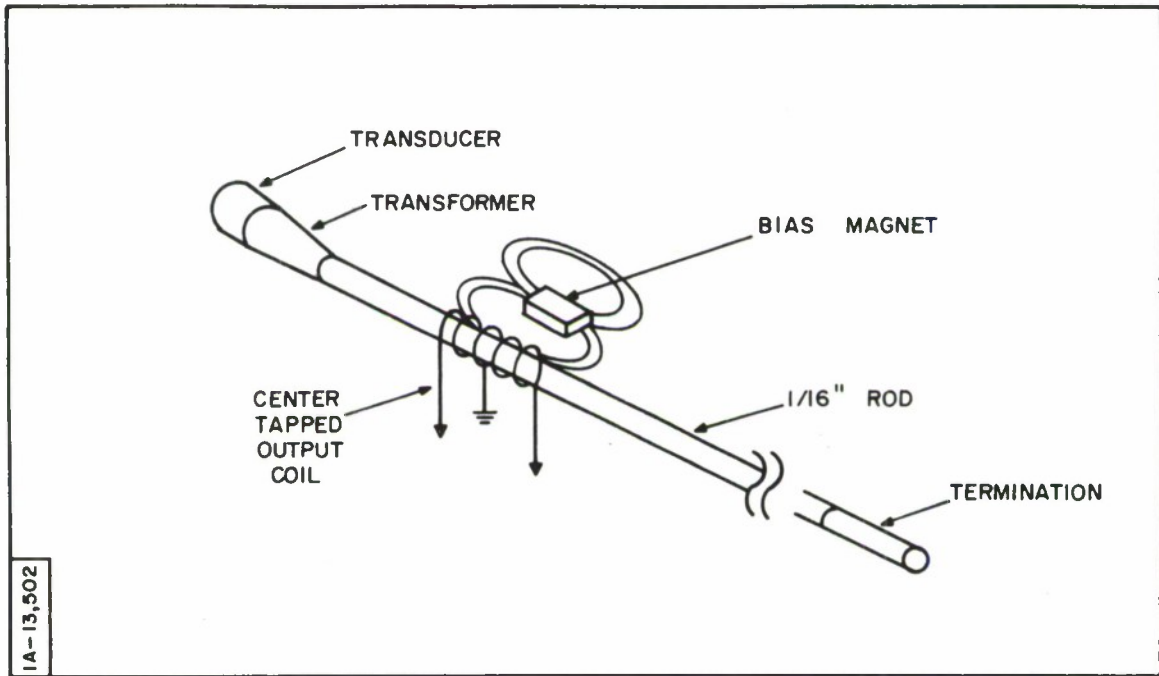
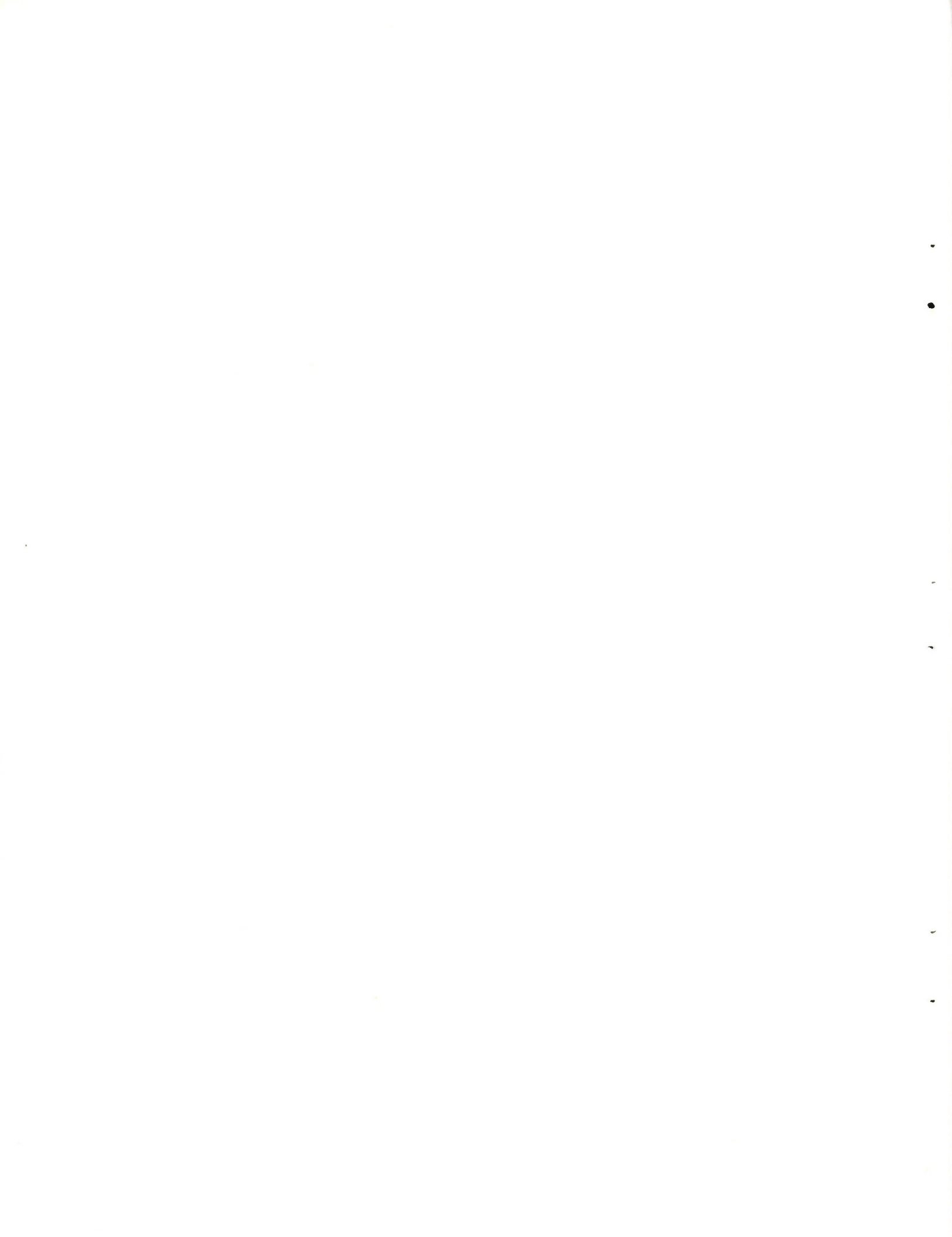


Fig. 75 Sketch of the magnetostrictive acoustic wire delay line developed at Lincoln Laboratory. (Taken from Lerner, Ref. 54, with permission.)



5.0 REFERENCES

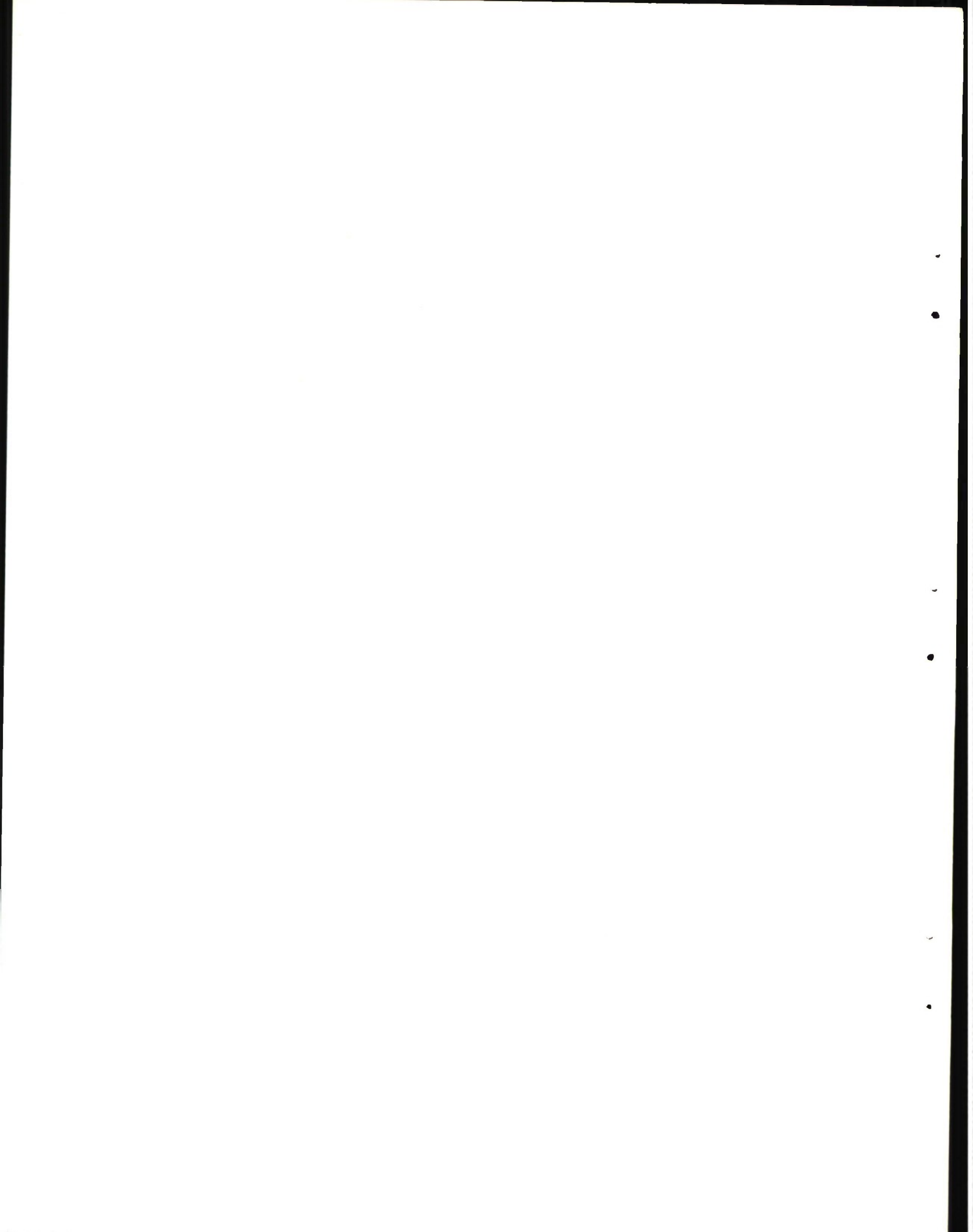
1. P. M. Woodward, Probability and Information Theory with Applications to Radar. New York: McGraw-Hill Book Company, Inc., 1953.
2. J. Freedman and L. Smullin, eds., Principles of High Power Radar Design. New York: McGraw-Hill (to be published late 1964). See particularly Chapter 2, by W. McC. Siebert.
3. W. McC. Siebert, Studies of Woodward's Uncertainty Function. Research Laboratory of Electronics, MIT, Cambridge, Massachusetts, Quarterly Progress Report, April 15, 1958.
4. J. Ville, Theorie et application de la notion de signal analytique. Cables et Transmission, Vol. 2, No. 1, 1948, 61-74.
5. S. Sussman, Least square synthesis of radar ambiguity functions. IRE Transactions on Information Theory, Vol. IT-8, No. 3, 1962.
6. C. W. Helstrom, Statistical Theory of Signal Detection. New York: Pergamon Press, 1960.
7. S. Applebaum and P. W. Howells, Waveform design for tomorrow's radars. Space/Aeronautics, October 1959.
8. E. N. Fowle, E. J. Kelley, and J. A. Sheehan, Radar system performance in a dense-target environment, 1961 IRE International Convention Record, Part IV, 136-145.
9. W. McC. Siebert, A radar detection philosophy. IRE Transactions on Information Theory, Vol. IT-2, 1956, 204-221.
10. E. L. Key, E. N. Fowle, and R. D. Haggarty, A method of designing signals of large time-bandwidth product. 1961 IRE International Convention Record, Part IV, 146-154.
11. C. E. Cook, Pulse compression - key to more efficient radar transmissions, Proceedings of the IRE, Vol. 48, No. 3, 1960, 310-316.
12. J. R. Klauder, A. C. Price, S. Darlington, and W. J. Albersheim, The theory and design of chirp radars. Bell Systems Technical Journal, Vol. 39, No. 4, 1960, 745-808.
13. E. N. Fowle, D. R. Carey, R. E. Vander Schuur, and R. C. Yost, A pulse compression system employing a linear FM Gaussian signal. Proceedings of the I. E. E. E., Vol. 51, No. 2, 1963.
14. R. W. Jacobus, A linear FM 1000:1 pulse compression system. The MITRE Corporation, Bedford, Massachusetts, Technical Memorandum TM-3529, January 8, 1963. (ESD-TDR-63-237)

15. R. Manasse, The use of pulse coding to discriminate against clutter. Lincoln Laboratory, Lexington, Massachusetts, MIT Group Report 312-12, August 1957.
16. C. H. Wilcox, The synthesis problem for radar ambiguity functions. Mathematics Research Center, The University of Wisconsin, Madison, Wisconsin, MRC Tech. Summary Report No. 157, April 1960.
17. E. C. Watters, A Note on the Design of Coded Pulses, Proceedings of the Pulse Compression Symposium, Rome Air Development Center, Griffiss Air Force Base, New York, TR-59-161, September 1959. (Not generally available.)
18. E. N. Fowle, A general method for controlling the time and frequency envelopes of FM signals. Lincoln Laboratory, Lexington, Massachusetts, MIT Group Report 41G-0008, June 5, 1961.
19. D. O. Sproule, and A. J. Hughes, Improvements in and relating to systems operating by means of wave trains. British Patent No. 604,429. Application Date: June 9, 1944.
20. R. H. Dicke, Object detection system. U. S. Patent No. 2,624,876, filed September 14, 1945.
21. S. Darlington, Pulse Transmission, U. S. Patent No. 2,678,997, filed December 31, 1949.
22. W. Cauer, (Title unknown), German Patent No. 892,772, December 19, 1950.
23. I. N. Sneddon, Fourier Transforms. New York: McGraw-Hill, 1951, pp. 282-285.
24. R. E. A. C. Paley, and N. Wiener, Fourier Transforms in the Complex Domain. Providence, R. I.: American Math. Society, 1934.
25. T. T. Taylor, Design of line-source antennas for narrow bandwidth and low side lobes. IRE Transactions on Antennas and Propagation, Vol. AP-3, No. 1, 1955.
26. N. Zierler, Several binary-sequence generators, Proceedings of American Mathematical Society, Vol. 7, 1956, 675-681.
27. R. M. Lerner, and A. M. Sherman, A tabulation of quadratic residues or Legendre sequences with respect to primes up to 1021. Lincoln Laboratory, Lexington, Massachusetts, MIT Group Report 36G-0047, July 27, 1960.

28. B. Elspas, A radar system based on statistical estimation and resolution considerations. Applied Electronics Laboratory, Stanford University, Palo Alto, California, TR 361-1, August 1955.
29. R. H. Barker, Group synchronizing of binary digital systems. Communication Theory, (Willis Jackson, ed.). London: Academic Press, 1958, 273-287.
30. D. DeLong, Three-phase codes. Lincoln Laboratory, Lexington, Massachusetts, MIT Group Report 47-28; July 1959.
31. E. L. Key, E. N. Fowle, and R. D. Haggarty, A method of side-lobe suppression in phase-coded pulse compression systems. Lincoln Laboratory, Lexington, Massachusetts, MIT Report TR-209, August 28, 1959.
32. E. N. Fowle, The design of FM pulse compression signals, IEEE Transactions on Information Theory, Vol. IT-10, No. 1, 1964.
33. E. N. Fowle, A note on the design of signals with ambiguity functions of the thumbtack shape. The MITRE Corporation, Bedford, Massachusetts, Technical Memorandum TM-3566. In preparation.
34. H. Miedema, Signal processing to obtain range and range-rate information on a single-pulse basis. Proceedings of the Eighth Annual Radar Symposium, The University of Michigan, Ann Arbor, Michigan, June 1962.
35. D. Richman, Superresolution. Proceedings of the Pulse Compression Symposium, Rome Air Development Center, Griffiss Air Force Base, New York, TR-59-161, September 1959. (Not generally available.)
36. F. P. Callahan, Jr., Enhanced accuracy radar pulses. Proceedings of the Pulse Compression Symposium, Rome Air Development Center, Griffiss Air Force Base, New York, TR-59-161, September 1959. (Not generally available.)
37. R. M. Lerner, Signals with uniform ambiguity functions. 1958 IRE International Convention Record, Part IV, pp. 27-36.
38. J. R. Klauder, The design of signals having both high range resolution and high velocity resolution. Bell System Technical Journal, Vol. 39, No. 4, 1960, 809-820.

39. T. Kailath, Measurement on time-variant communication channels. IRE Transactions on Information Theory, Vol. IT-8, No. 5, 1962.
40. J. B. Resnick, High resolution waveforms suitable for a multiple target environment. S. M. Thesis, Department of Electrical Engineering, MIT Cambridge, Mass., June 1962.
41. E. A. Guillemin, Synthesis of Passive Networks. New York: John Wiley and Sons, 1957.
42. M. Van Valkenburg, Introduction to Modern Network Synthesis. New York: John Wiley and Sons, 1960.
43. D. F. Tuttle, Network Synthesis. New York: John Wiley and Sons, 1958.
44. H. W. Bode, Network Analysis and Feedback Amplifier Design. Princeton, N. J.: D. Van Nostrand Co., Inc., 1945.
45. L. Pochhammer, J. reine angew. Math. (Crelle), Vol. 81, 1876, 324-336.
46. C. Chree, Transactions of the Cambridge Philosophical Society, Vol. 14, 1889, 250-269.
47. A. E. H. Love, Mathematical Theory of Elasticity. Cambridge, England University Press, 1934, p. 288.
48. J. E. May, Jr., Guided wave ultrasonic delay lines. A paper presented at 1962 Electronic Components Conference, Washington, D. C., May 9, 1962.
49. A.H. Meitzler, Ultrasonic delay lines using shear modes in strips. IRE Transactions on Ultrasonic Engineering, Vol. VE-7, No. 2, 1960.
50. J. E. May, Jr., Wire-type dispersive ultrasonic delay lines. IRE Transactions on Ultrasonic Engineering, Vol. VE-7, No. 2, 1960.
51. T. R. Meeker, Dispersive ultrasonic delay lines using the first longitudinal mode in a strip. IRE Transactions on Ultrasonic Engineering, Vol. VE-7, No. 2, 1960.
52. A. H. Fitch, Synthesis of dispersive delay characteristics by thickness tapering in ultrasonic strip delay lines. Journal of the Acoustical Society of America, Vol. 35, No. 5, 1963.
53. G. L. Turin, Introduction to matched filters. IRE Transactions on Information Theory, Vol. IT-6, No. 3; 1960.

54. R. M. Lerner, A matched filter detection system for complicated Doppler-shifted signals. IRE Transactions on Information Theory, Vol. IT-6, No. 3, 1960.
55. A. H. Meitzler, Ultrasonic delay lines for digital data storage. I. E. E. E. Transactions on Ultrasonic Engineering, Vol. VE-9, No. 2, 1962.



6.0 BIBLIOGRAPHY

S. Applebaum and P. W. Howells, Waveform design for tomorrow's radars. Space/Aeronautics, October 1959.

R. H. Barker, Group synchronizing of binary digital systems. Communication Theory, (Willis Jackson, ed.). London: Academic Press, 1958, 273-287.

H. W. Bode, Network Analysis and Feedback Amplifier Design. Princeton, N. J.: D. Van Nostrand Co., Inc., 1945.

F. P. Callahan, Jr., Enhanced accuracy radar pulses. Proceedings of the Pulse Compression Symposium, Rome Air Development Center, Griffiss Air Force Base, New York, TR-59-161, September 1959. (Not generally available.)

W. Cauer, (Title unknown), German Patent No. 892,772, December 19, 1950.

C. Chree, Transactions of the Cambridge Philosophical Society, Vol. 14, 1889, 250-269.

C. E. Cook, Pulse compression - key to more efficient radar transmissions. Proceedings of the IRE, Vol. 48, No. 3, 1960, 310-316.

S. Darlington, Pulse Transmission, U. S. Patent No. 2,678,997, filed December 31, 1949.

D. DeLong, Three-phase codes. Lincoln Laboratory, Lexington, Massachusetts, MIT, Group Report 47-28; July 1959.

R. H. Dicke, Object detection system. U. S. Patent No. 2,624,876, filed September 14, 1945.

B. Elspas, A radar system based on statistical estimation and resolution considerations. Applied Electronics Laboratory, Stanford University, Palo Alto, California, TR 361-1, August 1955.

A. H. Fitch, Synthesis of dispersive delay characteristics by thickness tapering in ultrasonic strip delay lines. Journal of the Acoustical Society of America, Vol. 35, No. 5, 1963.

E. N. Fowle, A general method for controlling the time and frequency envelopes of FM signals. Lincoln Laboratory, Lexington, Massachusetts, MIT Group Report 41G-0008, June 5, 1961.

E. N. Fowle, The design of FM pulse compression signals, IEEE Transactions on Information Theory, Vol. IT-10, No. 1, 1964.

E. N. Fowle, A note on the design of signals with ambiguity functions of the thumbtack shape. The MITRE Corporation, Bedford, Massachusetts, Technical Memorandum TM-3566. In preparation.

E. N. Fowle, D. R. Carey, R. E. Vander Schuur, and R. C. Yost, A pulse compression system employing a linear FM Gaussian signal. Proceedings of the I. E. E. E., Vol. 51, No. 2, 1963.

E. N. Fowle, E. J. Kelly, and J. A. Sheehan, Radar system performance in a dense-target environment, 1961 IRE International Convention Record, Part IV, 136-145.

J. Freedman and L. Smullin, eds., Principles of High Power Radar Design. New York: McGraw-Hill (to be published late 1964). See particularly Chapter 2, by W. McC. Siebert.

E. A. Guillemin, Synthesis of Passive Networks. New York: John Wiley and Sons, 1957.

C. W. Helstrom, Statistical Theory of Signal Detection. New York: Pergamon Press, 1960.

R. W. Jacobus, A linear FM 1000:1 pulse compression system. The MITRE Corporation, Bedford, Massachusetts, Technical Memorandum TM-3529, January 8, 1963. (ESD-TDR-63-237)

T. Kailath, Measurement on time-variant communication channels. IRE Transactions on Information Theory,

E. L. Key, E. N. Fowle, and R. D. Haggarty, A method of designing signals of large time-bandwidth product. 1961 IRE International Convention Record, Part IV, 146-154.

E. L. Key, E. N. Fowle, and R. D. Haggarty, A method of side-lobe suppression in phase-coded pulse compression systems. Lincoln Laboratory, Lexington, Massachusetts, MIT Report TR-209, August 28, 1959. .

J. R. Klauder, The design of signals having both high range resolution and high velocity resolution. Bell System Technical Journal, Vol. 39, No. 4, 1960, 809-820.

J. R. Klauder, A. C. Price, S. Darlington, and W. J. Albersheim, The theory and design of chirp radars. Bell System Technical Journal, Vol. 39, No. 4, 1960, 745-808.

R. M. Lerner, A matched filter detection system for complicated Doppler-shifted signals. IRE Transactions on Information Theory, Vol. IT-6, No. 3, 1960.

R. M. Lerner, Signals with uniform ambiguity functions. 1958 IRE International Convention Record, Part IV, pp. 27-36.

R. M. Lerner, and A. M. Sherman, A tabulation of quadratic residues or Legendre sequences with respect to primes up to 1021. Lincoln Laboratory, Lexington, Massachusetts, MIT Group Report 36G-0047, July 27, 1960.

A. E. H. Love, Mathematical Theory of Elasticity, Cambridge, England: University Press 1934, p. 288.

R. Manasse, The use of pulse coding to discriminate against clutter. Lincoln Laboratory, Lexington, Massachusetts, MIT Group Report 312-12, August 1957.

J. E. May, Jr., Guided wave ultrasonic delay lines. A paper presented at 1962 Electronic Components Conference, Washington, D. C., May 9, 1962.

J. E. May, Jr., Wire-type dispersive ultrasonic delay lines.: I. R. E. Transactions on Ultrasonic Engineering, Vol. VE-7, No. 2, 1960.

T. R. Meeker, Dispersive ultrasonic delay lines using the first longitudinal mode in a strip. IRE Transactions on Ultrasonic Engineering, Vol. VE-7, No. 2, 1960.

A. H. Meitzler, Ultrasonic delay lines for digital data storage. I. E. E. E. Transactions on Ultrasonic Engineering, Vol. VE-9, No. 2, 1962.

A. H. Meitzler, Ultrasonic delay lines using shear modes in strips. I. R. E. Transactions on Ultrasonic Engineering, Vol. VE-7, No. 2, 1960.

H. Miedema, Signal processing to obtain range and range-rate information on a single-pulse basis. Proceedings of the Eighth Annual Radar Symposium, The University of Michigan, Ann Arbor, Michigan, June 1962.

R. E. A. C. Paley, and N. Wiener, Fourier Transforms in the Complex Domain, Providence, R. I.: American Math. Society, 1934.

L. Pochhammer, J. reine angew. Math. (Crelle), Vol. 81, 1876, 324-336.

J. B. Resnick, High resolution waveforms suitable for a multiple target environment, S. M. Thesis, Department of Electrical Engineering, MIT, Cambridge, Massachusetts, June 1962.

D. Richman, Superresolution. Proceedings of the Pulse Compression Symposium, Rome Air Development Center, Griffiss Air Force Base, New York, TR-59-161, September 1959. (Not generally available.)

W. McC. Siebert, A radar detection philosophy. IRE Transactions on Information Theory, Vol. IT-2, 1956, 204-221.

W. McC. Siebert, Studies of Woodward's Uncertainty Function. Research Laboratory of Electronics, MIT, Cambridge, Massachusetts, Quarterly Progress Report, April 15, 1958.

- I. N. Sneddon, Fourier Transforms. New York: McGraw-Hill, 1951, pp. 282-285.
- D. O. Sproule, and A. J. Hughes, Improvements in and relating to systems operating by means of wave trains. British Patent No. 604, 429. Application Date: June 9, 1944.
- S. Sussman, Least square synthesis of radar ambiguity functions. IRE Transactions on Information Theory, Vol. IT-8, No. 3, 1962.
- T. T. Taylor, Design of line-source antennas for narrow bandwidth and low side lobes. IRE Transactions on Antennas and Propagation, Vol. AP-3, No. 1, 1955.
- G. L. Turin, Introduction to matched filters. IRE Transactions on Information Theory, Vol. IT-6, No. 3; 1960.
- D. F. Tuttle, Network Synthesis. New York: John Wiley and Sons, 1958.
- M. Van Valkenburg, Introduction to Modern Network Synthesis. New York: John Wiley and Sons, 1960.
- J. Ville, Theorie et application de la notion de signal analytique. Cables et Transmission, Vol. 2, No. 1, 1948, 61-74.
- E. C. Watters, A Note on the Design of Coded Pulses. Proceedings of the Pulse Compression Symposium, Rome Air Development Center, Griffiss Air Force Base, New York, TR-59-161, September 1959. (Not generally available.)
- C. H. Wilcox, The synthesis problem for radar ambiguity functions. Mathematics Research Center, The University of Wisconsin, Madison, Wisconsin, MRC Tech. Summary Report No. 157, April 1960.
- P. M. Woodward, Probability and Information Theory with Applications to Radar, New York: McGraw-Hill Book Company, Inc., 1953.
- N. Zierler, Several binary-sequence generators, Proceedings of American Mathematical Society, Vol. 7, 1956, 675-681.

DOCUMENT CONTROL DATA - R&D

(Security classification of title, body of abstract and indexing annotation must be entered when the overall report is classified)

1. ORIGINATING ACTIVITY (Corporate author) The MITRE Corporation Bedford, Mass.		2 a. REPORT SECURITY CLASSIFICATION Unclassified	
		2 b. GROUP	
3. REPORT TITLE The Design of Radar Signals			
4. DESCRIPTIVE NOTES (Type of report and inclusive dates) N/A			
5. AUTHOR(S) (Last name, first name, initial) Fowle, Evert N.			
6. REPORT DATE June 1965	7 a. TOTAL NO. OF PAGES 193	7 b. NO. OF REFS 55	
8 a. CONTRACT OR GRANT NO. AF 19(628)-2390	9 a. ORIGINATOR'S REPORT NUMBER(S) ESD-TR-65-97		
b. PROJECT NO. 750.0	9 b. OTHER REPORT NO(S) (Any other numbers that may be assigned this report) SR-98		
c.			
d.			
10. AVAILABILITY/LIMITATION NOTICES Qualified requestors may obtain from DDC. DDC release to CFSTI (formerly OTS) authorized.			
11. SUPPLEMENTARY NOTES		12. SPONSORING MILITARY ACTIVITY Directorate of Radar and Optics, Electronic Systems Division L. G. Hanscom Field, Bedford, Massachusetts	
13. ABSTRACT <p>This report discusses the design of radar signals. It is assumed that the radar receiver is matched to the signal so that the receiver output waveform, in the presence of signal Doppler frequency shift, is characterized by Woodward's two-dimensional signal correlation function. The signal correlation function is discussed, and certain of its properties are collected together. The problem of the detection of a target in the presence of many nearby targets is discussed, and an expression for the target capacity of a radar is developed in terms of the signal correlation function. There follows a discussion of the general problems of signal design for multiple target resolution and for detection of single targets in clutter. Signal waveforms are classified according to the type of modulation, and the design of waveforms of each type is considered in detail. The two-dimensional correlation function is given for each type of signal. Finally, the subject of techniques for generation and reception of signals is discussed.</p>			

